Surface Modification of Biodegradable Magnesium Implant Materials for Controlled Biodegradation

by

Afrah Al Hegy

A thesis submitted in partial fulfillment
of the requirements for the degree of
Doctor of Philosophy (PhD) in Materials Science

The Faculty of Graduate Studies
Laurentian University
Sudbury, Ontario, Canada

THESIS DEFENCE COMMITTEE/COMITÉ DE SOUTENANCE DE THÈSE
Laurentian Université/Université Laurentienne
Faculty of Graduate Studies/Faculté des études supérieures

Title of Thesis
Titre de la thèse: Surface Modification of Biodegradable Magnesium Implant Materials for Controlled Biodegradation

Name of Candidate
Nom du candidat: Al Hegy, Afrah

Degree
Diplôme: Doctor of Philosophy

Department/Program
Département/Programme: Materials Science

Date of Defence
Date de la soutenance June 18, 2019

APPROVED/APPROUVÉ

Thesis Examiners/Examinateurs de thèse:

Dr. Joy Gray-Munro
(Supervisor/Directrice de thèse)

Dr. Eric Gauthier
(Committee member/Membre du comité)

Dr. Louis Mercier
(Committee member/Membre du comité)

Dr. Hendra Herwaman
(External Examiner/Examinatrice externe)

Dr. Sabine Montaut
(Internal Examiner/Examinatrice interne)

Approved for the Faculty of Graduate Studies
Approuvé pour la Faculté des études supérieures
Dr. David Lesbarrères
Monsieur David Lesbarrères
Dean, Faculty of Graduate Studies
Doyen, Faculté des études supérieures

ACCESSIBILITY CLAUSE AND PERMISSION TO USE

Abstract

Magnesium and its alloys are promising candidates to be employed as a new generation of biodegradable metals in orthopaedic applications. However, the rapid degradation rate of magnesium alloys in the physiological environment has prevented their widespread application in medicine. The main objective of this thesis was to develop surface modification strategies that control the degradation rate of magnesium alloys in physiological environments and to provide an accurate assessment and evaluation of their biocompatibility *in vitro*. The overall thesis is composed of three individual projects.

The first project was to develop an accurate method to test the *in vitro* biocompatibility of magnesium alloys. In this study, the CyQUANT assay was used to quantitatively evaluate the *in vitro* biocompatibility of Mg AZ31 alloy by both direct and indirect methods. The results demonstrated that the CyQUANT assay provides a more complete assessment of the overall *in vitro* biocompatibility of biodegradable metals by combining both direct and indirect analyses.

In the second project, a multilayer coating consisting of a sol-gel silica layer followed by a mesoporous silica layer and finally a layer of calcium phosphate was developed. Surface characterization showed that a uniform and stable multilayer coating was successfully deposited on the Mg AZ31 alloy. *In vitro* characterization of the coatings confirmed this surface modification strategy significantly decreases the degradation rate of the magnesium alloy and that it is not cytotoxic.

Superhydrophobic surfaces decrease the corrosion rate of magnesium alloys, however, cell adhesion is inhibited. In the third project, a superhydrophobic magnesium alloy surface was modified with the cell adhesive molecule, MAPTrix-F-RGD and the influence of this surface

modification on cell adhesion was studied. The results demonstrate that although the MAPTrix-F-RGD molecule was successfully immobilized to the superhydrophobic magnesium alloy surface, cell adhesion was not improved. The complex surface topography of the superhydrophobic Mg AZ31 surface may be responsible for the observed cell behavior.

This thesis demonstrates that surface modification can be used to simultaneously control both the biodegradation rate and the biocompatibility of magnesium and its alloys, making these materials promising candidates for orthopaedic applications. In addition, it has been demonstrated that cell quantification assays based on the fluorescence of cyanine dyes are an excellent method for *in vitro* testing of these materials in direct contact with cells.

Keywords

Magnesium alloys, biodegradation, biocompatibility, surface modification, mesoporous silica, calcium phosphate, direct method, indirect method, CyQUANT assay, cell adhesion, cytotoxicity, superhydrophobic surface, fibronectin mimetic

Acknowledgments

I would first and foremost like to thank my supervisor Dr. Joy Gray-Munro for giving me the opportunity to study in her lab and for her support throughout my thesis as well as her patience, knowledge, and advice which allowed me to develop an understanding of this study. I would like to extend my thanks to my committee members Dr. Eric Gauthier and Dr. Louis Mercier for their time, support throughout my study and for reviewing my thesis. I would like to thank Dr. Eric Gauthier for giving me the opportunity to do the cell experiments in his lab under his supervision. I would like to thank all of my lab mates, past and present, especially Justin Campbell and Ryan Smith.

I would also like to share the accomplishment of this thesis with my Mother Salama Shibib for her encouragement and patience when it was most needed and a special thank you to my wonderful husband Habib Alkhames for his support and standing by my side throughout this entire journey. I would like to thank my kids (Mortaza, Amna, and Fatemah) for their patience and cooperation during my extended stay away from home during all my studies. I am extremely thankful to my loving and supportive sisters, brothers, all family members and friends for their continuous encouragement in completing my Ph.D.

Finally, I would like to thank Laurentian University for providing the opportunity to study and do the research in an excellent setting and I would like to acknowledge the financial support provided by the Ministry of Education in the Kingdom of Saudi Arabia.

Table of Contents

List of Tables

List of Figures

List of Reaction Schemes

List of Schematic Diagrams

List of Abbreviations

Mg AZ31	Magnesium Alloy containing 96 % Magnesium, 3% Aluminum, 1% Zinc
SBF	Simulated Body Fluid
ECM	Extracellular Matrix
HA	Hydroxyapatite
DCPD	Dicalcium Phosphate Dihydrate
FHA	Fluoridated Hydroxyapatite
ISO	International Organization for Standardization
BCS	Bovine Calf Serum
PBS	Phosphate Buffered Saline
C_{12}TAC	Dodecyltrimethylammonium Chloride
TEOS	Tetraethoxysilane
PDMS	Polydimethylsiloxane
MPTS	3-mercaptopropyltrimethoxysilane
RGD	Arginylglycylaspartic Amino Acid Sequence
MAP	Mussel Adhesive Proteins
DOPA	3,4-dihdryoxyphenylalanine
ATR-FTIR	Attenuated Total Reflectance-Fourier Transform Infrared Spectroscopy
FAA	Flame Atomic Absorption
SEM-EDS	Scanning Electron Microscopy-Energy Dispersive Spectroscopy
AFM	Atomic Force Microscope
IUPAC	International Union of Pure and Applied Chemistry
K_{sp}	Solubility product constant

List of Appendices

Chapter 1

1 Introduction

State-of-the-art orthopaedic surgical treatments depend greatly on the development of biomaterials used for the fixation of fractures and joint replacements. Biomaterials are artificial materials used in medical applications for the replacement and treatment of diseased or injured tissue in different parts of the body; some examples include cardiovascular, dental and orthopaedic implants [1]. Biomaterials provide a significant improvement to the health and well-being of humans. The human body may be subjected to various painful injuries such as strains, sprains, dislocations and fractures. Fractures are a break in the bone due to excessive external forces acting on the bone that are greater than the strength of the osseous tissue. The risk of fracture is highly dependent on age, gender, bone strength and the overall health of an individual [2].

Every year, millions of people suffer from bone fractures and degenerative joint diseases. The type of treatment required depends on the level of damage. In the case of degenerative joint diseases, bone replacement is typically needed. These permanent implants, such as artificial hips and knees, replace damaged tissue and therefore have to remain intact in the body. For this reason, they are most often manufactured from inert materials such as titanium, titanium alloys and cobalt-chrome alloys. In the case of fracture fixation, metallic pins, screws and plates may be surgically implanted to provide external support for the damaged bone tissue while it heals. This type of orthopaedic implant is meant to provide temporary support to prevent the treated bone from moving during the healing process [3].

The most commonly used materials for bone fracture fixation are typically metals such as stainless steel and titanium alloys. These materials were chosen due to their flexibility, high strength and excellent corrosion resistance [4]. However, a second surgery is needed to remove these temporary implants after tissue healing. This leads to potential re-damaging of the healed bone, discomfort for the patient and a significant cost to the health care system. An ideal temporary orthopaedic implant would provide the necessary mechanical strength during the initial stages after implantation but would gradually degrade and be replaced by new bone tissue as the patient healed. This would eliminate the need for a second surgery. Furthermore, the implant should produce non-toxic degradation products and degrade slowly enough that the implant maintains its mechanical strength until the bone tissue has healed sufficiently to provide load-bearing support [5].

1.1 Biodegradable Orthopaedic Biomaterials

New biodegradable implants for fracture fixation may provide significant advantages compared to the permanent implants currently used by orthopaedic surgeons. As mentioned previously, the use of biodegradable materials for fracture fixation would eliminate the need of removal surgery. Instead, these implants would be dissolved, absorbed, or excreted in the biological media to allow the surrounding tissue to proliferate and integrate with the implant and finally replace it. However, these materials need to maintain their mechanical properties until the implant is no longer needed for support [6].

Various materials have already been identified as biodegradable biomaterials and most of them are polymers. However, biodegradable polymers do not stimulate bone regeneration and

their mechanical properties are different from natural bone; thus, they do not provide enough support to the damaged bone [4]. Therefore, metallic material are more suitable for load-bearing applications compared with polymeric materials due to their high mechanical strength and fracture toughness [6]. In recent years, biomaterials scientists have proposed biodegradable metallic implants composed of chemically reactive metals such as iron and magnesium.

1.2 Magnesium as a Metallic Biodegradable Orthopaedic Biomaterial

The first clinical report of magnesium as an implant material was by the physician Edward C. Huse in 1878 [7]. He successfully stopped bleeding in vessels on several patients by using magnesium wire as a ligature. Other early reports, proposed the use of magnesium and its alloys for a variety of potential medical applications including magnesium plates, wires and tubes [7]. However, the high degradation rate of these early magnesium materials was a major drawback to their use in orthopaedics. Therefore, many physicians preferred to use other metallic materials with high corrosion resistance such as stainless-steel alloys and titanium alloys since the problem of controlling the corrosion of magnesium had not been appropriately solved. Consequently, despite its potential, research on the use of magnesium as a biomaterial was temporarily abandoned [7,8]. In the last two decades, research in this area has been reinvigorated due the development of better magnesium alloys and its unique properties as a biodegradable biomaterial. Among these unique properties is the biodegradability through anodic dissolution that results in the release of non-toxic magnesium ions that can be easily excreted in the urine [9]. In other words, magnesium implants can be gradually absorbed and the degradation products readily excreted by the body [10]. In addition to its biodegradability in the human body, these

materials have mechanical properties that are similar to natural bone making them a promising alternative to stainless steel and titanium alloys.

1.3 Biocompatibility of Magnesium in the Human Body

The biocompatibility of a material is an important key factor for successful implantation. The term biocompatibility has been defined by Williams as "The ability of a material to perform with an appropriate host response in a specific application" [11]. It means that the material should be compatible with the living tissue; it should be non-toxic and should not cause any immunological rejection.

Biocompatibility of metallic biomaterials is usually affected by corrosion processes in the human body. In metallic biomaterials, toxic metal ions (nickel, chromium, cobalt, etc.) are released in the body from corrosion and may lead to undesirable immune responses such as inflammation, cell apoptosis and other damaging tissue reactions. It was reported that exceeding the concentration limit of Cr (Co–Cr alloys), Nb, V and Ni (Ti-based) ions in the surrounding tissue or the body fluid may cause harmful tissue reaction. For example, Ni is an extremely cytotoxic, genotoxic, carcinogenic and mutagenic element [4]. Thus, these metallic implants do not have optimum biocompatibility.

Magnesium differs from other metallic biomaterials by having excellent biocompatibility. In fact, magnesium is the fourth most abundant inorganic element in the human body. The average adult human body weighs around 70 kg and contains approximately 21-28 g of magnesium [12]; 50 percent of this total body magnesium is stored in the skeletal system. To maintain appropriate magnesium levels in the body, humans need to absorb between 300 to 400

mg of magnesium daily [12,13]. Moreover, magnesium is also essential to human metabolic functions such as DNA/RNA stabilization and it acts as a co-factor for more than 300 different enzymatic reactions [13].

Magnesium influences many biological functions within the body and plays a very important role within the cell [13]. A number of studies demonstrate that divalent cations such as Mg^{2+} play a critical role in the remodeling and formation of bone tissue [4]. In addition, magnesium is one of the most important ions in the formation of the biological mineral phase, hydroxyapatite, on the surface of an implanted device. Some studies have reported that calcium phosphate can be formed on the surface of magnesium alloys exposed to both *in vitro* and *in vivo* environments [14]. This layer of calcium phosphate can form in direct contact with the surrounding tissue *in vivo* and can improve both the corrosion rate and the biocompatibility of magnesium in physiological solutions.

Moreover, it was reported that the presence of magnesium on orthopaedic implants could enhance osteoblastic cell adhesion and promote ideal osteogenesis. An *in vitro* study by Pietak et al. has shown that magnesium-based substrates can promote bone cell attachment on the implant surface [15]. Another article by Li et al. has shown that Mg-1Ca alloy did not induce toxicity to cells and had high activity of osteoblast and osteocytes around the alloy in an *in vivo* experiment [16].

1.4 Physical and Mechanical Properties of Magnesium in Comparison to Natural Bone

Materials used in orthopaedic applications should have very similar mechanical properties as natural bone. Metallic materials play an important role as biomaterials to assist with the repair of bone tissue that has been damaged or diseased. Commonly implanted metallic biomaterials include stainless steel, titanium and cobalt-chromium-based alloys [4]. However, most of the metallic biomaterials show significantly higher mechanical properties in comparison to natural bone. Biodegradable implants with the highest mechanical properties do not represent the best performance for orthopaedic application as this mismatch results in implant failure due to the stress shielding effect [17]. The stress shielding effect is the reduction in the density of bone tissue due to the removal of the normal stress on the bone after implantation. The bone in a healthy person will remodel in response to an applied load. Therefore, the bone will become weaker if the loading on bone decreases due to the difference in the stiffness between natural bone tissue and the implant material [18]. For example, a huge difference in elastic moduli between these metallic materials and natural bone causes the stress shielding effect. Therefore, a metallic biomaterial with lower elastic modulus is desired to effectively reduce the stress shielding effect and thereby improve bone remodeling.

Magnesium has physical and mechanical properties that are more similar to natural bone than traditional metallic implant materials. A brief summary is given in Table 1.1 which shows that the density of pure magnesium is approximately 1.74 g/cm^3, it is 2.5 times less dense than Ti alloy and 4.5 times less dense than steel making it the structural metal with a density closest to

that of human bone tissue (1.8 g/cm^3). The elastic modulus and compressive yield strength of magnesium are also the same order of magnitude as that of natural bone (Table 1.1) [6]. These similarities to natural bone should help in reducing or avoiding the stress shielding effect thus enhancing stimulation and remodeling of the bone tissue. Therefore, these mechanical properties contribute to making magnesium an ideal biomaterial for fracture fixation devices that provide good mechanical stability in the early stages of healing.

Table 1.1: Summary of the Physical and Mechanical Properties of Metallic Materials in Comparison to Natural Bone [6].

Properties	Natural bone	Pure magnesium	Ti alloy	Co-Cr alloy	Stainless steel
Density (g/cm^3)	1.8-2.1	1.74-2.0	4.4-4.5	8.3-9.2	7.9-8.1
Elastic modulus (GPa)	3-20	41-45	110–117	230	189-205
Compressive yield strength (MPa)	130-180	65-100	758-1117	450-1000	170-310
Fracture toughness (MPa/m$^{1/2}$)	3-6	15-40	55-115	N/A	50-200

1.5 Challenges for Using Magnesium as a Biodegradable Implant

The performance conditions of an ideal biodegradable magnesium-based material for orthopaedic applications should properly match the injured tissue reconstruction and healing

process to provide temporary mechanical support and then completely dissolve in the human body with an appropriate degradation rate. For a biodegradable material, as the degradation proceeds, the degeneration of mechanical integrity of the implant is expected [19]. This is illustrated in the Schematic Diagram (1.1) that shows the biodegradation and mechanical integrity of an ideal biodegradable implant during bone healing process. In general, the healing process of bone fracture occurs in three stages: inflammation, repair and remodelling [4,19]. The first stage of healing is inflammation when the immune system responds to the foreign body, this stage lasting for 1 to 7 days. In the repair stage, the implant integrates with new bone tissue as regeneration of tissue occurs over a period of 3-4 months depending on the fracture position and type. Finally, the remodelling stage is the longest in the healing process of the bone fracture. It involves regeneration and remodelling of the new bone by replacing the woven bone by cortical bone. This stage takes several months to years to be completed [19,20]. Unfortunately, most of the magnesium based orthopaedic implants degrade prior to complete healing causing implant failure.

Studies have shown that magnesium is highly degradable in both acidic solution and at the neutral pH conditions typically observed in the physiological environment [21]. Therefore, the high degradation rate of magnesium in the human body not only impacts the tissue healing process but can also lead to the loss of the mechanical integrity of the material implant causing the occurrence of a second fracture. As magnesium and its alloys have received much attention for biodegradable orthopaedic applications, several biodegradable Mg alloys have been developed but most of them are inadequate for medical implants due to a rapid degradation rate

and loss of mechanical integrity before the surrounding tissue has sufficiently healed. Magnesium alloy implants should maintain their mechanical properties for at least three months while the bone tissue healing occurs [20]. Therefore, it is important to control the degradation of magnesium implants after implantation into the human body as the rate of magnesium degradation is normally too fast in the initial stage.

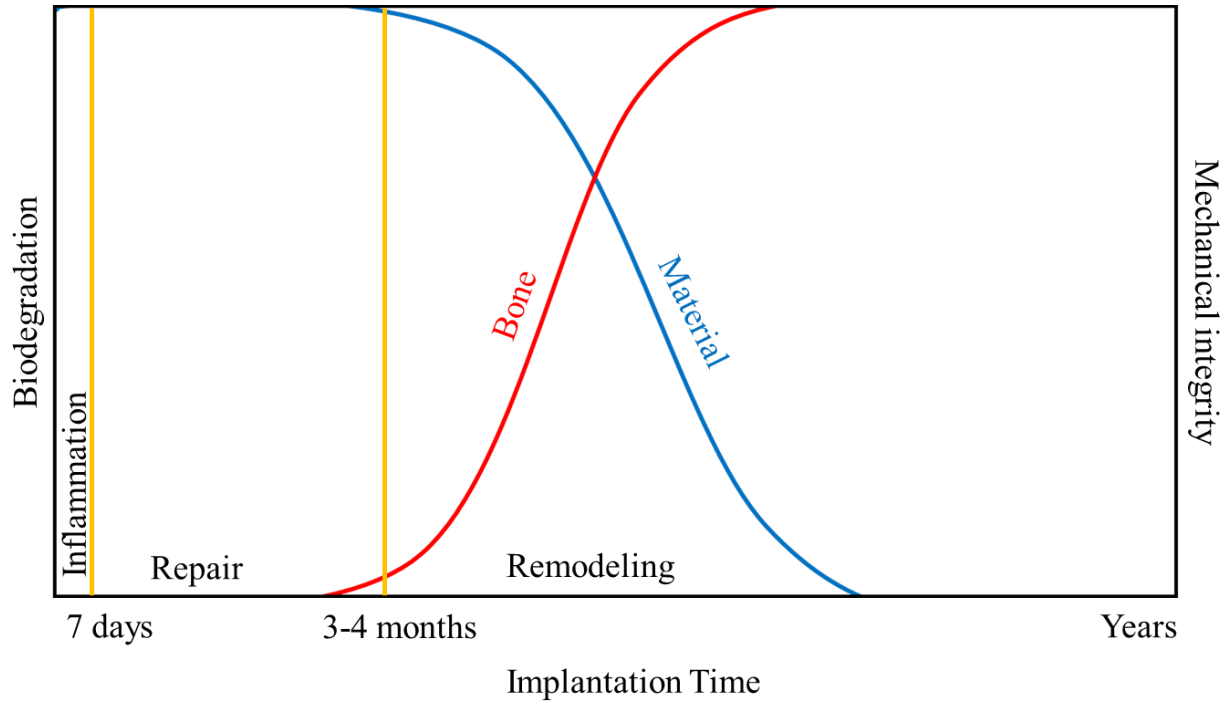

Schematic Diagram 1.1: The Schematic Diagram of the Biodegradation and Mechanical Integrity of Ideal Biodegradable Implants During the Bone Healing Process. Adapted from [19].

1.6 Degradation Process of Magnesium

The mechanism of degradation of metallic biomaterials occurs through corrosion of the materials by reaction with its environment under the influence of chemical, physical and electrochemical factors. The overall corrosion process of metallic materials involves electrochemical reactions to produce oxides, hydroxides and hydrogen gas. The rapid corrosion rate of magnesium in the physiological environment is the major problem that has limited the widespread use of magnesium alloys as biomaterials.

In aqueous solution, the corrosion reaction of pure magnesium proceeds by an electrochemical reaction with water as shown in Reaction Scheme 1.1. This reaction involves the anodic dissolution of magnesium and cathodic reduction of water. The products of this reaction are hydrogen gas, magnesium ions and hydroxide ions, leading to an increase in pH and ionic strength of the surrounding solution. These electrochemical reactions result in the formation of a magnesium hydroxide layer on the surface of magnesium that acts as a barrier layer between the magnesium substrate and the aqueous solution slowing the electrochemical reaction across the magnesium surface.

Reaction Scheme 1.1: General Corrosion Mechanism of Magnesium.

Anodic reaction: $Mg_{(s)} \rightarrow Mg^{2+}{}_{(aq)} + 2e^-$

Cathodic reaction: $2H_2O_{(l)} + 2e^- \rightarrow 2OH^-_{(aq)} + H_{2\,(g)}$

Product formation: $Mg^{2+}{}_{(aq)} + 2OH^-_{(aq)} \rightarrow Mg(OH)_{2\,(s)}$

Overall reaction: $Mg_{(s)} + 2H_2O_{(l)} \rightarrow Mg(OH)_{2\,(s)} + H_{2\,(g)}$

However, the physiological solution is a highly corrosive environment for magnesium and its alloys due to the presence of dissolved oxygen, proteins and electrolyte ions such as chloride [8,19]. These conditions play an important role in the accelerated corrosion of magnesium in body fluids. In the physiological environment, chloride ions react with the passive magnesium hydroxide layer leading to the formation of highly soluble magnesium chloride layer according to Reaction Scheme 1.2. Therefore, the underlying magnesium substrate is continually exposed to the corrosive media resulting in the occurrence of pitting corrosion of the magnesium substrate. Moreover, the corrosion in body fluids is influenced by various factors including pH, concentration and the types of ions, protein adsorption on orthopaedic biomaterials and influence of the biochemical reactions of surrounding tissues [4].

Reaction Scheme 1.2: Influence of Anions.

$$Mg(OH)_{2\,(s)} + 2Cl^-_{\,(aq)} \rightarrow MgCl_{2\,(aq)} + 2OH^-_{\,(aq)}$$

1.7 Types of Corrosion

There are two primary types of corrosion that can affect magnesium and its alloys in the physiological environment including pitting corrosion and galvanic corrosion.

1.7.1 Pitting Corrosion

Pitting corrosion is usually observed in the physiological environment due to the presence of aggressive ions such as chloride ions. Pitting is a type of localised corrosion associated with the breakdown of the hydroxide passivation layer in a corrosive environment. It is a serious type of corrosion, since the surface pits are difficult to detect due to the formation of corrosion

product [4]. After the pitting begins, magnesium materials can be corroded in a very short period of time resulting in reduction of the load bearing capacity in the case of orthopaedic applications [4,20]. Moreover, pitting corrosion increases the localised stress that may lead to the formation of cracks. The presence of stress corrosion cracking (SCC) and metal fatigue cracks in the pits can lead to an implant failure [4].

1.7.2 Galvanic Corrosion

Galvanic corrosion occurs when two dissimilar metals come in contact with each other in the same electrolyte and is due to the difference in electrochemical potential between these metals. Thus, the less noble metal acts as an anode which corrodes rapidly and produces by-products in the surrounding area [4,17].

Galvanic corrosion is the primary issue for magnesium and its alloys in orthopaedic applications due to the presence of different alloying elements and phases [17]. Magnesium is a highly active metal and always acts as an anode when it comes in contact with other metals (cathode) resulting in galvanic corrosion. Consequently, Mg and its alloys rapidly corrode. In addition, galvanic corrosion can result from the presence of impurities or intermetallic elements in the Mg matrix [4,20].

1.8 Biodegradation Process on Biocompatibility of Magnesium and Cell Responses

As it was discussed in the previous section, biocompatible material should not cause cell death, chronic inflammation or damage any cellular or tissue functions. Biodegradable

orthopaedic implants not only have to be biosafe in terms of cytotoxicity, they also need to have appropriate biodegradation rates and successful integration within the bone by interaction with the living tissue to guarantee the biocompatibility of the implant.

Osteoconduction and osseointegration are important factors for the biocompatibility of orthopaedic materials in the human body. Osteoconduction and osseointegration of the bone both depend on the response to a foreign material [22]. Osteoconduction is the process by which bone cells grow on the surface of the orthopaedic implant. Osseointegration is the stability of an implant achieved by a direct contact between living bone and implant without the growth of fibrous tissue at the bone-implant interface. Osseointegration of the implant depends on osteoconduction. If a material is too toxic to allow bone cell attachment on the surface, meaning that the material is not osteoconductive, it will not osseointegrate leading to the long-term poor performance of the implant long term [22].

Bone tissue is formed of four different types of cells: osteoblasts, osteocytes, bone lining cells and osteoclasts. Osteoblasts are located on the bone surface and contribute to bone formation and mineralization. Therefore, biocompatibility of magnesium is dependent on the behaviour of osteoblasts and their adhesion and proliferation on the implant surface [23].

To date, many studies have investigated the effect of magnesium on bone formation. It has been shown that magnesium has a significant effect on osteoblastic cell differentiation which indicated its effect on the acceleration of bone healing [17]. The biodegradation of magnesium implants in the human body led to the release of Mg^{2+} ions to surrounding tissue which resulted in stimulation of the local cells to form bone [17]. However, the rapid degradation of Mg alloy

implants leads to the release of high concentrations of Mg^{2+}, OH^{-}, H_2 and ions of alloying elements that negatively affect the cell viability and, therefore, its biocompatibility [8]. Although previous studies demonstrated that the hydrogen gas can be tolerated by human body, high amounts of hydrogen gas production within the implant environment and an increase in the local pH both have significant effects on the surrounding tissues [8,17]. Consequently, it can result in complications in the healing process.

Therefore, it is essential to increase the corrosion resistance to extend the lifetime of magnesium in the human body, giving the body enough time to deal with the biodegradation products and maintain its mechanical integrity until healing occurs. In addition, improving the biocompatibility of the magnesium surface can be considered to accelerate the healing process and regenerate new bone tissue around the magnesium implant.

1.9 Improving the Performance of Magnesium for Orthopaedic Application

The definition of biodegradable metals was given for the first time by Zheng and colleagues in 2014 as “Biodegradable metals (BMs) are metals expected to corrode gradually *in vivo*, with an appropriate host response elicited by released corrosion products, then dissolve completely upon fulfilling the mission to assist with tissue healing with no implant residues” [19]. This means the major metals used in the composition of biodegradable biomaterials should be absorbed by the human body and demonstrate appropriate degradation rates in the human body matching the bone healing process. Thus, it is essential to increase the corrosion resistance to maintain its mechanical properties and enhance the biocompatibility to ensure the

osteointegration and osteoconduction of the implant and, therefore, regeneration of new bone before degradation.

In spite of the advantageous properties that magnesium metal exhibits, the commercially available pure metal cannot provide either the appropriate mechanical properties or corrosion resistance for orthopaedic application. There are currently a number of strategies that have been investigated to obtain suitable degradation rates and provide appropriate mechanical properties, as well as improve the biocompatibility and the osteointegration potential of magnesium for orthopaedic biomaterials. Some of these strategies include using high purity alloys, addition of new alloying elements, surface modification and deposition of protective coatings.

1.10 Alloying

Magnesium alloys are of a particular interest for many applications since they have enhanced mechanical properties and corrosion resistance in comparison to the unalloyed metal [24]. An alloy is a mixture of metals or a mixture of a metal and other elements. Alloys of Mg can be binary, ternary or more [6]. It is essential to choose an appropriate element which can enhance mechanical properties and corrosion resistance but is also non-toxic to guarantee the biocompatibility of the implant. Therefore, biomaterial scientists recently focussed on investigating biologically safe magnesium alloys containing non-toxic elements such as Ca, Zr, Zn, Mn, Sr, Li, Sn, Si, Bi, Cd, Ag [6,25]. The composition of various magnesium alloys is given in table 1.2.

Table 1.2: Composition of Various Magnesium Alloys

Magnesium alloy	Nominal Composition (weight %)
Mg AZ31	3% Aluminium, 1 % Zinc, Balance Magnesium
Mg AZ61	6% Aluminum, 1% Zinc, Balance Magnesium
Mg AZ91	9% Aluminum, 1% Zinc, Balance Magnesium
Mg ZK40	4% Zinc, less than 1% Zirconium, Balance Magnesium
Mg-6Zn-1Ca	6% Zinc, 1% Calcium, Balance Magnesium
Mg-0.5Ca	0.5% Calcium, Balance Magnesium
Mg-1Ca	1% Calcium, Balance Magnesium

For instance, Ca is a well-known alloying element for accelerating bone growth and improving corrosion resistance [17,26,27]. Li et al. developed binary Mg-Ca alloys with different amount of Ca. Alloys of high Ca content were shown to be very brittle which was detrimental for their mechanical properties. However, alloys with low content (1 wt% of Ca) showed a slow degradation rate *in vitro* and *in vivo*. Also, the study indicated that Mg-1Ca alloys were not cytotoxic to cells. This study indicated that the mechanical properties and biocorrosion resistance of Mg-Ca alloys are adjustable by controlling Ca content [27]. Another study by Rad et al. suggested Mg-0.5Ca alloy as a great candidate for biodegradable implants due to its high corrosion resistance [28]. Sr is also considered one of the promising biocompatible alloying

elements in magnesium alloys. Studies showed that Sr significantly enhances the osteoblastic activity and bone formation *in vivo*, which improves its biocompatibility [17,27,29]. Li et al. studied the biodegradation of Mg-Zr-Sr alloys *in vitro* and *in vivo*. The study demonstrated that addition of less than 2% Sr significantly decreased the corrosion rate for Mg-Zr-Sr and Mg-Sr alloys; an improvement in biocompatibility was also observed [29].

Zn is one of the common alloying elements for magnesium. The presence of zinc in magnesium alloys can increase the tolerance limits and reduce the effect of impurities. Also, it increases strength without decreasing flexibility [6,17]. Studies showed that the presence of 6% Zn in magnesium alloys decreases the corrosion rate of the material [30]. In addition to improving the mechanical properties and the corrosion resistance of magnesium, it was also demonstrated that the presence of Zn in magnesium alloys enhances osteoblastic cell proliferation. A study by Hong et al. further indicated that ZK40-Mg and AZ31-Mg alloys enhance cell proliferation compared to pure Mg [31].

Aluminum is often used as an alloying element for magnesium to enhance the corrosion resistance. The corrosion rate of magnesium alloys decreases rapidly with increasing aluminum content due to a decrease in the impurity level with increasing Al content and the formation of the more noble β-phase acts as a barrier to the progression of the corrosion attack [32]. However, the presence of high concentrations of aluminum can be considered toxic for humans. Therefore, it is highly recommended to use aluminum with low concentrations in biomaterial applications. Even though the biocompatibility of aluminum is limited, it seems to be an acceptable alloying element for magnesium in the human body [17]. An *in vivo* study performed by Witte et al.

indicated that alloyed Mg with different concentrations of Al did not show any cytotoxic or neurotoxic effects up to 9 wt% of Al and the osteoblastic activity around the implant was increased with increasing amount of Al up to 9 wt%. Therefore, the small amount of Al ions that are released during the degradation of magnesium can be tolerated by the human body [33].

AZ31, AZ61, and AZ91 are common Mg-Al-Zn alloys with reasonable corrosion rates. Huang et al investigated the *in vivo* degradation behavior of a Mg-Al-Zn (AZ31) alloy implanted into rabbits. After a nine-week period, formation of a thin layer of calcium phosphate was shown around the implants and the *in vivo* degradation rate of Al-Zn containing Mg alloys was slower than that of pure Mg [34]. AZ31 is the alloy that was used in this project, A and Z correspond to aluminum and zinc, which are present in the alloy with concentrations of 3 % and 1 % by mass respectively. This alloy has a good combination of suitable mechanical properties, corrosion resistance and low concentration of aluminum.

1.11 Surface Modification

Despite of the possible alloying process of magnesium to improve its degradation rate and mechanical properties, magnesium alloys may remain very reactive in physiological environments. Thus, surface modification is an additional way to provide an optimum biodegradable orthopaedic implant. Surface modification is one of the most effective ways to simultaneously control the biodegradation rate and improve the surface biocompatibility of magnesium alloys.

To fully understand the impact of surface modification, it is very important to have a good knowledge of the influence of surface characteristic on the orthopaedic implants and their cell responses.

1.11.1.1 Surface Characteristics

Orthopaedic implants not only have to be non-toxic and stable in terms of cytotoxicity and degradation, they also have to match the structure of bone to enhance the interaction between the implant surface and the living tissue.

The hierarchical structure of human bone should be highly considered in orthopaedic biomaterial designs to successfully replace tissue in the bone. Human compact bone is a composite natural material with macro to nano scale features in a hierarchical structure [35]. Therefore, to achieve a high grade of compatibility with host tissue, this range of scale should be taken into account.

Understanding surface characteristic of the implants is key in order to achieve excellent biocompatibility of the orthopaedic biomaterial with the host tissue. Moreover, the biomaterial surface is a major factor influencing the success or failure of the implantation process due to the direct contact of the implant surface and the host tissue.

1.11.1.2 Surface Roughness

Surface roughness is a significant factor for the osseointegration rate and biomechanical fixation of orthopaedic implant to bone [35]. Several studies have shown that increasing the surface roughness at the micro-scale range improves the rate of new bone formation as a result of

an increase in protein adsorption and cellular activity [17,35]. Zareidoost et al. studied the relationship of implant surface roughness and cell response and established that osteoblastic cell adhesion and proliferation are correlated to surface roughness. It was found that the cell viability and proliferation on rough surfaces etched with HCl-HF-H_3PO_4 was higher than on the polished surfaces [36].

In particular, in a study of magnesium alloys, a significant increase in bone cell adhesion was observed by increasing the surface roughness of a magnesium alloy from 3.40 nm to 23.40 nm through deposition of a rough and dense layer of HA/TiO_2 composite coating on magnesium alloys [37].

Thus, mimicking the bone surface with a combination of macro, micro and nano scale roughness on the implant surface may enhance osseointegration of the implant due to an increase in hydroxyapatite deposition and cellular activity. Various methods are employed to create such microstructural surface features including blasting, acid-etching, anodization and plasma-spraying [35].

1.11.1.3 Porous Structure

Pore size and morphology have a considerable impact on cell attachment and proliferation. It was demonstrated that the size and structure of the pore play a very important role in designing orthopaedic implants [17]. Studies have shown that pores with a hexagonal structure increase cell attachment more than the pores with spherical structure. However, it was found that the mechanical properties of implants decrease with increasing the pore size resulting in brittle behavior [38].

Due to the influence of porous structures on mechanical properties, a significant concern for orthopaedic applications, porous materials have been proposed as a coating on implant surfaces to improve the cell attachment and proliferation resulting in successful osseointegration of the orthopaedic implant [39,40,41]. Moreover, porous surface implants have been effectively used as a drug delivery coating by incorporation of drugs into the pores [42-43].

1.11.1.4 Wettability

Wettability (hydrophobicity/hydrophilicity) is one of the parameters affecting the biological response of the biomaterial. In general, wettability can be influenced by four primary surface characteristics: roughness, chemical composition, surface energy, and heterogeneity. The surface wettability of biomaterials can be controlled by surface modification techniques, such as ion implantation, surface coating, chemical etching, and laser surface modification techniques [44].

Hydrophilic surfaces typically enhance cell adhesion on the implant surface [45]. A study by Lim et al. detected the effect of the surface wettability of biomaterials on the osteoblast response by producing model substrates with various water contact angles ranging from 0^{o} to 120^{o}. They observed that human osteoblastic cells showed a strong positive correlation in cell adhesion and proliferation with biomaterial surface wettability. The osteoblastic cells exhibited greater adhesion and proliferation on hydrophilic surfaces than on hydrophobic surfaces [46].

1.11.2 Type of Surface Modification

Surface modification is primarily employed to controlling the degradation rate of magnesium alloys to maintain their mechanical properties and also to improve the surface biocompatibility of magnesium alloys for orthopaedic applications. These surface modification methods have been classified by Wang et al. into three types: chemical modification, physical modification, or a combination of these two methods [47,48].

In recent years, researchers have focused on the combination of both chemical and physical modification. Generally, chemical modification is used as a pre-treatment to the physical process to improve adhesion. These double modifications on the substrate surface are more effective in improving the biodegradation resistance of substrates [47].

1.11.2.1 Chemical Modification

This type of modification is associated with the removal of the native oxide layer and its replacement with a new phase on the surface. The main advantage of this new phase is its improved adhesion to the substrate due to chemical bonding. Chemical surface modifications include: acid etching, alkaline treatment, fluoride treatment, anodization, and ion implantation [48].

1.11.2.1.1 Acid Etching

Acid etching could be adopted to remove the native oxide layer followed by creating uniform and compact layers leading to a lower degradation rate [47]. Gray-Munro et al. investigated the effect of acid etching as a pre-treatment on the degradation rate of the AZ31

magnesium alloy in SBF solutions. The magnesium alloys were immersed in a 90% (v/v) phosphoric acid solution at 55°C for 30 s, then neutralized in 100 g/L NaOH solution for 30 s. More homogenous and dense films of $Mg_3(PO_4)_2$ layers were produced on the top of etched magnesium alloys compared with the unetched alloys leading to a significant decrease on the overall degradation rate in SBF (Simulated Body Fluids) [49].

1.11.2.1.2 Alkaline Treatment

A new passive layer is deposited on the surface of magnesium alloys after soaking in alkaline solutions leading to the formation of passive layer consisting of $Mg(OH)_2$, $MgCO_3$, and MgO [48]. It has been reported that an alkaline treatment by soaking the samples in 1 M NaOH has a significant effect on improving the degradation rate of magnesium due to the creation of a passive layer on the substrate surface [50-51]. Another study by Gu et al. investigated the influence of an alkaline heat-treatment on Mg-Ca alloy for controlling the biodegradation rate. The magnesium alloys were soaked in three different alkaline solutions (Na_2HPO_4, Na_2CO_3 and $NaHCO_3$) for 24 h, and subsequently heat treated at 773 K for 12 h. The results indicated that the degradation rate of alkaline heat-treated Mg-Ca alloy in SBF were significantly decreased in comparison to the untreated alloy. Also, the cytotoxicity evaluation demonstrated that none of the alkaline heat-treated Mg-Ca alloys were cytotoxic to L-929 cells [52].

1.11.2.2 Physical Modification

Physical modification, also called physical coating can be employed by various strategies to create protective coatings on the Mg substrate. These types of coatings provide a physical

barrier between the metal and the corrosive environment. The deposition of a coating can also improve the biocompatibility and osteointegration of an implant [8,47,48]. Examples of physical surface modification include sol-gel processes, biomimetic methods (calcium phosphate and superhydrophobic coating) as well as multifunctional coatings.

1.11.2.2.1 Sol-gel Coating

The sol-gel process is an environmentally friendly method. It is one of the most popular methods to prepare a protective barrier coating. Sol-gel coatings have shown great chemical stability, oxidation control and improved corrosion resistance for different metal substrates such as aluminum, copper, steel, magnesium and their alloys. The sol-gel process has attracted a great deal of attention in the fields of ceramics, polymer chemistry, organic and inorganic chemistry and also plays an essential role in the production of novel organic-inorganic hybrid materials [53].

The sol-gel process involves the synthesis of an oxide network through reactions of the precursor solution in a liquid. The overall sol-gel process consists of two chemical reactions: the first is a hydrolysis reaction and the second is a condensation reaction. The hydrolysis reaction produces the sol, while the condensation reaction forms a gel on the substrate producing a thin film. The coating deposited through the sol-gel process is influenced by the initial reaction conditions such as pH, temperature, molar ratio of water to precursor solution and solvent composition. For instance, synthesis of the coating at high temperature leads to a porous, nanocrystalline coating with a controlled microstructure [4,19].

Hu et al. prepared a nano TiO_2 coating on AZ31 by the sol-gel method and investigated the relationship of the degradation rate of Mg alloy with the annealing temperature and time. The results indicated that the degradation rate increased with the annealing temperature higher than 350 °C as the size of nano-spherical TiO_2 particles of the coating increased and led to an increased degradation rate. On the other hand, the degradation rate was decreased gradually by the prolongation of the annealing time. It was concluded that the best improvement in degradation rate was obtained when the sol-gel coated samples were annealed at 250 °C for 3 h [54].

Organosilane coatings have also been employed as protective and biocompatible coatings on Mg alloy for orthopaedic applications. There are several advantages of using organosilanes as protective barrier coatings such as its hydrophobic Si-O-Si networks, lower galvanic reactions with Mg, greater adhesive ability, easy chemical modification and low cytotoxicity [4]. Gaur et al. developed a sol-gel silane coating on Mg alloy (Mg-6Zn-1Ca (wt%)) using a mixture of the silanes diethylphosphatoethyltriethoxysilane (DEPETES) and bis-[3-(triethoxysilyl)propyl] tetrasulfide (BTESPT) to improve the degradation rate of magnesium alloys. The *in vitro* biodegradation evaluation indicated that the silane-based sol-gel coating provided a significant decrease in degradation rate of the coated magnesium alloys as compared to the bare Mg alloy. The degradation protection of this coating was attributed to the formation of highly dense Si-O-Si networks [55].

1.11.2.2.2 Calcium Phosphate Coating

The orthopaedic implant should have a bioactive surface to bond directly with the bone tissue for successful osseointegration. Calcium phosphate coatings have been prepared on magnesium substrates with various techniques to deposit different types of calcium phosphate coatings including hydroxyapatite (HA), fluoridated hydroxyapatite (FHA), and brushite (DCPD). Calcium phosphate coating has been shown to improve both the bioactivity and the overall biocompatibility of implants [19].

Biomimetic calcium phosphate deposition is one of the most useful techniques investigated for coating the surface of orthopaedic implants. The biomimetic deposition technique is used to provide a bone-like apatite (calcium phosphate) on the surface of orthopaedic implants. Therefore, the surface becomes more bioactive resulting in improved osseointegration of the implant into the human bone [19,56]. The biomimetic process is based on simple chemical immersion techniques to produce calcium phosphate coatings on the substrate using different kinds of solutions such as SBF (Simulated Body Fluids). Cao et al. prepared a Ca-P coating on AZ31 Mg alloys using the biomimetic method by immersing Mg alloys into 1.5 times SBF (Simulated Body Fluids) at pH 7.4 and 37^{o}C. The corrosion resistance and cytocompatibility of the biomimetic calcium phosphate coating was investigated. The results showed that the corrosion resistance of the biomimetic Ca-P coating Mg alloys was significantly improved compared to uncoated magnesium alloys. Moreover, the biomimetic coating showed no cytotoxic effects to the cells. Furthermore, additional modification of this coating through the

immobilization of the RGDC peptide into the biomimetic coating resulted in a significant enhancement of cellular responses [56].

Additionally, calcium phosphate coatings have been widely prepared by electrodeposition techniques using the acidic $Ca(NO_3)_2$, $NH_4H_2PO_4$, and $NaNO_3$ electrolyte systems. Song et al. used an electrodeposition technique to develop three kinds of calcium phosphate coatings (brushite, hydroxyapatite and fluoridated hydroxyapatite). The degradation behavior and bioactivity of these coatings on magnesium alloys was investigated. The results showed that all these coatings decreased the degradation rate of Mg-Zn alloys compared to uncoated alloys. However, fluoridated hydroxyapatite (FHA) coating on magnesium alloy was more stable than the brushite DCPD and hydroxyapatite HA coatings as it remained intact after immersion in modified simulated body fluid (m-SBF) for one month. It was also shown that HA and FHA coatings improved the bioactivity and mineralization ability (formation of bone-like apatite layer) of a Mg-Zn alloy demonstrated by the higher Ca/P ratio of the precipitates compared to the DCPD coating [57].

1.11.2.2.3 Superhydrophobic Coating

The development of a superhydrophobic surface is one of the most recent strategies to improve the corrosion resistance of Mg alloys. In general, superhydrophobic surfaces are surfaces with high water contact angles greater than 150° and low sliding angles that are smaller than 5°. Superhydrophobic surfaces have been employed for many special functions such as anti-corrosion, self-cleaning, anti-bacterial, and water-repellent surfaces. Superhydrophobic surfaces can be obtained by various strategies such as wet chemical reaction, hydrothermal reaction,

electrochemical deposition, self-assembly, phase separation, electrospinning, sol-gel, and polymerization reactions [58].

The best-known natural example of a superhydrophobic surface comes from the lotus leaf. The superhydrophobicity of the lotus leaf can be mimicked on man-made surfaces. This is generally accomplished through a two-step surface modification: the first step is to form a surface with a micro/nanostructured roughness. A thin hydrophobic layer is then deposited leading to an overall superhydrophobic surface [58,59].

Zhang et al. fabricated a superhydrophobic surface on magnesium alloy AZ31 through combination of a hydrothermal treatment method to get the hierarchical rough structures and post modification with low energy stearic acid. This superhydrophobic surface had a water contact angle of 157.6°. The corrosion results in 3.5% NaCl showed that the superhydrophobic coatings significantly improved the corrosion resistance of the AZ31 alloy [59].

In addition to their excellent corrosion resistance, superhydrophobic surfaces has been used in biomedical applications as a surface to control protein adsorption, cellular interaction, and bacterial growth [60].

Although superhydrophobic surfaces decrease the rapid degradation of magnesium alloys, the interaction between the cells and the implants is also reduced leading to a decrease in the ability of the implant to induce bone regeneration thus limiting its biocompatibility. However, there are very limited studies carried out in this area. Therefore, novel strategies need to be designed to improve the cell adhesion and proliferation of the superhydrophobic surface for the development of biodegradable orthopaedic implants.

1.11.2.2.4 Multifunctional Coatings

To overcome the limitation of magnesium and its alloys for orthopaedic application, protective coatings can be used as a multifunctional implant coating that not only control the degradation rate of the implant but also offer improved biocompatibility. For example, barrier coatings loaded with bone growth factors to accelerate the healing process, or antibiotic drugs to prevent inflammation may be effective. The surface modification of barrier coatings through immobilization of biomolecules or cell adhesive ligands such as RGD surface may efficiently bio-mimic the natural extracellular matrix environment to enhance cell adhesion.

Luo et al. developed a polymer coating on pure magnesium loaded with an anti-inflammatory dexamethasone drug. The polymer coatings significantly improved the corrosion resistance of magnesium. In addition, the polymeric coating was successfully loaded with dexamethasone which may control the inflammatory tissue response to Mg implants during implantation. Therefore, using a polymer coating loaded with a drug can improve both the degradation rate and biocompatibility of magnesium [61].

Moreover, Yang et al. investigated the effect of covalent attachment of RGD peptides onto AZ31 magnesium alloy surfaces using mixed organosilane coatings to improve the corrosion resistance. This study demonstrated an increase in both cell adhesion and proliferation onto the magnesium alloys by immobilization of RGD peptides on the protective coating [62].

1.12 Conclusions

In this literature survey several strategies have been proposed for coating magnesium and its alloys in order to achieve the required improvements for successful implementation of these materials as a mainstream biomaterial. These various coating strategies have shown lowered corrosion rates as well as enhanced bioactivity and biocompatibility, making magnesium and its alloys promising candidates to be used as biodegradable biomaterials in orthopedic applications.

However, future studies are also recommended to design the optimal magnesium implant for a biomedical application. In order to design materials for orthopaedic applications, not only the degradation rate of magnesium must be controlled, but also the mechanical properties and biological behaviours such as cell attachment, cell proliferation and cytocompatibility must also be investigated.

References

1. Parida, P., A. Behera, and S. C. Mishra. "Classification of biomaterials used in Medicine." *International Journal of Advances in Applied Sciences* 1.3 (2012): 31-35.
2. Radha, R., and D. Sreekanth. "Insight of magnesium alloys and composites for orthopedic implant applications-a review." *Journal of Magnesium and Alloys* 5.3 (2017): 286-312.
3. Goodman, S.B., et al. "The future of biologic coatings for orthopaedic implants." *Biomaterials* 34.13 (2013): 3174-3183.
4. Agarwal, S., et al. "Biodegradable magnesium alloys for orthopaedic applications: A review on corrosion, biocompatibility and surface modifications." *Materials Science and Engineering: C* 68 (2016): 948-963.
5. Navarro, M., et al. "Biomaterials in orthopaedics." *Journal of the Royal Society Interface* 5.27 (2008): 1137-1158.
6. Kumar, K., R. S. Gill, and U. Batra. "Challenges and opportunities for biodegradable magnesium alloy implants." *Materials Technology* 33.2 (2018): 153-172.
7. Witte, F. "The history of biodegradable magnesium implants: a review." *Acta Biomaterialia* 6.5 (2010): 1680-1692.

8. Walker, J., et al. "Magnesium biomaterials for orthopedic application: a review from a biological perspective." *Journal of Biomedical Materials Research Part B: Applied Biomaterials* 102.6 (2014): 1316-1331.

9. Carboneras, M., M. C. García-Alonso, and M. L. Escudero. "Biodegradation kinetics of modified magnesium-based materials in cell culture medium." *Corrosion Science* 53.4 (2011): 1433-1439.

10. Xu, R., et al. "Controllable degradation of biomedical magnesium by chromium and oxygen dual ion implantation." *Materials Letters* 65.14 (2011): 2171-2173.

11. Hollinger, J. O., ed. *An introduction to biomaterials*. CRC Press, (2011).

12. Bogden, J. D., and M. Klevay, L. *Clinical nutrition of the essential trace elements and minerals: the guide for health professionals*. New Jersey: Humana Press (2000).

13. Gupta, M., and M.N.L Sharon. *Magnesium, magnesium alloys, and magnesium composites*. Hoboken, New Jersey: Wiley (2011).

14. Wang, Y., et al. "Corrosion process of pure magnesium in simulated body fluid." *Materials letters* 62.14 (2008): 2181-2184.

15. Pietak, A., et al. "Bone-like matrix formation on magnesium and magnesium alloys." *Journal of Materials Science: Materials in Medicine* 19.1 (2008): 407-415.

16. Li, Z., et al. "The development of binary Mg–Ca alloys for use as biodegradable materials within bone." *Biomaterials* 29.10 (2008): 1329-1344.

17. Sezer, N., et al. "Review of magnesium-based biomaterials and their applications." *Journal of Magnesium and Alloys* (2018): 23-43.

18. Ridzwan, M. I. Z., et al. "Problem of stress shielding and improvement to the hip implant designs: a review." *Journal of Medical Science* 7.3 (2007): 460-467.

19. Zheng, Y. F., et al. "Biodegradable metals." *Materials Science and Engineering: R: Reports* 77 (2014): 1-34.

20. Poinern, G.E., et al. "Biomedical magnesium alloys: a review of material properties, surface modifications and potential as a biodegradable orthopaedic implant." *American Journal of Biomedical Engineering* 2.6 (2012): 218-240.

21. Song, G. "Control of biodegradation of biocompatable magnesium alloys." *Corrosion Science* 49.4 (2007): 1696-1701.

22. Albrektsson, T., and C. Johansson. "Osteoinduction, osteoconduction and osseointegration." *European Spine Journal* 10.2 (2001): S96-S101.

23. Florencio-Silva, R., et al. "Biology of bone tissue: structure, function, and factors that influence bone cells." *BioMed Research International* 2015 (2015): 421746.

24. Gusieva, K., et al. "Corrosion of magnesium alloys: the role of alloying." *International Materials Reviews* 60.3 (2015): 169-194.

25. Li, L., et al. "Corrosion and biocompatibility improvement of magnesium-based alloys as bone implant materials: a review." *Regenerative Biomaterials* 4.2 (2017): 129-137.

26. Li, H. F., et al. "Development of biodegradable Zn-1X binary alloys with nutrient alloying elements Mg, Ca and Sr." *Scientific Reports* 5 (2015): 10719.

27. Li, Z., et al. "The development of binary Mg-Ca alloys for use as biodegradable materials within bone." *Biomaterials* 29.10 (2008): 1329-1344.

28. Rad, H.R.B., et al. "Microstructure analysis and corrosion behavior of biodegradable Mg–Ca implant alloys." *Materials & Design* 33 (2012): 88-97.

29. Li, Y., et al. "Mg-Zr-Sr alloys as biodegradable implant materials." *Acta Biomaterialia* 8.8 (2012): 3177-3188.

30. Zhang, S., et al. "Research on an Mg-Zn alloy as a degradable biomaterial." *Acta Biomaterialia* 6.2 (2010): 626-640.

31. Hong, D., et al. "In vitro degradation and cytotoxicity response of Mg-4% Zn–0.5% Zr (ZK40) alloy as a potential biodegradable material." *Acta Biomaterialia* 9.10 (2013): 8534-8547.

32. Pardo, A., et al. "Corrosion behaviour of magnesium/aluminium alloys in 3.5 wt.% NaCl." *Corrosion Science* 50.3 (2008): 823-834.

33. Witte, F., et al. "In vivo corrosion of four magnesium alloys and the associated bone response." *Biomaterials* 26.17 (2005): 3557-3563.

34. Huang, J., et al. "In vivo study of degradable magnesium and magnesium alloy as bone implant." *Frontiers of Materials Science in China* 1.4 (2007): 405-409.

35. Bauer, S., et al. "Engineering biocompatible implant surfaces: Part I: Materials and surfaces." *Progress in Materials Science* 58.3 (2013): 261-326.

36. Zareidoost, A., et al. "The relationship of surface roughness and cell response of chemical surface modification of titanium." *Journal of Materials Science: Materials in Medicine*23.6 (2012): 1479-1488.

37. Amaravathy, P., et al. "Bioactive HA/TiO2 coating on magnesium alloy for biomedical applications." *Ceramics International* 40.5 (2014): 6617-6630.

38. Lake, S. P., et al. "Pore size and pore shape–but not mesh density-alter the mechanical strength of tissue ingrowth and host tissue response to synthetic mesh materials in a porcine model of ventral hernia repair." *Journal of the Mechanical Behavior of Biomedical Materials* 42 (2015): 186-197.

39. Wang, X., et al. "Mesoporous bioactive glass coatings on stainless steel for enhanced cell activity, cytoskeletal organization and AsMg immobilization." *Journal of Materials Chemistry* 20.31 (2010): 6437-6445.

40. Gu, X. N., et al. "Corrosion resistance and surface biocompatibility of a microarc oxidation coating on a Mg-Ca alloy." *Acta Biomaterialia* 7.4 (2011): 1880-1889.

41. Inzunza, D., et al. "Synthesis of nanostructured porous silica coatings on titanium and their cell adhesive and osteogenic differentiation properties." *Journal of Biomedical Materials Research Part A: An Official Journal of The Society for Biomaterials* 102.1 (2014): 37-48.

42. Xia, W., et al. "Mesoporous titanium dioxide coating for metallic implants." *Journal of Biomedical Materials Research Part B: Applied Biomaterials* 100.1 (2012): 82-93.

43. Gultepe, E., et al. "Nanoporous inorganic membranes or coatings for sustained drug delivery in implantable devices." *Advanced Drug Delivery Reviews* 62.3 (2010): 305-315.

44. Ho, Y. H., H. D. Vora, and N. B. Dahotre. "Laser surface modification of AZ31B Mg alloy for bio-wettability." *Journal of Biomaterials Applications* 29.7 (2015): 915-928.

45. Lim, J. Y., and H. J. Donahue. "Biomaterial characteristics important to skeletal tissue engineering." *Journal of Musculoskeletal and Neuronal Interactions* 4.4 (2004): 396-398.

46. Lim, J. Y., et al. "Systematic variation in osteoblast adhesion and phenotype with substratum surface characteristics." *Journal of Biomedical Materials Research Part A: An Official Journal of The Society for Biomaterials* 68.3 (2004): 504-512.

47. Wang, J., et al. "Surface modification of magnesium alloys developed for bioabsorbable orthopedic implants: a general review." *Journal of Biomedical Materials Research Part B: Applied Biomaterials* 100.6 (2012): 1691-1701.

48. Liu, C., et al. "Biodegradable magnesium alloys developed as bone repair materials: a review." *Scanning* 2018 (2018): 9216314.

49. Gray-Munro, J. E., C. Seguin, and M. Strong. "Influence of surface modification on the in vitro corrosion rate of magnesium alloy AZ31." *Journal of Biomedical Materials Research Part A: An Official Journal of The Society for Biomaterials* 91.1 (2009): 221-230.

50. Assadian, M., et al. "Effects of Alkaline Treatment on Corrosion Behavior of Biodegradable Magnesium." *Advanced Materials Research* 1125 (2015): 441-444.

51. Lorenz, C., et al. "Effect of surface pre-treatments on biocompatibility of magnesium." *Acta Biomaterialia* 5.7 (2009): 2783-2789.

52. Gu, X. N., et al. "A study on alkaline heat treated Mg–Ca alloy for the control of the biocorrosion rate." *Acta Biomaterialia* 5.7 (2009): 2790-2799.

53. Wang, D., and G. P. Bierwagen. "Sol–gel coatings on metals for corrosion protection." *Progress in Organic Coatings* 64.4 (2009): 327-338.

54. Hu, J., et al. "In vitro degradation of AZ31 magnesium alloy coated with nano TiO_2 film by sol–gel method." *Applied Surface Science* 257.21 (2011): 8772-8777.

55. Gaur, S., R. S. Raman, and A. S. Khanna. "In vitro investigation of biodegradable polymeric coating for corrosion resistance of Mg-6Zn-Ca alloy in simulated body fluid." *Materials Science and Engineering: C* 42 (2014): 91-101.

56. Cao, L., et al. "RGDC Peptide-induced biomimetic calcium phosphate coating formed on AZ31 magnesium alloy." *Materials* 10.4 (2017): 358.

57. Song, Y., et al. "Electrodeposition of Ca–P coatings on biodegradable Mg alloy: in vitro biomineralization behavior." *Acta Biomaterialia* 6.5 (2010): 1736-1742.

58. Yeganeh, M., and N. Mohammadi. "Superhydrophobic surface of Mg alloys: A review." *Journal of Magnesium and Alloys* (2018): 59-70.

59. Zhang, F., et al. "Fabrication of the superhydrophobic surface on magnesium alloy and its corrosion resistance." *Journal of Materials Science & Technology* 31.11 (2015): 1139-1143.

60. Falde, E. J., et al. "Superhydrophobic materials for biomedical applications." *Biomaterials* 104 (2016): 87-103.

61. Luo, X., and X. T. Cui. "Electrochemical deposition of conducting polymer coatings on magnesium surfaces in ionic liquid." *Acta Biomaterialia* 7.1 (2011): 441-446.

62. Yang, X., et al. "Influence of mixed organosilane coatings with variable RGD surface densities on the adhesion and proliferation of human osteosarcoma Saos-2 cells to magnesium alloy AZ31." *Bioactive Materials* 2.1 (2017): 35-43.

Chapter 2

2 Objectives

Conventionally used metallic biomaterials such as stainless steel and titanium alloys often result in stress shielding and metal ion release after implantation. Moreover, a secondary surgery may be necessary to remove the implant after tissue healing. Biodegradable metallic materials that can provide the required stability during the initial stages of healing and promote tissue regeneration as they degrade would eliminate both the toxic corrosion products associated with traditional metallic implants and the need for a second surgery. The innate biodegradation of magnesium metal makes it and its alloys suitable candidates for biodegradable materials due to their excellent biocompatibility coupled with outstanding physical and mechanical properties that are similar to natural bone. However, the rapid degradation rate of magnesium and its alloys in the physiological environment has restricted their widespread application in the biomedical field since uncontrolled degradation could result in failure of the implant due to the loss of mechanical integrity. In addition, surface modifications that can promote cell adhesion and proliferation are of interest to optimize integration of these implants into the body.

Thus, researchers have been working to enhance magnesium-based biomaterials with a variety of surface modifications in order to control their degradation rate and their biocompatibility.

The main objective of this thesis was to develop surface modification strategies that result in controlled degradation of magnesium alloys in physiological environments while simultaneously enhancing the biocompatibility of the surface. The thesis contains three

individual studies that are summarized below. In the first project a method for quantifying the cytotoxicity and cell adhesion/proliferation of magnesium alloys by both direct and indirect method was evaluated. In the second project a multi-layered coating was developed; the surface chemistry of the coating, its influence on the biodegradation rate of the magnesium alloy and its cytotoxicity were studied. In the third project, the preliminary results of a study on the immobilization of a cell adhesive ligand to the surface of a superhydrophobic magnesium alloy and its influence on the biocompatibility of the samples is reported.

Project 1: Evaluation of the Biocompatibility of Magnesium Alloys by Direct and Indirect Methods

In order to evaluate newly designed biomaterials, it is essential to develop accurate testing methods to determine the biocompatibility of magnesium and its alloys to ensure that they are safe for use in medical applications. According to the International Organization for Standardization (ISO), various methods and conditions are suggested to evaluate the *in vitro* biocompatibility of recently developed biomaterials including direct and indirect techniques that quantify the cytotoxicity and cell adhesion/proliferation in the presence of biomaterials. The direct method involves direct contact between the material and the cultured cells while the indirect method involves exposing healthy, growing cells to an extract created by immersing the material in cell culture medium for a specified period of time. The current ISO standards were developed for the testing of medical devices in general and not specifically for degradable magnesium materials or other oxidizable metallic materials. Therefore, the most commonly used assays employed are not useful for these types of materials due to a false positive result that

occurs when the assay dye is reduced by the electrons released during metal oxidation. The MTT assay is an example of an assay that depends on chemical reduction of the dye molecules for cell quantification leading to a false positive in the presence of a corroding metal.

$$Metal \rightarrow Metal^{n+} + ne^{-}$$

This has led to a preponderance of studies that test the cytotoxicity of the soluble degradation products of the biodegradable metals via an indirect method and few articles that quantify cell adhesion/proliferation directly in the presence of the biodegradable metal. In addition, this false positive has caused some materials scientists to avoid these *in vitro* tests altogether and proceed directly to *in vivo* testing. While *in vivo* testing gives a more complete evaluation of the biocompatibility of an implant material, *in vitro* testing is still an essential screening tool to choose the most likely candidate materials and thus minimize the number of animals that must be sacrificed.

Therefore, it is very important to establish an alternative *in vitro* assay that can be used in a direct method to more accurately mimic the expected *in vivo* conditions. In this study, a non-common assay was evaluated for its ability to determine the biocompatibility of magnesium alloys by both direct and indirect methods. The CyQUANT assay uses a dye molecule that strongly fluoresces when bound to cellular nucleic acids and, therefore, does not undergo a colorimetric change in response to cellular metabolic reduction. This assay is not subject to the same false positive result that has been observed with other assays. The key objectives of this study were:

- To show that a cyanine dye-based assay can be used to evaluate cell adhesion/proliferation in direct contact with magnesium metals with no false positive result.
- To evaluate the CyQUANT assay as a tool to quantify the biocompatibility of magnesium alloys by both direct and indirect methods.

Project 2: Development of a Biocompatible Calcium Phosphate Coating with Improved Degradation Resistance for Biodegradable Magnesium Implant Materials

As discussed above, the rapid degradation of magnesium has prevented its widespread use in medical applications. Therefore, the key objectives of this project were:

- To develop a multi-layered surface modification strategy for magnesium alloys that controls both the degradation rate and the biocompatibility of these materials. The multilayers consist of an initial sol-gel silica layer, followed by a spin coated of mesoporous silica layer and finally a calcium phosphate layer
- To optimize the coating conditions for each layer by characterizing the surface chemistry and topography of each layer at various deposition condition.
- To produce multi-layer coating that are uniform, stable and biocompatible
- To characterize the biodegradation rate and of the optimized multi-layered coating.

Project 3: Preliminary Results on Immobilization of a Fibronectin Mimetic to the Surface of Superhydrophobic Magnesium and its Influence on Cell Adhesion

Superhydrophobic surfaces are of interest for corrosion control due to their extreme water repellence. However, while superhydrophobic surfaces have been shown to decrease the corrosion rate of magnesium alloys, superhydrophobic surfaces have also been shown to inhibit cell adhesion which is an important factor for cell survival and proliferation at implant surfaces. The arginylglycylaspartic acid (RGD) amino acid sequence is an amino acid sequence found in fibronectin, an important extracellular matrix (ECM) that mediates cell adhesion to surfaces. MAPTRix-F-RGD is a mussel adhesive protein that contains the RGD peptide. Mussel adhesive protein is a "super glue" that readily adheres to virtually any substrate, even very low surface energy superhydrophobic materials. The key objectives of this project were:

- To reproduce a superhydrophobic surface on magnesium alloy AZ31.
- To develop a method for the immobilization of the MAPTrix-F-RGD protein to the superhydrophobic Mg AZ31.
- To study the influence of this surface modification on Saos-2 osteoblast adhesion to the modified surfaces in comparison to unmodified superhydrophobic surfaces

In this study, the best conditions for deposition of MAPTrix-F-RGD protein on superhydrophobic magnesium surfaces were determined and the surface chemistry was characterized. The number of cells adhered to the modified and unmodified superhydrophobic surfaces were quantified to determine if the presence of cell adhesive ligands has any impact on the cell adhesive properties of the surface.

Chapter 3

3 Evaluation of the Biocompatibility of Magnesium Alloys by Direct and Indirect Methods

Afrah Al Hegy, Joy E. Gray-Munro, Eric R. Gauthier

Dept. of Chemistry and Biochemistry and Materials Science Program, Laurentian University, Sudbury, Ontario, Canada, P3E 2C6

(Manuscript)

Abstract

Magnesium and its alloys are promising candidates to be employed as a new generation of biodegradable metals in orthopaedic applications due to their excellent biocompatibility, biodegradability, and mechanical properties that are similar to natural bone. However, direct *in vitro* assessment of these materials in the presence of cells is complicated by degradation products from the alloy that lead to a false positive for the most commonly used cell adhesion and cell proliferation assays. In this paper, the cyanine dye was used to quantitatively evaluate the *in vitro* biocompatibility of a Mg AZ31 alloy by both direct and indirect methods. The cytotoxicity of the corrosion products was evaluated via an indirect method; a 25% decrease in cell viability compared to control samples was observed. Moreover, direct assessment of cell adhesion and proliferation showed a statistically significant increase in cell number at the surface after 72 hours. In addition, the degradation rate and surface characteristics of the Mg AZ31 alloy were evaluated in direct and indirect tests. The degradation rate was unaffected by the presence of cells while evidence of an increase in calcium phosphate deposition on the magnesium alloy surface in the presence of cells was observed. This study demonstrates that the cyanine dye provides a more accurate assessment of the overall *in vitro* biocompatibility of biodegradable metals than the more commonly used assays reported in the literature to date.

Keywords: Magnesium alloys, biocompatibility, direct method, indirect method, cyanine dye, CyQUANT assay, cell adhesion, cell proliferation, cytotoxicity

3.1 Introduction

Biomaterials are used in the replacement and treatment of diseased or injured tissue in different parts of the body; some examples include cardiovascular, dental and orthopaedic implants [1]. The development of biomaterials for orthopaedic applications has been a significant challenge to biomaterials scientists. The optimum biomaterials for orthopaedic implants should be non-toxic and biocompatible with the human body [2]. Furthermore, they should have excellent mechanical properties for the intended application and for applications such as fracture fixation, these biomaterials should be biodegradable to prevent the need for additional surgery to remove the implant after healing has occurred [3].

Magnesium and its alloys are a promising alternative for biodegradable orthopaedic implants that decrease stress shielding and enhance new bone growth due to their biodegradability, biocompatibility, and mechanical properties that are similar to natural bone. The biodegradability of magnesium provides a good advantage for short term implants that can dissolve after healing without the need of a second surgery to remove the implant.

Although magnesium itself is biocompatible [4,5], the degradation process in physiological environments that are rich in chloride ions can cause several complications for the surrounding tissues due to the rapid pH change and hydrogen gas production. The electrochemical reaction that occurs is shown in Reaction Scheme 3.1. Magnesium metal is oxidized to produce magnesium ions while water is reduced to form hydroxide ions and hydrogen gas [6].

Reaction Scheme 3.1: General Degradation Mechanism of Magnesium.

Anodic reaction: $Mg_{(s)} \rightarrow Mg^{2+}{}_{(aq)} + 2e^-$

Cathodic reaction: $2H_2O_{(l)} + 2e^- \rightarrow 2OH^-{}_{(aq)} + H_{2\,(g)}$

Product formation: $Mg^{2+}{}_{(aq)} + 2OH^-{}_{(aq)} \rightarrow Mg(OH)_{2\,(s)}$

General reaction: $Mg_{(s)} + 2H_2O_{(l)} \rightarrow Mg(OH)_{2\,(s)} + H_{2\,(g)}$

Mg alloys contain small amounts of additional elements such as aluminum, zinc, manganese and rare earth elements that enhance the mechanical strength and corrosion resistance of these materials. In addition, alloying elements that play an important role in biological activity such as calcium and strontium may also be present. The release of magnesium ions, hydroxide ions, hydrogen gas, and other alloying elements during the biodegradation process affects the overall biocompatibility of magnesium alloys. Therefore, it is essential to develop accurate testing methods to assess their biocompatibility and to ensure that they are safe for use in medical applications [7].

According to the International Organization for Standardization (ISO), various methods and conditions are suggested to evaluate the biocompatibility of recently developed biomaterials. These methods include both direct and indirect techniques [8,9].

For magnesium and its alloys, an indirect method is the most common way to evaluate their biocompatibility. This indirect method involves studying the effects of cell culture media that have been pre-conditioned through exposure to the biodegradable material on already growing cells [7]. This indirect test evaluates the effect of the soluble degradation products on

the cell viability. Many studies use this indirect method of evaluation for magnesium because a false positive is commonly observed when the assays are conducted in the presence of the magnesium material [10]. For example, the MTT assay, which is commonly used to directly quantify cell proliferation at the surface of biomaterials, involves the conversion of the yellow tetrazolium salt into a purple formazan dye by chemical reduction. Using this assay in the presence of biodegradable metals leads to a false positive result as the MTT dye is reduced by the electrons released during metal oxidation (Reaction Scheme 3.1) [10].

Although evaluating the cytotoxicity of the degradation products for biodegradable materials is one indicator of their biocompatibility, cell adhesion and cell proliferation at the surface of these materials are also important factors to consider. Therefore, in order to fully evaluate the *in vitro* biocompatibility of biodegradable magnesium, it is also important to develop direct tests for the quantification of cell adhesion and proliferation on the surface of the metal.

The determination of cellular nucleic acid content provides a reasonable measure of cell numbers. These types of assays do not rely on a colorimetric change due to chemical reduction but rather take advantage of the interaction of a fluorescent dye with cellular DNA and thus should not exhibit the false positive result discussed above. This makes them suitable for quantifying cell adhesion and proliferation directly in the presence of a biodegradable metal. The cyanine dyes bind to double helical DNA by either intercalation between the base pairs of DNA or insertion into the minor groove of the double helical DNA resulting in high fluorescence enhancement [11].

The general structure of cyanine dyes consists of two nitrogen centers that are typically part of two heterocyclic aromatic groups, linked by a conjugated polymethine chain that has an odd number of carbon atoms. Some of the most common heterocyclic aromatic groups are quinoline, indole, benzoxazole, and benzothiazole. The general structure of cyanine dyes is shown in Figure 3.1.

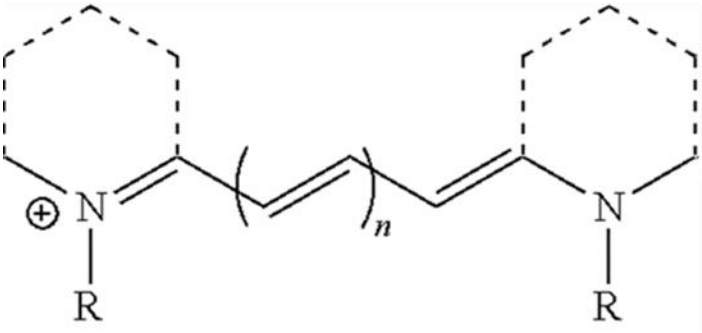

Figure 3.1: The General Structure of Cyanine Dye

Cyanine dyes can be classified as either symmetrical or unsymmetrical dyes. The symmetrical dyes are formed of identical heterocyclic aromatic groups linked at the same position whereas asymmetrical dyes contain either two different heterocycles or identical heterocyclic aromatic groups linked at different positions. The structure of the dyes plays a very important role in how they interact with the DNA [12,13,14]. Cyanine dyes have properties of both intercalators and minor groove binders and thus, either one or both of these binding modes has been observed. The planar heterocycles of the dye readily intercalate between the base pairs of DNA whereas the semiflexible polymethine chain allows the molecule to twist and follow the minor groove [12]. Upon binding, cyanine dyes exhibit significant fluorescence enhancement as a result of restricted internal rotation of the dye molecules.

The CyQUANT assay that was used in this study is an example of an assay that is based on the binding of a cyanine dye to nucleic acids. It is a quick and reliable method to evaluate the biocompatibility of a material and can detect as few as 10-50 cells and as high as 25,000-50,000 cells depending on cell type. The linear range of this assay can be further extended to cell numbers as high 100,000-250,000 cells by increasing the cyanine dye concentration [11].

In contrast to indirect techniques that evaluate cell viability in the presence of pre-conditioned cell media, direct methods allow for evaluation of the biocompatibility of magnesium alloys in the presence of the biocorrosion process. The effect of Mg ions that dissolve in cell culture media, the rapid pH change, the hydrogen gas produced and the deposition of corrosion products during biocorrosion all have an influence on biocompatibility. However, direct evaluation methods have been avoided by many researchers for biodegradable magnesium materials due to false positive results from the most commonly used assays [7,10].

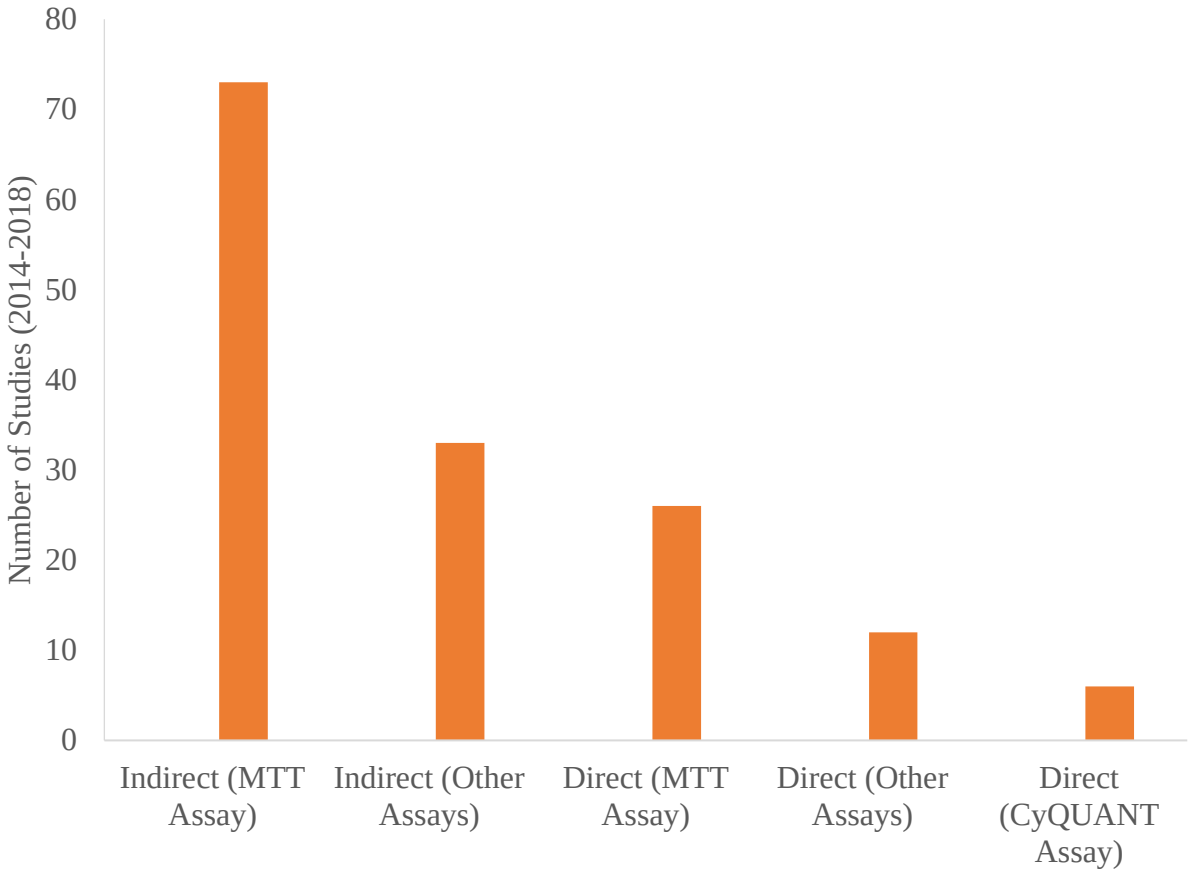

Figure 3.2: Survey of Methods Used to Evaluate the Biocompatibility of Magnesium Materials in Publications from 2014-2018. A Complete List of the References Used to Prepare this Figure can be Found in Appendix 1.

Figure 3.2. shows the results of our literature survey of the methods used to evaluate the biocompatibility of magnesium materials from 2014 to 2018. Of the 150 journal articles surveyed, 70% reported using an indirect method to evaluate biocompatibility. As shown in Figure 3.2, the most common method used to evaluate the biocompatibility of magnesium was the indirect method with the MTT assay. Other assays used for the indirect method include the

MTS, WST-1, WST-8 and Alamar Blue assays. All of these assays undergo a colorimetric change when a dye is chemically reduced in response to cellular metabolism and are therefore unsuitable for quantifying cell adhesion/proliferation in the presence of magnesium due to the expected false positive result. Despite the known false positive, the MTT assay was also employed in a direct biocompatibility test in 17% of the articles surveyed. Moreover, about 8% of the articles evaluated the biocompatibility of magnesium by a direct method using other assays that also undergo a colorimetric change via chemical reduction. Overall only 4% of the articles reviewed evaluated biocompatibility by a direct method that did not employ an assay that would be expected to give false positive results. This literature survey highlights the need for a reliable method to quantify cell adhesion/proliferation for cells in direct contact with magnesium biomaterials. The CyQUANT assay, used in only 6 of the 150 articles surveyed, should not result in a false positive and can be used to quantify cell numbers by both direct and indirect methods.

The objective of this research was to demonstrate the applicability of the cyanine dye for the *in vitro* evaluation of the biocompatibility of biodegradable magnesium materials by both direct and indirect methods.

3.2 Experimental Details

3.2.1 Materials

Mg AZ31 foil (0.81mm thickness) was purchased from Alfa Aesar (US). Acetone (reagent grade) was purchased from Caledon Laboratory Chemicals (Canada). Bovine Calf Serum (BCS) and Trypan Blue were purchased from Fisher Scientific (Canada). McCoy's 5a

culture medium and Trypsin/EDTA (1X) were purchased from Corning (Canada). Phosphate Buffered Saline (PBS) (1X) and Penicillin-Streptomycin Solution were purchased from HyClone (Canada). The CyQUANT Cell Proliferation Assay kit was purchased from Life technologies (Canada). Ethyl alcohol (95%) and methanol were purchased from Commercial Alcohols (Canada). All chemicals were used as received without further purification. The Saos-2 cell line was purchased from American Type Culture Collection (ATCC, Bethesda, MD USA).

3.2.2 Preparation of Mg AZ31 Alloys

Mg AZ31 alloy sheets were cut into circular discs with a diameter of 1.27 cm. These discs were polished on both sides with a 320 grit P400 grinding paper and oil-based lubricant (Buehler). In order to remove any excess polishing oil from the surface of the alloys, the samples were sonicated in acetone for 20 minutes and then rinsed in deionized water for 30 seconds. Finally, the samples were air dried.

3.2.3 Cell Culture

Human osteosarcoma Saos-2 cells were cultured in McCoy's 5a cell culture medium containing 15% Bovine Calf Serum and 1% penicillin/streptomycin at 37^{o}C in a 5% CO_2 humidified atmosphere. The cell culture medium was changed every two days. Once the cells grew to 70-80% confluence, they were washed with warm (37^{o}C), sterile PBS and detached from the flask with Trypsin/EDTA and then centrifuged at 2500 rpm for 5 minutes. The supernatant was discarded, and the cells were resuspended in fresh McCoy's medium. The number of cells in the suspension was determined by the trypan blue dye using a Neubauer hemocytometer.

3.2.4 Direct Method Procedure

The Mg Alloy samples were sterilized in 70% ethanol for 20 minutes and then rinsed with warm PBS. The samples were placed in the wells of a 24-well plate, 25,000 cells in 2 mL of McCoy's medium were added to each well and the plate was incubated for 24, 48, and 72 hrs at 37^{o}C in a 5% CO_2 atmosphere. After the desired incubation period, a 25 µL aliquot was taken from the cell culture medium and diluted to 25 mL with 2% HNO_3 in a volumetric flask to determine the amount of Mg ions dissolved in the cell culture medium. Subsequently, the Mg alloys were rinsed with warm PBS in order to remove non-adherent cells, then the plate was frozen at -20ºC at least 24 h for the cells to lyse. For cell number determination, the plate was allowed to thaw and processed for the CyQUANT assay, according to the supplier's instructions. Briefly, 200 µl of CyQUANT solution was added to each sample and incubated for 5 minutes. At the end of the incubation period, 100 µL of the CyQUANT solution was pipetted from each well to a black fluorescent 96-well plate (Costar) and the fluorescence intensity of each solution was measured with a Fluostar Optima spectrofluorometer. The cell number was then determined using a calibration curve of cell number vs. fluorescence intensity. In addition, cells grown on the bare well surface (in the absence of magnesium discs) was used as a positive control group for cell adhesion while the blank consisted in Mg AZ31 disks incubated in culture medium in absence of cells. The experiment was repeated two times on different days to ensure the reliability of the results. Each individual experiment was an analysis of 3 samples at each incubation time.

The percentage of Saos-2 cells adhered directly to the Mg AZ31 surface as a function of time was determined using this direct method. The quantitative data were reported as a percentage of the number of cells attached to the surface in comparison to the initial number of cells seeded (25,000 cells). The cell adhesion percentage was calculated by the following equation:

$$Cell\ Adhesion\% = \left(\frac{number\ of\ adhered\ cells}{25{,}000}\right) * 100$$

The lack of false positive for the CyQUANT assay was tested through a control experiment that measured the fluorescence of the dye in the presence of magnesium but in the absence of cells. The fluorescence intensity measured in the absence of cells was very low, usually in the range (125-375).

3.2.5 Indirect Method Procedure

3.2.5.1 Preparation of Magnesium Conditioned Media (Magnesium Extract)

Prior to the indirect experiment, all magnesium alloy samples were sterilized in 70% ethanol for 20 minutes followed by washing with warm PBS. The Mg alloy samples were placed in individual wells of a 24-well plate that contained only cell culture medium (2 mL of McCoy's medium) and then incubated for 24, 48, and 72 hrs at 37^{o}C in a 5% CO_2. After the incubation periods, a 25 µL aliquot of the cell culture medium was taken from each well and diluted to 25 mL using 2% HNO_3 in a volumetric flask. The Mg alloys were then rinsed in water and set aside

for further analysis (Section 3.2.6). Cell culture medium was used as a control to compare the concentrations of magnesium ions in the presence vs absence of magnesium alloy samples.

3.2.5.2 Evaluation of Cell Viability

To determine the effect of magnesium on the viability of cells, 15,000 cells were seeded in a 96-well plate in triplicate. Cells were incubated at 37^{o}C in a 5% CO_2 atmosphere for 24 hours to allow cell attachment to the plate surface. After 24 hours of incubation, the cell culture medium was removed and 200 µL of the magnesium extract (Mg-conditioned medium) was added to a 96-well plate with the already growing cells. The plate was then incubated for 24 hrs at 37^{o}C in a 5% CO_2 atmosphere. After 24 hrs, the magnesium conditioned medium was removed, and the cells in the 96-well plates were rinsed with warm PBS in order to remove non-adherent cells, then the plate was frozen at -20^{o}C overnight for the cells to lyse. The cell numbers were then determined using the CyQUANT assay as described above. Cells grown in the absence of magnesium extract were used as a control group to determine the cell viability. The entire experiment was repeated two times on different days to ensure the reliability of the results. Each individual experiment tested 3 samples of each type set (cells only, 24 hours extract medium, 48 hours extract medium, 72 hours extract medium).

The percentage of viable Saos-2 cells in the presence of magnesium alloy conditioned extract that had been pre-conditioned for 24, 48 and 72 hours was determined using this indirect method. The quantitative data are reported as a percentage of the number of cells in the presence of Mg conditioned cell culture media in comparison to the number of cells in the absence of Mg

conditioned cell culture media (control). The cell viability percentage was calculated by the following equation:

$$Cell\ viability\% = \left(\frac{number\ of\ viable\ cells\ exposed\ to\ Mg\ extract}{number\ of\ viable\ cells\ in\ control\ sample}\right) * 100$$

3.2.6 Instrumental Analysis

3.2.6.1 Attenuated Total Reflectance-Fourier Transform Infrared Microscopy (ATR-FTIR)

Attenuated total reflection Fourier transform infrared microscopy (ATR- FTIR) was used to analyze the surface of the Mg AZ31 alloy discs after exposure to the cells and the cell culture medium in the direct method and to the cell culture medium alone in the indirect method. A Bruker Optics Hyperion infrared microscope with an attenuated total reflectance objective and a germanium crystal was employed. The main goal of this technique was to determine the chemical functional groups present on the surface of the magnesium alloys after the direct and indirect method. The spectra were taken in three spots for each sample and were corrected with the atmospheric compensation function of the OPUS software to remove water vapour and CO_2 from the spectra.

3.2.6.2 Flame Atomic Absorption Spectroscopy (FAAS)

A Perkin Elmer AA analyst 400, flame atomic absorption spectrometer was used to determine the degradation rate of the magnesium alloys after exposure to the cells and the growth medium in the direct method and to the growth medium alone in the indirect method.

This technique was used to measure the concentration of magnesium ions that have been released into the cell culture medium in the presence and absence of the cells. The amount of magnesium released from the samples was quantified using a calibration curve for standards of known concentrations of magnesium (0.05, 0.1, 0.2, 0.5 mg/L). Unmodified cell culture medium was used as the control. The results are reported as the average ± standard deviation for three different samples of each type.

3.2.6.3 Scanning Electron Microscopy-Energy Dispersive X-ray Spectroscopy (SEM-EDS)

Scanning electron microscopy was used to evaluate the surface topography of the samples after the direct and indirect cell tests. SEM images were obtained using a digital scanning electron microscope (JEOL 6400) operated at 20 kV with a beam current of 1 nA. Energy Dispersive X-ray Spectroscopy (EDS) was used to determine the elemental composition of the degradation products on the surface. Samples to be analyzed were coated with a thin film of carbon to render the sample conductive.

3.2.7 Statistical Analysis

Quantitative results are reported as an average±standard deviation of multiple sample trials. The number of samples used in each data is indicated in the figure captions. Statistical significance of the observed differences in the cell adhesion% and cell viability% data was determined with a paired student t-test. A value of $p < 0.05$ was assumed to indicate statistically significant differences.

3.3 Results and Discussion

3.3.1 Evaluation of the Biocompatibility of Mg AZ31 Alloy by CyQUANT Assay

The main objective of this study was to compare the usefulness of the CyQUANT assay in a direct and indirect method for evaluating the biocompatibility of magnesium alloy AZ31 *in vitro*. This assay is a quick and reliable technique that can be readily adapted for use in direct and indirect methods. The CyQUANT assay does not depend on a reaction with cellular metabolic products but instead is based on the interaction of a dye with the cellular nucleic acids.

3.3.1.1 Direct Method

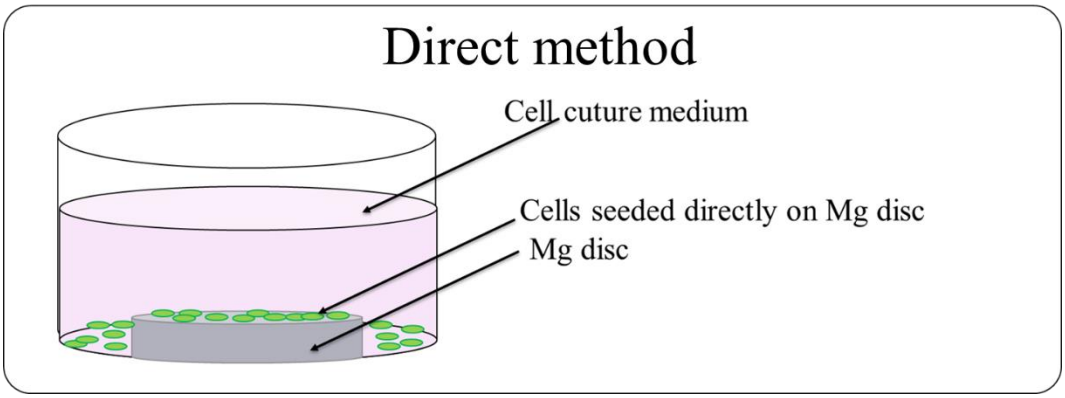

Schematic Diagram 3.1: The Schematic Diagram of the Direct Method

In the direct method, cells were grown directly on the surface of the Mg AZ31 discs for a selected time interval (24 hrs, 48 hrs, and 72 hrs) as shown in Schematic Diagram 3.1. After the incubation time, the magnesium disc was removed, and the non-adherent cells were rinsed from the surface in order to quantify only the cells adhered to the Mg alloy surfaces.

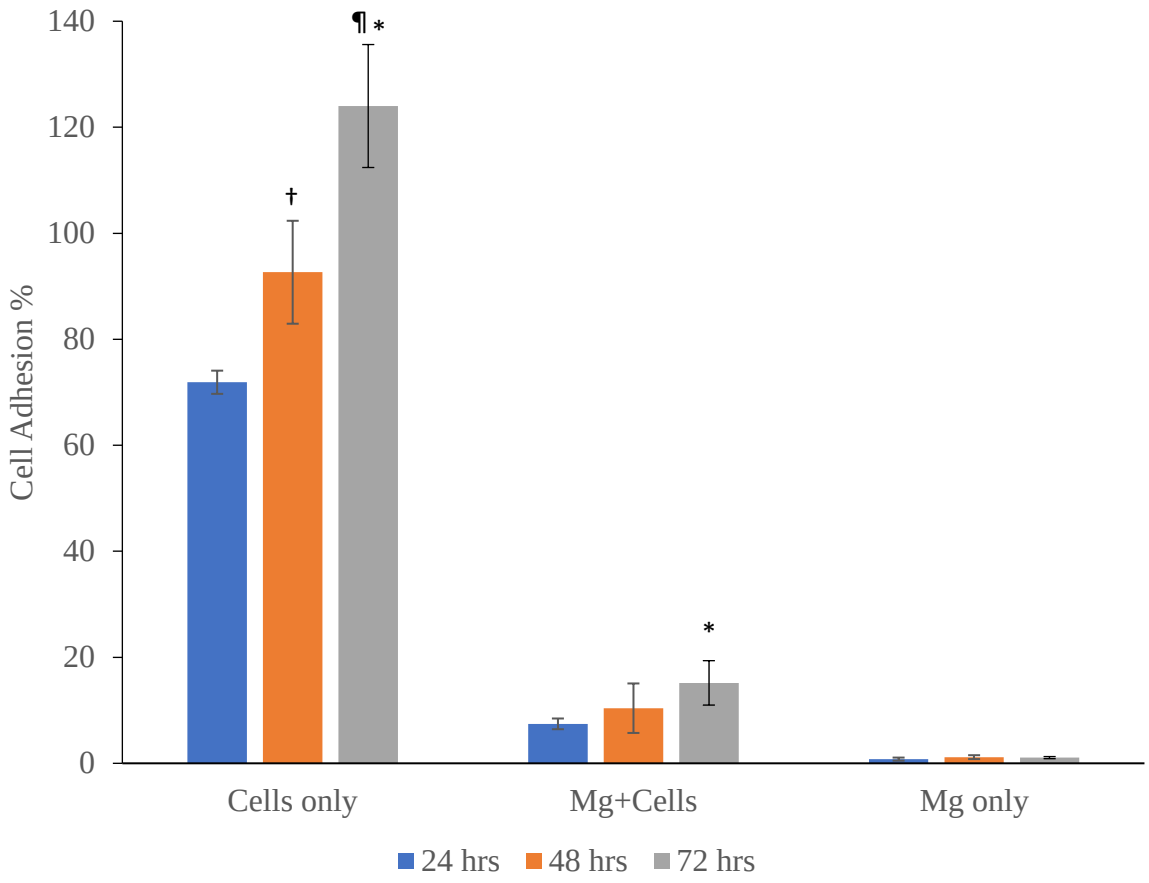

Figure 3.3: The Percentage of Saos-2 Cells Adhered to the Mg AZ31 Surface as a Function of Time Evaluated by the Direct Method. Results are Reported as a Percentage of the Number of Cells Attached to the Surface in Comparison to Initial Number of Cells Seeded. "Cells only" is the Data for the Control Group Grown in the Cell Culture Plate while "Mg+Cells" is the Data for Cells Attached to the Mg AZ31 Surface. Data are the Average of 6 Samples (3 Replicates of 2 Independent Experiments). * Indicates $p<0.05$ between 24 hrs and 72 hrs, ¶ Indicates $p<0.05$ between 48 hrs and 72 hrs, and † Indicates $p<0.05$ between 24 hrs and 48 hrs.

Figure 3.3 shows the percentage of cells adhered to the Mg AZ31 samples after incubation periods of 24, 48, and 72 hours. The results show that the percentage of cells on the positive control (cells only) increased as a function of time indicating cell proliferation in the well. Also, the percentage of cells on the Mg AZ31 alloy surface increased significantly over time but with overall low cell numbers in comparison to the control samples. The low percentage of cells on the Mg AZ31 surface may be attributed to the corrosion of the magnesium alloy surface in aqueous environments resulting in the production of hydrogen gas bubbles and an increase in pH of growth medium. However, the results show a statistically significant difference in cell number on the magnesium alloy sample after 72 hours. In fact, after 72 hours the cell number increases by 105% on the magnesium alloy surface in comparison to an increase of only 70% for the control samples. This indicates that although the initial adhesion of cells to the magnesium samples is low, the adhered cells were able to proliferate significantly over 72 hours. Thus, using the CyQUANT assay, we were able to show that Mg AZ31 has the ability to promote cell adhesion and cell proliferation over time.

3.3.1.2 Indirect Method

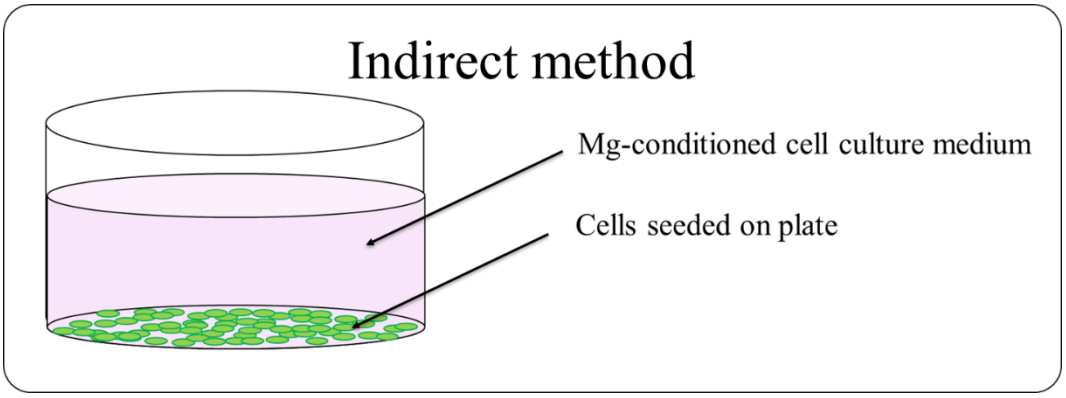

Schematic Diagram 3.2: Schematic Diagram of the Indirect Method

In the indirect method, cells were growing on the surface of a plastic 96-well plate are exposed to cell culture medium that had been pre-conditioned with magnesium alloy for 24, 48 and 72 hours as shown in Schematic Diagram 3.2. After incubation of the cells in the presence of the conditioned medium for 24 hours, the magnesium conditioned cell culture medium was removed, the wells rinsed with PBS to remove non-adherent cells and the number of viable cells determined with the CyQUANT assay. Cells grown in well (in the absence of magnesium extract) were applied as a control group in this study to determine the cell viability for each sample group.

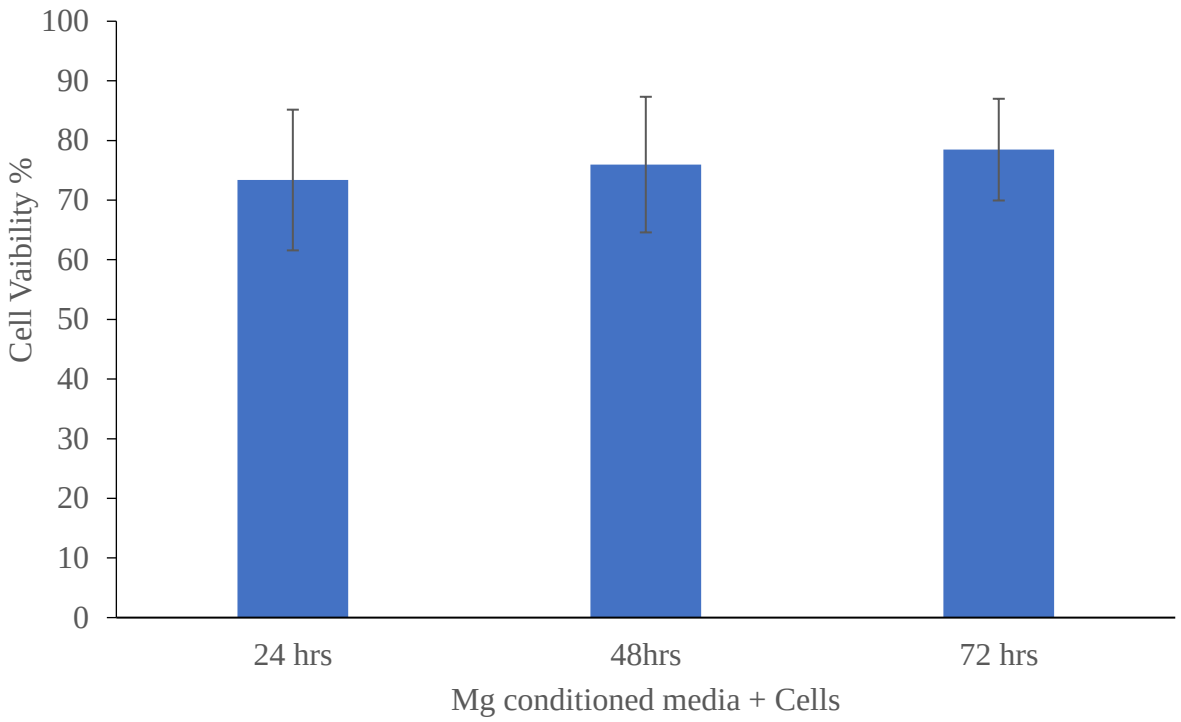

Figure 3.4: The Percentage of Saos-2 Cell Viability Using the Indirect Method in the Presence of Mg Alloy Conditioned Extracts that had been Pre-conditioned for 24, 48 and 72 hours. The Quantitative Data are Reported as a Percentage of the Number of Viable Cells in the Presence of Mg Alloy Conditioned Extract Compared to Number of Viable Cells in Unmodified Cell Culture Medium (Control). Data are the Average of 6 Samples (3 Replicates of 2 Independent Experiments).

Due to the biodegradation of the Mg alloy samples, magnesium ions, hydroxide ions and ions of alloying elements are released into the cell culture medium. The rise in pH and the presence of potentially toxic ions may negatively affect the cell viability. Figure 3.4 shows the viability of Saos-2 cells in the presence of the Mg-conditioned medium after 24, 48 and 72 hours.

It was observed that the cells exposed to the conditioned Mg AZ31 extract had similar cell viability regardless of conditioning time. According to ISO, if the cell viability is reduced by more than 30%, the material is considered to be cytotoxic [9]. However, these results show that cell growth in the Mg alloy conditioned cell culture medium for 24, 48 and 72 hours all decreased the cell viability by only 25% on average. No statistically significant difference in the percentage of cell viability was noted for the different conditioned media ($p > 0.05$).

Determination of the Biodegradation Rate of Mg alloy AZ31 in the Cell Culture Medium in the Presence and Absence of Cells

In order to evaluate the influence of cells on the biodegradation rate of Mg AZ31, the amount of magnesium dissolved in cell culture medium as a function of time was determined by flame atomic absorption spectroscopy (FAAS). Magnesium ions are released into cell culture medium as the magnesium metal is oxidized to Mg^{2+} in the aqueous solution.

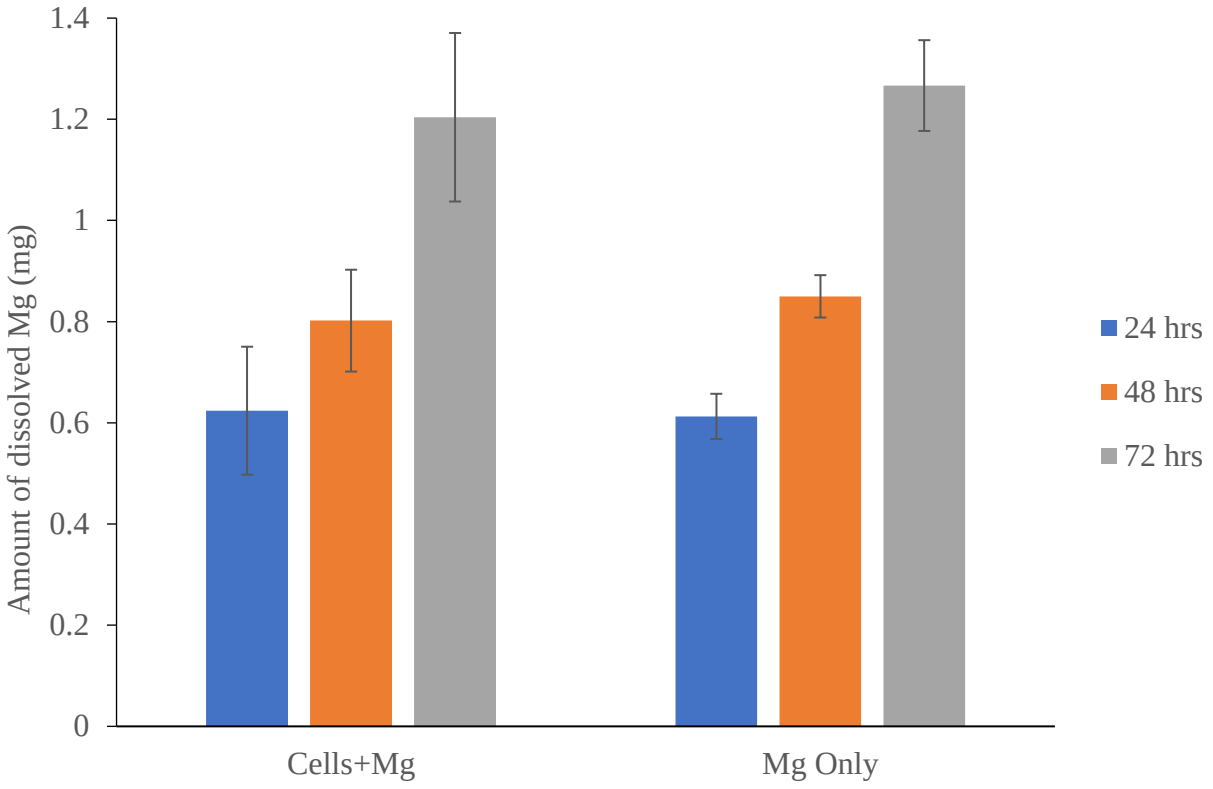

Figure 3.5: The Amount of Mg Dissolved as a Function of Time in the Cell Culture Medium in the Presence and Absence of Cells. Each Data Point Represents an Average of 3 Samples; the Error Bars are the Sample to Sample Standard Deviations.

Figure 3.5 shows a graph of the amount of magnesium dissolved into the cell culture medium as a function of time over a 72-hour period in the presence (direct method) and absence (indirect method) of cells. The amount of Mg ions released into the cell culture medium was the same in the presence (direct) and absence (indirect) of cells. Therefore, the cells did not inhibit or enhance the corrosion of Mg alloys AZ31 up to 72 hours. However, Agha et al. reported that the influence of cells on the degradation of pure Mg and Mg alloys was more apparent after 14 days

of immersion than 4 days of immersion in cell culture medium in their study on the degradation of magnesium in the presence and absence of osteoblast cells. A decrease in the degradation rate of pure Mg and Mg-10Gd was observed in the presence of cells compared with the samples in the absence of cells. These results were attributed to the formation of more hydroxyapatite in the presence of osteoblast cells which increased over time [15]. This will be discussed in more detail in later sections.

In addition, although the concentration of magnesium in the cell culture medium at 72 hours was close to two times the amount measured at 24 hours there was no increase in the observed cell cytotoxicity measured by the indirect method. For the direct method, cell proliferation was observed despite the increase in magnesium ions in the cell culture medium. These results are consistent with the literature as it has been previously reported that increased magnesium ions levels stimulate new bone growth [16,17]. Numerous of studies have stated the enhancement of bone growth around the corroded magnesium implant *in vivo* [18,19,20]. As has been shown in the literature, the presence of magnesium on orthopaedic implants may enhance osteoblastic cell adhesion *in vitro*. Pietak et al. has shown that magnesium-based substrates can promote bone cell attachment on the implant surface in an *in vitro* experiment [21]. Furthermore, Li et al. have shown that Mg-1Ca alloy did not induce toxicity to cells and had high activity of osteoblast and osteocytes around the alloy in an *in vivo* experiment [20].

3.3.2 Characterization of the Surface of Mg AZ31 Alloy after Direct and Indirect Methods

After each incubation time, the samples were analyzed by SEM-EDS in order to evaluate the morphology and surface elemental composition of the magnesium alloy after exposure to the mixture of the cells and the cell culture medium in the direct method and to the unmodified cell culture medium in the indirect method. The samples were also analyzed by ATR-FTIR in order to identify the precipitation products on the surface. One of the expected degradation products on the surface of magnesium alloys after exposure to the cell culture medium solution is calcium phosphate [22] due to their low solubility in aqueous solution, particularly at elevated pH.

As the magnesium alloy degrades, the pH rises, resulting in precipitation of calcium phosphate species such as hydroxyapatite as shown in reaction scheme 3.2.

Reaction Scheme 3.2: Precipitation Reactions

$$10Ca^{2+}_{(aq)} + 6PO_4^{3-}{}_{(aq)} + 2OH^-_{(aq)} \rightarrow Ca_{10}(PO_4)_6(OH)_{2\,(s)}$$

Furthermore, other precipitation products are possible on magnesium alloy surfaces after exposure to cell culture media such as other calcium phosphates, magnesium phosphate, magnesium hydroxide and magnesium carbonate [23].

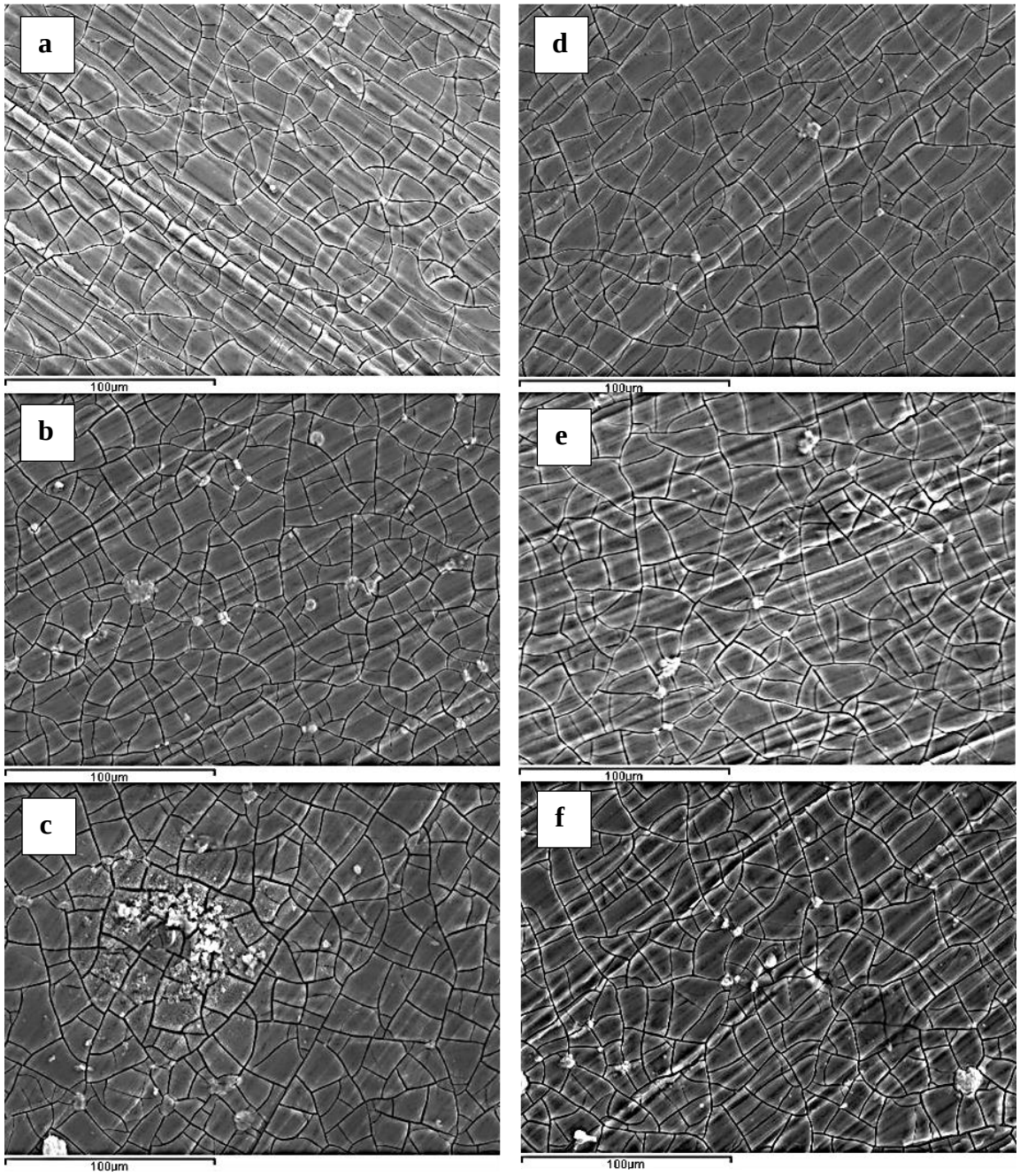

Figure 3.6: SEM Images of the Magnesium Alloy AZ31 Surface after the Direct and Indirect Methods. (a, b, c) Samples after 24, 48,72 hours by the Direct Method, (d, e, f) Sample after 24, 48,72 hours by the Indirect Method. Scale Bar = 100 µm.

Figure 3.6. shows representative SEM images of the surface of the Mg AZ31 alloy samples after incubation in the cell culture medium in the presence (a, b, c) or absence (d, e, f) of osteoblast cells. The SEM image of a polished bare magnesium surface before testing showed that the polished Mg AZ31 surface was flat with lines due to polishing (image is not shown). The SEM images of all of the samples after either the direct or indirect test are completely covered with a layer of corrosion product. The cracking of the layer is due to dehydration of the corrosion product as it dries. This layer was readily observed on the magnesium substrate after 24 hrs of exposure to the cell culture medium both in the presence and absence of cells. Thus, the presence of cells in the culture medium does not change the surface morphology of the layer deposited on the magnesium alloy surface. The presence of both calcium and phosphorus on these surfaces was confirmed by EDS indicating that the deposited layer is calcium phosphate as expected. This will be discussed in more detail in subsequent sections.

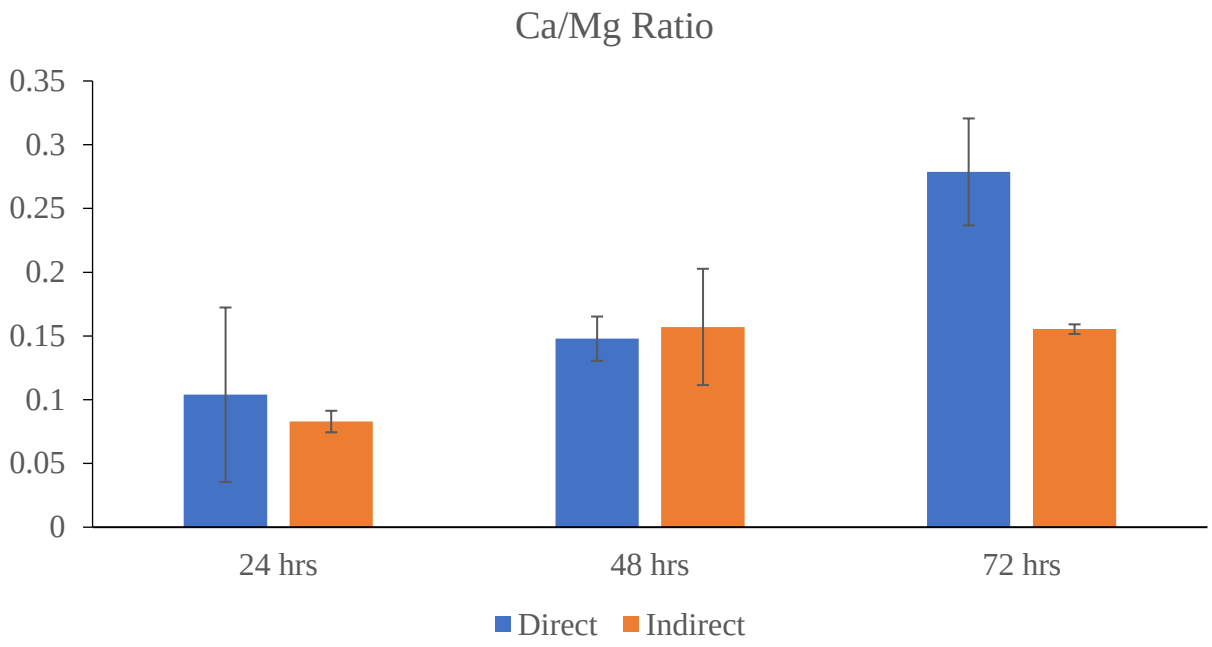

Figure 3.7: The Ratio of Weight Percentage for Ca/Mg Deposited on the Surface of Mg AZ31 after the Direct and Indirect Methods. Each Data Point Represents an Average of 3 Samples and 9 Spots on each Samples; the Error Bars are the Sample to Sample and Spot to Spot Standard Deviations.

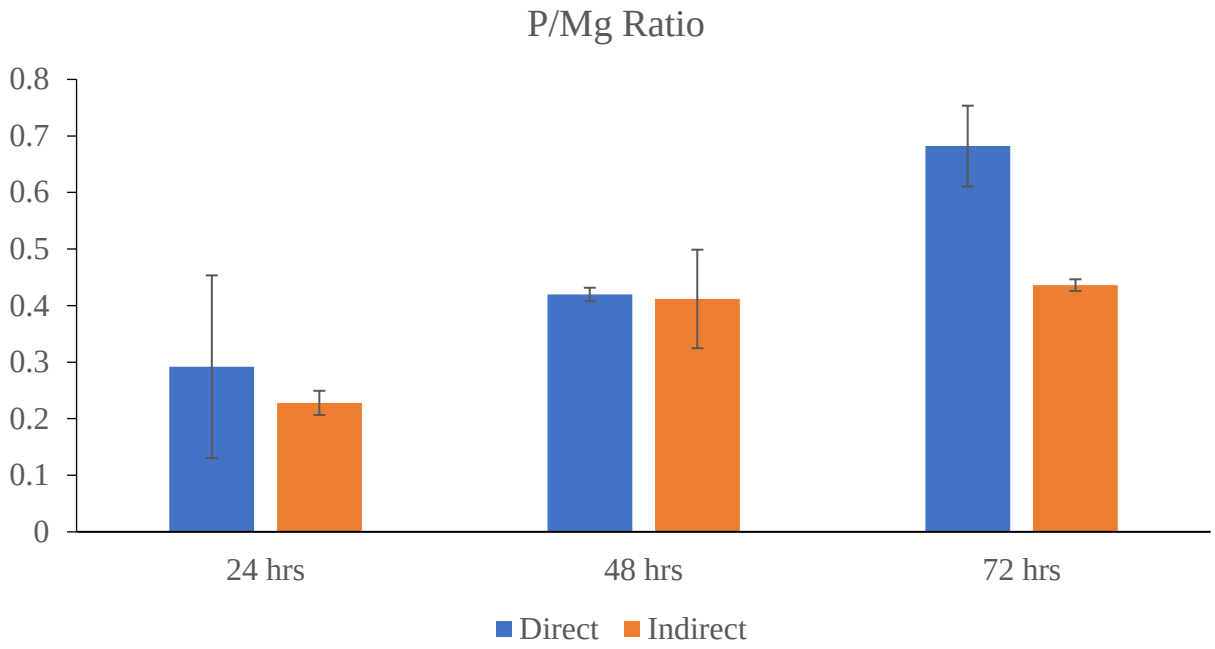

Figure 3.8: The Ratio of Weight Percentage for P/Mg Deposited on the Surface of Mg AZ31 after the Direct and Indirect Methods. Each Data Point Represents an Average of 3 Samples and 9 Spots on each Samples; the Error Bars are the Sample to Sample and Spot to Spot Standard Deviations.

All of the samples were analyzed by EDS in order to determine the elemental composition of the degradation products that had been formed on the surface of the magnesium alloy after both the direct and indirect cell tests.

Figure 3.7 shows the Ca/Mg ratio while Figure 3.8 shows the P/Mg ratio as a function of time for samples exposed to cell culture media alone (indirect test) and cell culture medium and cells (direct test). The EDS results indicate that the Ca/Mg and P/Mg ratio on the surface of Mg alloys for both the direct and indirect methods was slightly increased with increased incubation

time from 24 to 48 hrs. After 72 hrs, the ratio of Ca/Mg and P/Mg that was deposited on the surface of the Mg alloys after the direct method increased indicating an increase in the thickness of the calcium phosphate layers in the presence of cells with increasing incubation time. In comparison, the ratios of Ca/Mg and P/Mg on the surface of Mg AZ31 in the absence of cells (indirect method) after 72 hrs were not increased. Thus, although the morphologies are similar as seen in Figure 3.6, the thickness of the calcium phosphate layer appears to be influenced by the presence of cells.

These results can be attributed to the ability of the Saos-2 osteoblast cells to produce calcium phosphate as has been reported in numerous of studies. Human osteoblast cells play an important role in the formation of bone by inducing and regulating the mineralization of the extracellular matrix. Saos-2 cells can also more closely mimic the *in vivo* environment than other commonly used osteoblast cell lines [15,24,25,26]. Agha et al. found more hydroxyapatite on a magnesium surface in the presence in comparison to the absence of cells. Specifically, their study reported that finding more Ca and P contents near the cells than underneath the cells [15].

In addition, Strzelecka-Kiliszek, et al. compared the formation of minerals on two selected osteoblastic cell models: osteosarcoma Saos-2 cells and human foetal hFOB 1.19 cells and it was observed that Saos-2 cells had higher amount and composition of minerals compared to hFOB 1.19 cells and that Saos-2 cells mineralized better than hFOB 1.19 cells since the ratio of calcium to phosphate was closer to hydroxyapatite. Therefore, the choice of osteoblast cell line is an important consideration for the direct method since each cell line shows different characteristics in terms the extracellular matrix and mineralization production [27].

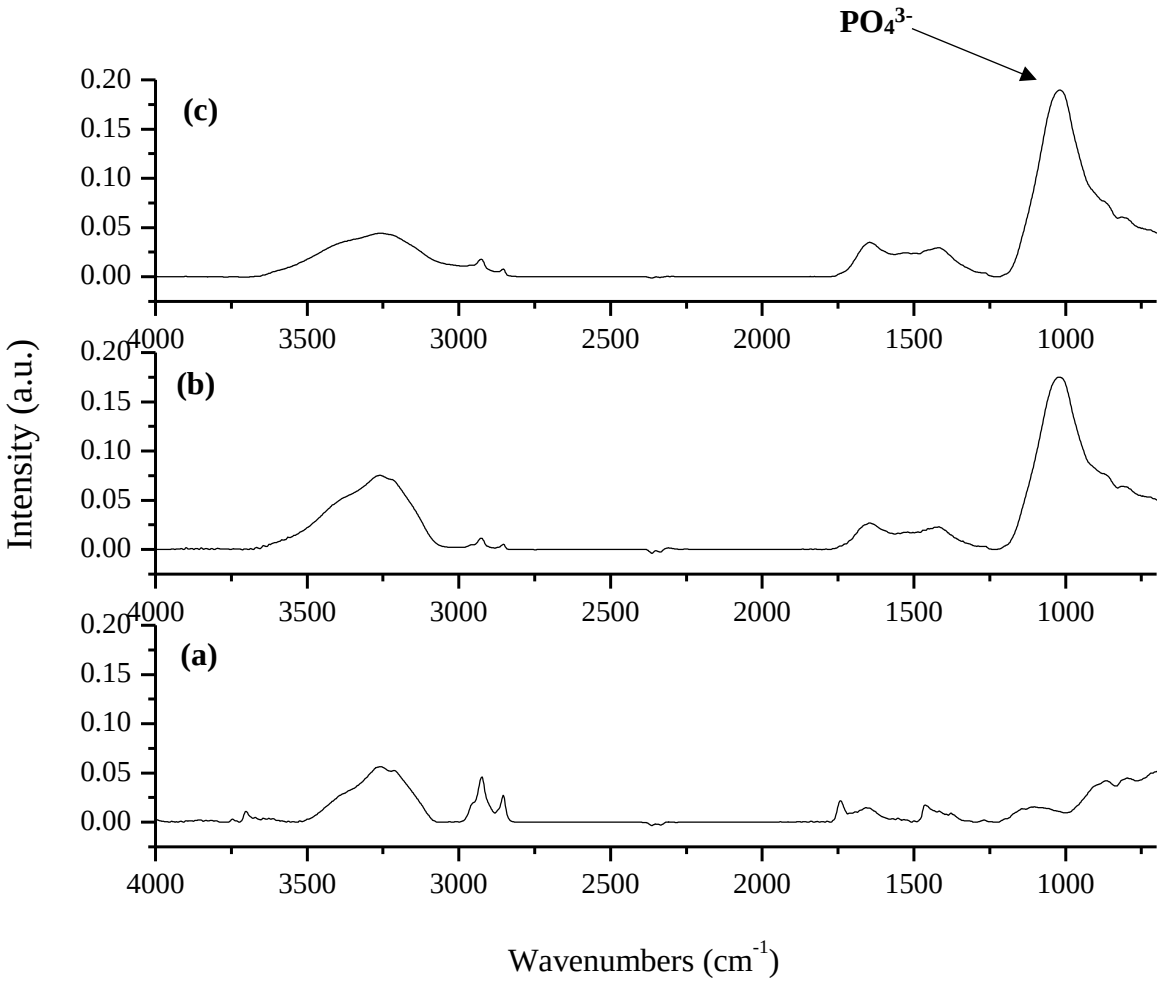

Figure 3.9: IR Spectra of MgAZ31 after the Direct and Indirect Methods (72 hour Incubation Time). (a) Sample before Test, (b) Sample after Direct Method and (c) Sample after Indirect Test.

The magnesium alloy was also analyzed by ATR-FTIR in order to further identify the precipitation products on the surface. Figure 3.9 shows IR spectra of MgAZ31 surface before and after exposure to the cells. The IR spectrum for a polished and cleaned magnesium alloy has a

small peak at 3700 cm^{-1} (O-H stretch) which indicates the presence of Mg-OH bonds at the surface. A broad peak at 3000 cm^{-1} (O-H stretch) was also observed coupled with a peak at 1640 cm^{-1} (O-H bend) due to the surface adsorbed water. Carbonate (CO_3^{2-}) is also observed at (1450 cm^{-1}) due to the reaction of the magnesium substrate with carbon dioxide in the atmosphere. Furthermore, peaks at 2850-2930 cm^{-1} (CH_2/CH_3 stretch) were observed indicating a small amount of organic contamination on the surface. As shown in Figure 3.9, all the sample surfaces exhibited a strong phosphate peak at 1050 cm^{-1} confirming that the phosphorus peak observed in the EDS spectra which is due to the presence of phosphate, PO_4^{3-}, at the magnesium alloy surface. Furthermore, the carbonate peak at (1450 cm^{-1}) is still observed after the direct and indirect test; this is attributed to the presence of carbonate within the deposited surface layer. The deposition of this calcium phosphate layer on the surface of the Mg alloy may lead to enhanced bone-implant contact and induce early bone formation [19,20]. Therefore, the presence of cells in direct contact with this layer is a very important factor for the evaluation of the biocompatibility of magnesium biomaterials.

3.3.3 Comparison of the Direct and Indirect Methods using the CyQUANT Assay

Each material developed for medical applications must be biocompatible, which means it does not have toxic or carcinogenic effects and also can be tolerated by the human body without inducing inflammation or injury to the surrounding tissue [28]. *In vitro* studies of the biocompatibility of a material are an important preliminary step to investigate the potential safety of using these materials for *in vivo* studies [29]. The *in vitro* study of the biocompatibility of

biodegradable magnesium alloys is mainly carried out using cell culture [29]. There are two primary methods that have been adapted from the international standards organization for evaluating the biocompatibility of biomedical devices [8,9]. The first method involves direct contact between the material and the cultured cells (direct method). The second method is to evaluate the compatibility of the materials with cells using an indirect method in which growing cells are exposed to an extract created by immersing the material in cell culture medium for a period of time.

The most commonly used assays for both of these methods are colorimetric assays that depend on a chemical reduction reaction. Using these assays for magnesium materials in a direct method leads to a false positive result as the dye is reduced by the electrons released during the oxidation of the magnesium substrate itself [29]. Consequently, the indirect method is the most popular method for analyzing the biocompatibility of Mg based biomaterials. Although some authors have reported analyzing samples exposed to only magnesium (the blank) and then subtracting the signal obtained from the samples in the presence of cells, this is still problematic because the observed intensity of the magnesium “blank” depends on the corrosion rate of the sample [30]. This can be influenced by the mechanism of corrosion of the alloy especially in the case of pitting corrosion where high sample to sample variability may be observed. The corrosion rate may also be influenced by the presence of the cells themselves.

The CyQUANT assay used in this study is an excellent alternative as it is an assay based on nucleic acid binding and can therefore be used in both indirect and direct biocompatibility tests. In this paper, the results obtained from the direct methods using the CyQUANT assay

indicated the ability of Mg AZ31 to promote cell adhesion and cell proliferation over time. Moreover, the extremely low fluorescence measurements observed for Mg AZ31 alloys without cells indicates that the CyQUANT assay does not yield a false positive result in the presence of magnesium. Therefore, this assay provides a better assessment of the overall behaviour of cells with Mg based biomaterials because the cells are growing in a direct contact with the biomaterial and are therefore exposed to all environmental changes in the cell culture medium, including Mg ion release, an increase in pH, hydrogen gas production and the deposition of biodegradation products.

In addition, the CyQUANT assay was also used in an indirect method in this study. The results indicated that the Mg alloy conditioned cell culture medium was only slightly cytotoxic to the cells.

The results of this study have demonstrated that the CyQUANT assay can be employed in both direct and indirect methods to obtain a more complete analysis of the biocompatibility of biodegradable metallic biomaterials.

3.4 Conclusion

This research demonstrates that the cyanine dye (CyQUANT assay) can be used to evaluate the *in vitro* biocompatibility of biodegradable magnesium alloys by both direct and indirect methods. A particular advantage of this assay is the ability to quantitatively measure cell numbers directly on the surface of magnesium biomaterials allowing for a more complete evaluation of the behaviour of cells in the presence of all of the degradation products that are produced when magnesium alloys biodegrade. The combined results from the direct and indirect

biocompatibility tests performed in this study indicate that cell proliferation readily occurs on Mg AZ31 surfaces and that the soluble products of biodegradation are only slightly cytotoxic.

References

1. Parida, P., A. Behera, and S. C. Mishra. "Classification of biomaterials used in medicine." *International Journal of Advances in Applied Sciences* 1.3 (2012): 31-35.

2. Ratner, B. D., et al. "Biomaterials science." *Plasma Processing of Polymers*. Netherlands*:* Kluwer Academic Publisher (1997): 453-464.

3. Malekani, J., et al. "Biomaterials in orthopedic bone plates: a review." Proceedings of the 2nd Annual International Conference on Materials Science, Metal & Manufacturing (M3 2011). *Global Science and Technology Forum* (2011): 71-77.

4. Staiger, M. P., et al. "Magnesium and its alloys as orthopedic biomaterials: a review." Biomaterials 27.9 (2006): 1728-1734.

5. Yang, J. X., et al. "In vivo biocompatibility and degradation behavior of Mg alloy coated by calcium phosphate in a rabbit model." *Journal of Biomaterials Applications* 27.2 (2012): 153-164.

6. Song, G., and A. Atrens. "Recent insights into the mechanism of magnesium corrosion and research suggestions." *Advanced Engineering Materials* 9.3 (2007): 177-183.

7. Han, H.S., et al. "Conventional and improved cytotoxicity test methods of newly developed biodegradable magnesium alloys." *Metals and Materials International* 21.6 (2015): 1108-1117.

8. International Organization for Standardization, ISO 10993-5. "Biological evaluation of medical devices-Part 5: Tests for in Vitro Cytotoxicity." (2009): 10993-5.

9. International Organization for Standardization, ISO 10993-12. "Biological evaluation of medical devices-Part 12: Sample preparation and reference materials." (2012): 10993-109912.

10. Fischer, J., et al. "Interference of magnesium corrosion with tetrazolium-based cytotoxicity assays." *Acta Biomaterialia* 6.5 (2010): 1813-1823.

11. Jones, L. J., et al. "Sensitive determination of cell number using the CyQUANT® cell proliferation assay." *Journal of Immunological Methods* 254.1-2 (2001): 85-98.

12. Armitage, B. A. "Cyanine dye-DNA interactions: intercalation, groove binding, and aggregation." *DNA Binders and Related Subjects*. Springer, Berlin, Heidelberg, 2005. 55-76.

13. Bruijns, B. B., Roald M. T., and Johannes GE G. "Fluorescent cyanine dyes for the quantification of low amounts of dsDNA." *Analytical Biochemistry* 511 (2016): 74-79.

14. Shindy, H. A. "Fundamentals in the chemistry of cyanine dyes: A review." *Dyes and Pigments* 145 (2017): 505-513.

15. Agha, N. A., et al. "The degradation interface of magnesium-based alloys in direct contact with human primary osteoblast cells." *PloS One* 11.6 (2016): e0157874.

16. Zheng, Y. F., X. N. Gu, and F. Witte. "Biodegradable metals." *Materials Science and Engineering: R: Reports* 77 (2014): 1-34.

17. Witte, F. "The history of biodegradable magnesium implants: a review." *Acta Biomaterialia* 6.5 (2010): 1680-1692.

18. Witte, F., et al. "Biodegradable magnesium scaffolds: Part II: Peri-implant bone remodeling." *Journal of Biomedical Materials Research Part A* 81.3 (2007): 757-765.

19. Witte, F., et al. "In vivo corrosion of four magnesium alloys and the associated bone response." *Biomaterials* 26.17 (2005): 3557-3563.

20. Li, Z., et al. "The development of binary Mg-Ca alloys for use as biodegradable materials within bone." *Biomaterials* 29.10 (2008): 1329-1344.

21. Pietak, A., et al. "Bone-like matrix formation on magnesium and magnesium alloys." *Journal of Materials Science: Materials in Medicine* 19.1 (2008): 407-415.

22. Wang, Y., et al. "Corrosion process of pure magnesium in simulated body fluid." *Materials Letters* 62.14 (2008): 2181-2184.

23. Willumeit, R., et al. "Chemical surface alteration of biodegradable magnesium exposed to corrosion media." *Acta Biomaterialia* 7.6 (2011): 2704-2715.

24. Gordon, J. A., et al. "Bone sialoprotein expression enhances osteoblast differentiation and matrix mineralization in vitro." *Bone* 41.3 (2007): 462-473.

25. Neve, A., A. Corrado, and F. P. Cantatore. "Osteoblast physiology in normal and pathological conditions." *Cell and Tissue Research* 343.2 (2011): 289-302.

26. Müller, W. E., et al. "Mineralization of bone-related SaOS-2 cells under physiological hypoxic conditions." *The FEBS Journal* 283.1 (2016): 74-87.

27. Strzelecka-Kiliszek, A., et al. "Characteristics of minerals in vesicles produced by human osteoblasts hFOB 1.19 and osteosarcoma Saos-2 cells stimulated for mineralization." *Journal of Inorganic Biochemistry* 171 (2017): 100-107.

28. Li, L., et al. "Corrosion and biocompatibility improvement of magnesium-based alloys as bone implant materials: a review." *Regenerative Biomaterials* 4.2 (2017): 129-137.

29. Walker, J., et al. "Magnesium biomaterials for orthopedic application: a review from a biological perspective." *Journal of Biomedical Materials Research Part B: Applied Biomaterials* 102.6 (2014): 1316-1331.

30. Charyeva, O., et al. "Biocompatibility of magnesium implants in primary human reaming debris-derived cells stem cells in vitro." *Journal of Orthopaedics and Traumatology* 17.1 (2016): 63-73.

Chapter 4

4 Development of a Biocompatible Calcium Phosphate Coating with Improved Degradation Resistance for Biodegradable Magnesium Implant Materials

Afrah Al Hegy, Joy Gray-Munro, Eric R. Gauthier

Dept. of Chemistry and Biochemistry and Materials Science Program, Laurentian University, Sudbury, Ontario, Canada, P3E 2C6

(Manuscript)

Abstract

In recent years, there has been growing interest in using magnesium alloys as a new generation of biodegradable materials for orthopaedic applications. However, the rapid degradation of magnesium in physiological environments has prevented its widespread use in medicine. Therefore, surface modification with coatings that slow the degradation rate while also enhancing the biocompatibility of magnesium alloys are of significant interest. In this study, a multilayer coating system consisting of a sol-gel silica layer followed by a mesoporous silica layer and finally a layer of calcium phosphate was designed to meet this goal.

The coating conditions were optimized and the surface characterization results indicate that the multilayer coating of silica sol-gel, mesoporous silica, and calcium phosphate was successfully deposited on magnesium AZ31 alloy. The results from the corrosion test in NaCl solution demonstrate that the optimized multi-layer coating has excellent corrosion resistance. The *in vitro* biodegradation test in physiological solutions confirmed that the multi-layer coating provides an effective protection for the Mg alloy substrate from rapid degradation. Moreover, the cytotoxicity tests showed that the protective layer has no cytotoxic effect on Saos-2 osteoblast cells. These *in vitro* studies confirm that the use of multi-layered coatings consisting of sol-gel silica and calcium phosphate is an effective strategy for controlling both the degradation rate and biocompatibility of magnesium alloys for medical applications.

Keywords: Magnesium alloys, biodegradation, surface modification, mesoporous silica, calcium phosphate

4.1 Introduction

In recent years, magnesium and its alloys have received much attention as potential orthopaedic biomaterials due to their excellent biocompatibility, biodegradability, and mechanical properties that are similar to natural bone. These properties have made magnesium alloys a promising alternative for biodegradable orthopaedic implants that decrease stress shielding and enhance new bone growth [1]. The biodegradability of magnesium provides a good advantage for short term implants that are no longer necessary after healing because the need for a second surgery to remove the implant is eliminated. Unfortunately, the degradation rate of magnesium is fast due to its high chemical and electrochemical reactivity [1,2]. This high degradation rate may result in the loss of implant strength prior to healing. Therefore, the main goal of this study was to create a non-cytotoxic, multi-layered coating to control the degradation rate of magnesium alloys in body fluids.

Many articles have discussed the formation of a covalently bonded protective silica layer on a variety of substrates such as magnesium alloys, aluminum alloys, iron, stainless steel and other metals [3,4,5]. Vasconcelos and his group have demonstrated that sol-gel silica coatings can provide good corrosion protection for stainless steel in a simple salt solution containing 3.5% NaCl [5]. Consequently, a sol-gel silica layer was chosen as the first layer of the multilayer system. It was expected that this layer would not only enhance corrosion resistance but would also improve the adhesion of the mesoporous silica particles by providing Si-OH surface functional groups on magnesium that can undergo a condensation reaction with the Si-OH groups on the surface of the mesoporous silica particles thus forming a strong covalent bond

between the particles and the magnesium surface. The interaction of silane with metal surfaces occurs in two steps according to the sol-gel process. The first step is the hydrolysis of the silane. This occurs when the alkoxy groups react with water to form reactive silanol groups (Si-OH). The second step is the condensation of silane molecules. In this step, the silanol groups can react with each other to form siloxane bonds (Si-O-Si) or they can react with surface hydroxyl groups to form Si-O-Metal bonds. These reactions are shown in reaction scheme 4.1 below:

Reaction Scheme 4.1: Silane Chemistry

1- The hydrolysis of the silane molecules - (sol formation)

2- The condensation of the silane molecules - (gel formation)

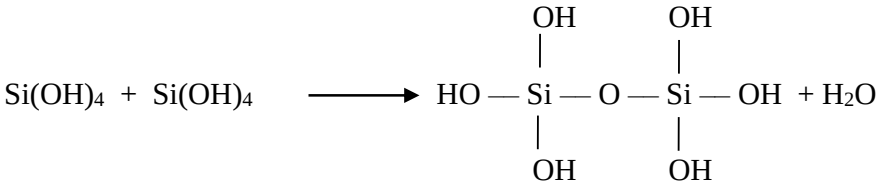

3- The formation of a silane film on metal surfaces

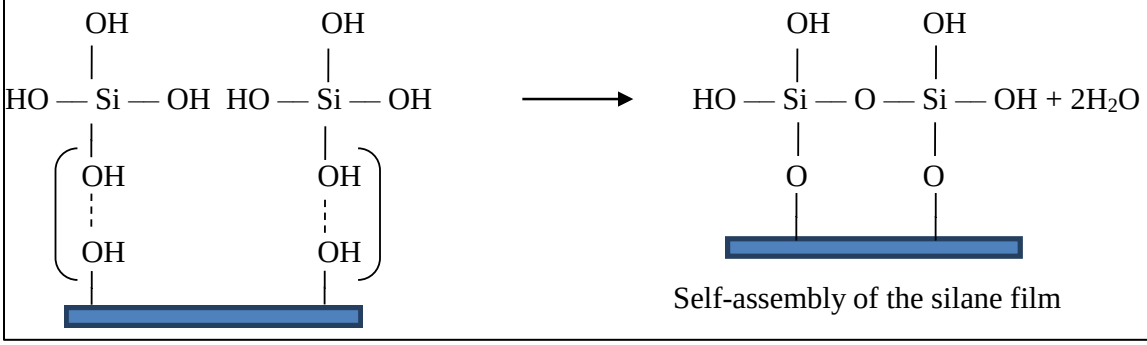

The second layer is a spin-coated mesoporous silica layer. Mesoporous silica is an inorganic material synthesized in the presence of a surfactant or a block co-polymer, which acts as a template, and a silica precursor molecule. Porous materials have been classified by IUPAC according to their pore size; macropores have a diameter greater than 50 nm, micropores have a diameter less than 2 nm and mesopores have a diameter from 2-50 nm. Mesoporous silica materials are synthesized through a combination of the sol-gel processes and self-assembly of the surfactant. A silicate-surfactant species is formed followed by condensation of the siloxane network to form hexagonal arrays and finally the surfactant is removed to produce the mesoporous structure [6]. Mesoporous silica materials have begun to attract attention for biomedical applications due to their high surface areas, high pore volumes, and good biocompatibility [6]. Mesoporous silica materials have been used as a biomaterial coating on different substrates such as titanium, glass and stainless steel due to its biocompatibility, bioactivity, and its ability to be used as a drug-delivery coating [7,8,9]. For example, Ehlert and his co-workers have successfully developed a local drug delivery and biocompatible coating on glass by using mesoporous silica that was loaded with the antibacterial drug ciprofloxacin to prevent bacterial infections after implantation [9]. These materials have been shown to have good bioactivity and the ability to stimulate osteoblast proliferation and differentiation at implant surfaces. Furthermore, they have been shown to be non-toxic and non-inflammatory to mammalian tissues. Gomez-Vega et al. have indicated that mesoporous silica coatings on different substrates (glass, silicon, and titanium), can form apatite when they are immersed in a simulated body fluid [7]. Also, Wang et al. used a mesoporous bioactive glass coating on stainless steel to improve implant-bone integration. The authors reported that the mesoporous

structure of the coating was responsible for protein adsorption followed by osteoblastic cell attachment, proliferation and differentiation [8]. The toxicity and the mechanism of excretion of mesoporous silica materials *in vivo* were also investigated by injecting mesoporous silica particles into a live mouse tail which did not show any evidence of toxic effects during the one month study and the particles of silica were excreted in the urine [10]. The spin-coating technique has been widely used to prepare mesoporous silica coating on many different substrates including glass, silicon and titanium [7,11,12]. Compared to other techniques, spin-coating has several advantages including thin and uniform coating thickness, a low volume of solution is needed for each sample, fast evaporation of solvent and it is a rapid procedure [11,13,14].

The final layer of the coating is a calcium phosphate layer. Biocompatible ceramics such as calcium phosphates are biodegradable inorganic coatings that can be used to enhance the corrosion resistance of metallic implants as well as to improve their surface bioactivity. Calcium phosphate has been used as a coating due to its bioactivity, excellent biocompatibility, non-toxicity, and bone inductivity [15]. It has previously been used as a coating on titanium in order to improve osteointegration and osteoconductivity [16,17]. Recently, calcium phosphate coatings have been used as a protective coating on magnesium alloys [15,18]. Cui et al. reported that a Ca-P coating significantly decreased the degradation rate of AZ31Mg alloy in 3.0% NaCl solution and was very effective in protecting the substrate from rapid degradation [15]. Moreover, Xu et al. evaluated the *in vitro* and *in vivo* behaviour of the surface bioactivity of a calcium phosphate coated magnesium alloy. *In vitro* cell evaluation results showed that cells had

good adherence and proliferation on the Ca-P-coated magnesium alloy thus demonstrating that Ca-P coatings can provide excellent biocompatibility for magnesium alloys. *In vivo* studies of a calcium phosphate coated magnesium alloy demonstrated that the Ca-P coating provided the magnesium alloy with good bioactivity and promoted early bone growth at the implant/bone interface [19].

The objective of this study was to develop a surface modification strategy for magnesium alloys that controls both the degradation rate and the biocompatibility of these materials. In this project, a multilayer system has been developed for this purpose. The multilayers consist of:

1) an initial sol-gel silica layer to enhance corrosion resistance

2) a spin coated mesoporous silica layer to enhance the stability of the subsequent calcium phosphate layer through ingrowth of the calcium phosphate film into the pores of the mesoporous particle layer

3) a layer of calcium phosphate to improve the corrosion resistance as well as provide optimum biocompatibility of the magnesium substrate

4.2 Material and Methods

4.2.1 Materials

Mg AZ31 foil (0.81 mm thickness) was purchased from Alfa Aesar (US). Tetraethoxysilane (TEOS), sodium hydroxide, ammonium hydroxide, dodecyltrimethylammonium chloride, calcium phosphate monobasic and Hanks Balanced salt

solution (Table 4.1) were purchased from Sigma-Aldrich (Canada). Acetone (reagent grade) was purchased from Caledon Laboratory Chemicals (Canada). Bovine Calf Serum (BCS) was purchased from Fisher Scientific (Canada). McCoy's 5a and Trypsin/EDTA (1X) were purchased from Corning (Canada). Phosphate Buffered Saline (PBS) (1X) and Penicillin-Streptomycin Solution were purchased from HyClone (Canada). CyQUANT cell proliferation assay was purchased from Life technologies (Canada). Ethyl alcohol (95%) and methanol were purchased from Commercial Alcohols (Canada). All chemicals were used as received without further purification. The Saos-2 cell line was purchased from American Type Culture Collection (US) and cultured for further experiments.

Table 4.1: Composition of Hanks Balanced Salt Solution.

Component	Concentration (g/L)
$CaCl_2$. $2H_2O$	0.185
$MgSO_4$ (anhyd)	0.09767
KCl	0.4
KH_2PO_4(anhyd)	0.06
$NaHCO_3$	0.35
Na_2HPO_4(anhydrous)	8.0
D-Glucose	0.04788

4.2.2 Sample Preparation

The AZ31 magnesium alloy was cut into circular discs with a diameter of 1.27 cm and then polished to a one-micron surface finish to remove the gross oxide layer. In order to clean and remove any excess polishing oil from the surface of the alloys, they were sonicated in acetone for 20 minutes and then rinsed in deionized water for 30 seconds. Then, the samples were immersed into an alkaline bath (0.05 M NaOH, pH 12.5) at 50 °C for one hour to promote the formation of surface hydroxyl groups.

4.2.3 Coating Processes

An overview of the coating process used is shown in Schematic Diagram 4.1. In brief, the magnesium alloy AZ31 samples were polished, cleaned and alkaline aged. A multi-layer coating was then deposited on the substrate. The multilayers consist of an initial sol-gel silica layer, followed by a spin coated of mesoporous silica layer and finally a layer of calcium phosphate.

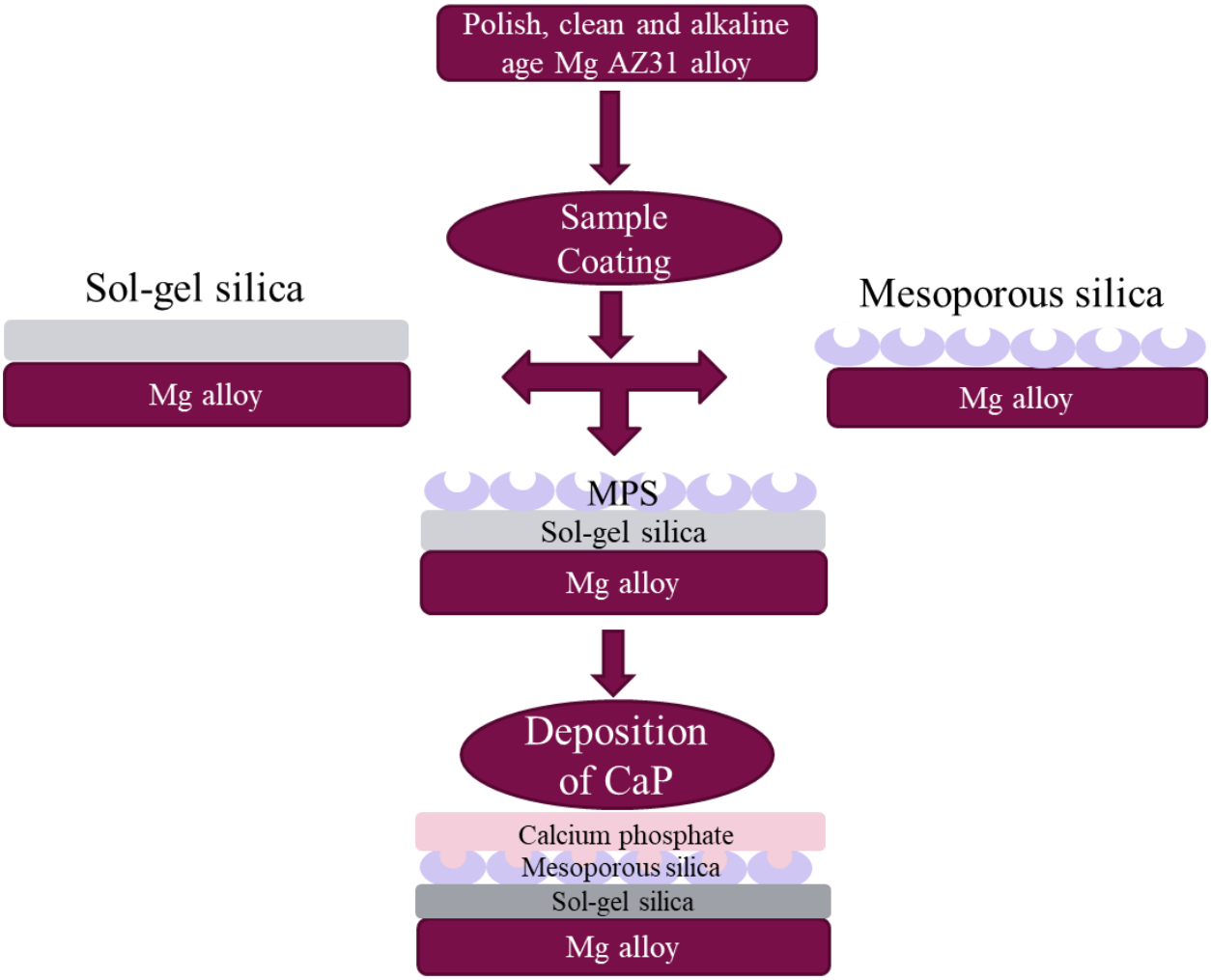

Schematic Diagram 4.1: An Overview of the Coating Process

4.2.3.1 Sol-gel Silica Layer

The silane coating solution was prepared by using a 6% (v/v) TEOS, 14% (v/v) deionized water, 6% (v/v) ammonium hydroxide, and 74% (v/v) methanol as a solvent. The solution was allowed to stir for 24 hours to ensure complete hydrolysis before coating. Then the samples were

immersed in the solution for 20 min. After coating, the samples were dried before curing in an oven for 1h at 100 °C.

4.2.3.2 Mesoporous Silica Layer

The mesoporous silica layer was spin-coated from solution onto the magnesium substrate. The mesoporous silica coating solutions were prepared by using TEOS as a silica precursor and the cationic surfactant C_{12}TAC (dodecyltrimethylammonium chloride) as the templating agent in deionized water, ammonium hydroxide, and methanol as the solvent. The molar ratio of TEOS: C_{12}CAT: deionized water, methanol, and ammonia was 1:0.4:774:1501:72. Therefore, 100 mL of methanol was mixed with 0.248 g of C_{12}TAC, 17.7 mL of deionized water, 8 mL of 28% aqueous ammonia solution and 0.368 mL of TEOS. The solution was pre-hydrolyzed for 1h prior to spin coating. Subsequently, 100 μL of the coating solution was pipetted onto the substrate, which were spun for a minute at 2000 rpm. This process was repeated until the required number of layers was deposited. The samples were cured for 1h after coating. To remove the surfactant, the coated samples were calcined at 350°C for 3h.

4.2.3.3 Calcium Phosphate Layer

The calcium phosphate layer was deposited by dip coating the sol-gel silica+mesoporous silica coated substrates in an aqueous calcium phosphate solution. The calcium phosphate coating solution was prepared by dissolving monocalcium phosphate ($Ca(H_2PO_4)_2$) in deionized water (pH ~ 4.5); the solution was stirred overnight to ensure complete dissolution.

The Mg AZ31 samples were immersed into 25 mL of the calcium phosphate solution; both 3 mM and 6 mM concentrations were tested. The coating process was further optimized as a function of deposition time (1, 3, and 7 days) to determine the best coating conditions for a stable and uniform calcium phosphate layer on the surface of the mesoporous silica coated magnesium alloy. After coating, the samples were rinsed with deionized water and then air dried.

4.2.4 Magnesium Release Rate in NaCl Solution

The degradation rate of the coated samples compared to uncoated Mg AZ31 was evaluated by monitoring the amount of magnesium released into solution as a function of time upon immersion in 3.5% (w/v) NaCl solution at room temperature. The samples were mounted in epoxy to ensure a uniform surface area and surface chemistry for the corrosion test. Each sample was immersed in 40 mL of NaCl solution. At 24 hour intervals, the solutions were mixed well and a 100 μL aliquot was taken from the solution and diluted to 10 mL in a 2% nitric acid solution. The concentration of magnesium in the diluted solutions was determined using flame atomic absorbance spectroscopy with a Perkin Elmer AA analyst 400 spectrometer. Quantification was performed using a calibration curve of known concentrations of magnesium (0.05, 0.1, 0.2, and 0.5 mg/L).

4.2.5 *In Vitro* Degradation Study in Simulated Body Fluid (SBF)

To compare the degradation rates of the coated samples to the uncoated magnesium alloy, the concentration of magnesium ions was measured as a function of time by flame atomic absorbance spectroscopy as described in section 4.2.4. The mounted samples were immersed into 40 mL of Simulated Body Fluid (SBF). The samples were stored at 37 °C to mimic *in vivo*

conditions according to ASTM standard. The solutions were changed daily over a one week period. Each day, a 100 µL aliquot was taken from the solution, diluted to 10 mL with 2% HNO_3 in a volumetric flask and processed for the flame atomic absorbance spectroscopy. Finally, the samples were removed from the solution after seven days and they were rinsed with deionized water. The samples were dried prior to further analysis.

4.2.6 Cytotoxicity Test

The cytotoxicity was evaluated using an indirect method: already growing cells were exposed to a magnesium alloy conditioned culture medium prepared by incubating the uncoated and coated magnesium samples in cell culture medium for 72 hours at 37ºC in a 5% CO_2 atmosphere.

4.2.6.1 Preparation of Magnesium Alloy Conditioned Extract

Prior to the cytotoxicity experiment, all samples were sterilized in 70% ethanol for 10 minutes followed by washing with warm (37ºC), sterile PBS. The uncoated and coated Mg alloys were placed in a 24-well plate that contained cell culture medium only (2 mL of McCoy's medium/ per well) and then incubated for 72 hrs at 37ºC in a 5% CO_2 atmosphere. Then, the conditioned medium was used for the indirect test.

4.2.6.2 Cell Culture

Human osteosarcoma Saos-2 cells were cultured in McCoy's 5a cell culture medium containing 15% Bovine Calf Serum and 1% penicillin/streptomycin at 37ºC in a 5% CO_2 atmosphere. The cell culture medium was changed every two days. Once the cells grew to about

70-80% confluence, they were washed with PBS and detached from the flask with Trypsin/EDTA and then centrifuged at 2500 rpm for 5 minutes. The supernatant was discarded, and the cells were resuspended in fresh McCoy's medium. The number of cells in the suspension was determined by the trypan blue dye using a Neubauer hemocytometer. Then, the cells were used for the indirect experiment.

4.2.6.3 Indirect Test

15,000 cells were seeded in a 96-well plate in triplicate for each sample type. Cells were incubated at 37℃ in a 5% CO_2 for 24 hours to allow attachment to the plate surface. After 24 hours of incubation, the cell culture medium was removed and replaced by 200 µL of the magnesium conditioned medium. The plate was then incubated for another 24 hrs at 37℃ in a 5% CO_2 atmosphere. After 24 hrs, the magnesium conditioned media were removed, the cells in the 96-well plates were rinsed with warm PBS in order to remove non-adherent cells, and the plate was frozen at -20ºC at overnight for the cells to lyse. Cells cultured in fresh, non-conditioned medium was used as a control group.

4.2.6.4 Cytotoxicity Assay

The cell numbers were determined using the CyQUANT assay. The CyQUANT assay does not depend on a reaction with cellular metabolic products as other assays do but rather on the interaction of a dye with the cellular nucleic acids. The cell numbers can be determined by measuring the fluorescence intensity of the DNA-bound dye.

The CyQUANT assay was used according to the supplier's instructions. 200 µL of CyQUANT solution was added to each sample and incubated for 5 minutes. At the end of the incubation period, 100 µL of the CyQUANT solution was pipetted from each well to a black fluorescent 96-well plate (Costar) and the fluorescence intensity of each solution was measured with a Fluostar Optima spectrofluorometer. The cell number was then determined using a calibration curve of known number of cells vs. fluorescence intensity. The experiment was repeated two times to ensure the reliability of the results. The experiments were run on different days in triplicate. Uncoated and coated samples were analyzed in comparison to the control (cells grown in non-conditioned cell culture medium).

The cell viability was reported as a percentage of the number of viable cells in the presence of magnesium conditioned extract in cell culture media in comparison to the number of viable cells in the absence of magnesium extract in cell culture media (control). The cell viability percentage was calculated as the following equation:

$$Cell\ viability\% = \left(\frac{number\ of\ viable\ cells\ exposed\ to\ Mg\ extract}{number\ of\ viable\ cells\ in\ control\ sample}\right) * 100$$

4.2.7 Surface Characterization

4.2.7.1 Attenuated Total Reflection Fourier Transform Infrared Microscopy (ATR-FTIR)

Attenuated total reflection Fourier transform infrared microscopy (ATR-FTIR) was used to analyze the surface of the alloys after each step to determine the chemical functional groups

on the surface of the coated Mg alloys. A Bruker Optics Hyperion infrared microscope equipped with an attenuated total reflectance objective and a germanium crystal was employed. The resolution of the spectrometer was 4 cm^{-1} and 100 scans were taken per spectra. Spectra were collected at three spots for each sample. The spectra were corrected with the atmospheric compensation function of the OPUS software to remove water vapour and CO_2 from the spectra. In addition, the baseline for each spectrum was corrected using the OPUS software.

4.2.7.2 Atomic Force Microscopy (AFM)

Atomic force microscopy (AFM) was used to characterize the surface morphology of the as-deposited mesoporous silica coatings on the surface. A Bruker multimode AFM III D was used to capture the images in tapping mode. Bruker AFM TESPA probes with a resonant frequency of approximately 320 KHz were used. An image area of 5 μm x 5 μm was scanned at a scan rate of 0.5 Hz and 512 samples/line. The images were flattened using the Nanoscope Analysis software and are presented without any further modification.

4.2.7.3 Scanning Electron Microscopy and Energy Dispersive X-ray Spectroscopy (SEM-EDS)

Scanning electron microscopy and energy dispersive X-ray spectroscopy (SEM-EDS) were used to evaluate the surface morphology and surface chemical composition of the samples. SEM images were obtained using a JEOL 6400 field emission SEM operated at 20kV, 1 nA and 10^{-6} Torr. An Oxford EDS detector was used to determine the elemental composition of the

sample surface. Samples to be analyzed were coated with a thin film of carbon to render the sample conductive.

4.2.7.4 Flame Atomic Absorption Spectroscopy (FAAS)

Flame atomic absorption spectroscopy (FAAS) was performed with a Perkin Elmer AA analyst 400 spectrometer. This technique was used to measure the concentration of magnesium ions that had been released into the solution during the degradation tests. The concentration measurements were done by using a calibration curve for standards of known concentrations of magnesium (0.05, 0.1, and 0.2 mg/L). An SBF control set was used to compare the concentrations of magnesium ions in the SBF solution with the solutions that had been exposed to the coated and uncoated magnesium alloy. The samples for analysis were prepared as previously described in sections 4.2.4 and 4.2.5.

4.3 Results and Discussion

4.3.1 Optimization of the Multi-layered Coating Conditions

Surface modification is one of the most effective ways to create an optimum biodegradable orthopedic implant. In this study, a multi-layered biocompatible and protective coating surface was developed to control the biodegradation rate and improve the surface biocompatibility of a magnesium alloy. The surface chemistry and morphology of each layer was characterized and the conditions were optimized to give a final multilayered coating with the optimized degradation resistance. This was determined by immersing the samples in a 3.5% sodium chloride solution for up to one week and comparing the amount of magnesium released

for the coated samples in comparison to the control samples. The multilayered coating that gave the lowest magnesium release was designated as the best overall coating.

4.3.1.1 Deposition of the Sol-Gel Silica Coating (Layer 1)

In order to enhance the corrosion resistance of the Mg alloy and improve the adhesion of the mesoporous silica particles (layer 2) on the surface, a sol-gel silica layer was deposited. This layer is capable of covalently bonding to the magnesium alloy surface through the formation of Mg-O-Si groups via a condensation reaction between the silanol groups of the hydrolyzed TEOS molecules and surface Mg-OH functional groups. In addition, silanol (Si-OH) present at the surface of this coating can covalently bond to the mesoporous silica particles through a condensation reaction between the silanol groups at the surface of the coating and the silanol groups on the surface of the mesoporous silica particles. The surface chemistry and morphology of the as-deposited sol-gel silica coated samples were characterized by infrared microscopy and high-resolution scanning electron microscopy (HRSEM), respectively.

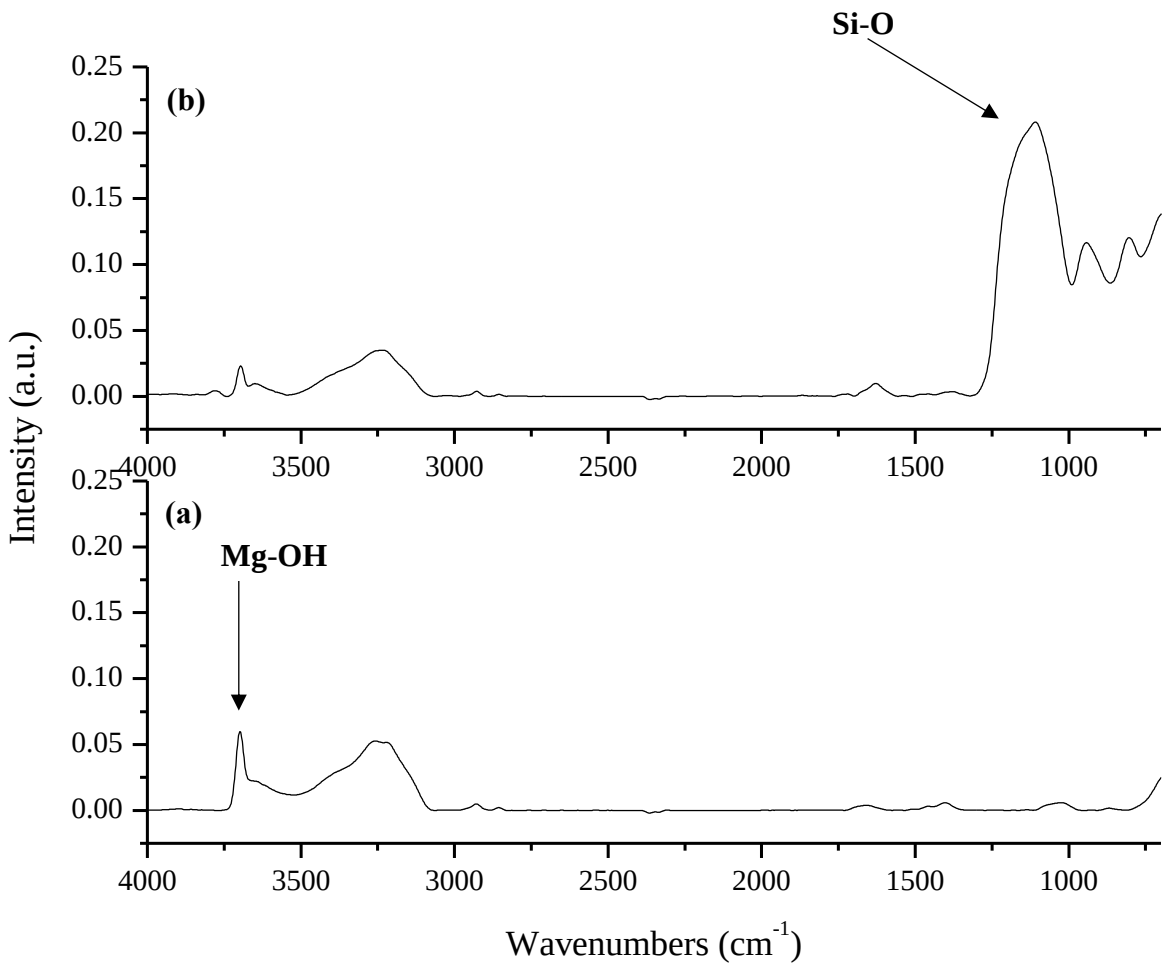

Figure 4.1: IR Spectra of Mg Alloy Before and After Coating with Sol-gel Silica (TEOS Concentration 6% (v/v), Deposition Time 20 Minutes). (a) Polished Magnesium Alloy AZ31 before coating (Control) and (b) Sol-gel Silica Coated Magnesium Alloy AZ31.

Figure 4.1 shows representative infrared spectra for the Mg alloy before and after coating with sol-gel silica. The surfaces of the magnesium alloy samples were polished, cleaned and alkaline aged prior to coating. Figure 4.1 (a) shows an IR spectrum of Mg AZ31 alloy after

surface pre-treatment. This spectrum has a sharp peak (O-H stretch) at 3700 cm^{-1} which indicates the presence of crystalline $Mg(OH)_2$. The formation of hydroxyl groups on the surface of the magnesium alloy is very important for covalent bond formation between the metal and the sol-gel silica coating. Moreover, a broad peak (O-H stretch) from 3000 to 3500 cm^{-1} and a peak (O-H bend) at 1640 cm^{-1} were observed which can be attributed to either surface adsorbed water and/or non-crystalline magnesium hydroxide on the surface. A carbonate (CO_3^{2-}) peak is also observed at 1450 cm^{-1} due to the reaction of the magnesium surface with carbon dioxide in the atmosphere. In addition, despite the extensive cleaning regimen, peaks at 2850-2930 cm^{-1} (CH_2/CH_3 stretch) were also observed indicating that a small amount of organic contamination is still present on the surface after the pre-treatment process.

Figure 4.1 (b) shows a representative infrared spectrum of the sol-gel silica coated magnesium alloy prepared by immersing the pretreated magnesium alloy sample in a 6% (v/v) TEOS solution for a deposition time of 20 minutes. These specific coating conditions for the sol-gel silica layer were chosen based on our previous studies which had demonstrated that high TEOS concentration coupled with long deposition time resulted in non-uniform films whereas high TEOS concentration with low deposition time produced sol-gel silica film with good thickness and uniformity that can be employed as a protective layer on Mg alloys [20].

As shown in Figure 4.1 (b), a new broad peak was observed after coating at 1050-1250 cm^{-1} which is attributed to the Si-O stretch and confirms the condensation of the hydrolysed TEOS to form a sol-gel silica coating on the surface of the magnesium alloy. It was also observed that the intensity of both the $Mg(OH)_2$ peak at 3700 cm^{-1} and the carbonate peak at 1450 cm^{-1} decrease.

The decrease in intensity of the substrate further confirms the presence of the coating on the surface as the sampling depth of the ATR-FTIR technique is limited to a maximum of 1 μm. However, this peak at 3700 cm^{-1} may also be attributed to the presence of silanol (Si-OH) groups which would further confirm successful deposition of the sol-gel silica layer.

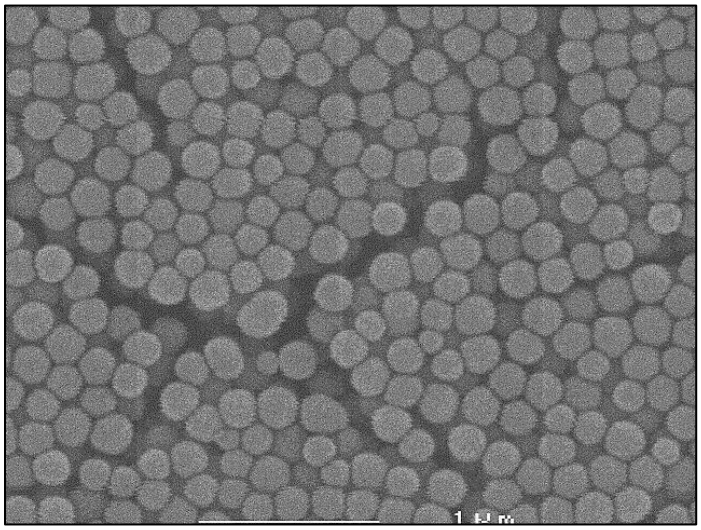

Figure 4.2: High-Resolution Scanning Electron Microscopy (HRSEM) Image of Sol-gel Silica Coated Mg Alloy (TEOS Concentration 6% (v/v), Deposition Time 20 Minutes).

Figure 3.2 shows a high-resolution SEM image of the sol-gel silica coated magnesium alloy surface (6% (v/v) TEOS, deposition time -20 minutes). The image shows that the deposited TEOS layer is composed of particles that have an ordered hexagonal structure. An ordered hexagonal structure was obtained due to the use of basic catalysis during coating formation. In basic catalysis, the hydrolysis rate of the molecules is slower, but the condensation rate is faster which leads to the production of compact colloidal particles [21]. The size of these particles is approximately 150-200 nm in diameter and they are distributed across the entire surface.

Furthermore, all of the sol-gel silica coated samples analyzed have similar morphologies indicating excellent sample to sample reproducibility of the coating.

From the IR spectra and HRSEM image results obtained after the deposition of the sol-gel silica coating, it is clear that the sol-gel silica layer was successfully deposited with good thickness and uniformity. It is therefore an appropriate method to enhance corrosion resistance and to improve the adhesion of the mesoporous silica particles by a further condensation reaction through the Si-OH at the surface of the sol-gel coating and those on the surface of the mesoporous silica particles from layer 2.

4.3.1.2 Optimization of the Mesoporous Silica Coating Conditions (Layer 2)

The second layer of the multi-layered coating is a spin-coated mesoporous silica layer. This type of coating was chosen due to the possibility of enhanced stability of the subsequent calcium phosphate layer due to ingrowth of the calcium phosphate into the pores of the mesoporous silica layer.

4.3.1.2.1 Optimization of the Mesoporous Silica Coating Conditions on Bare Magnesium Alloys

To determine the best coating conditions for the mesoporous silica layer without having interference from the underlayer of sol-gel silica, the effect of the number of spin coated layers on the structure and uniformity of the mesoporous silica coating was investigated first on bare magnesium. The mesoporous silica coated samples were analyzed by infrared microscopy to

determine the chemical functional groups on the surface and to ensure the successful deposition of the mesoporous silica layer on the surface of the magnesium alloy. Furthermore, atomic force microscope (AFM) was used to characterize the surface morphology of the mesoporous silica coatings as a function of the number of spin-coated layers.

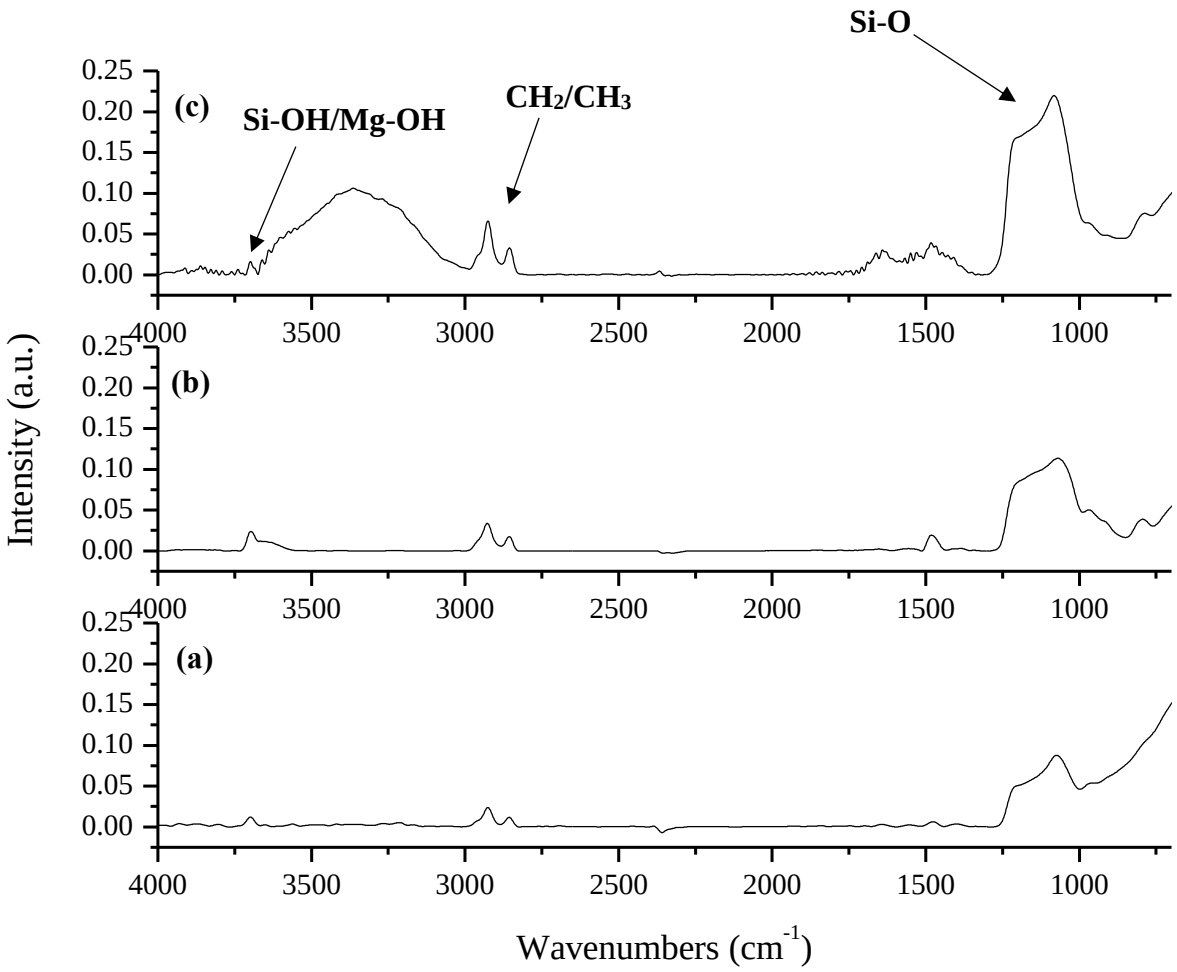

Figure 4.3: IR Spectra for as Deposited Mesoporous Silica Layers on Bare Magnesium Alloy as a Function of the Number of Treatments. (a) 3 Spin-treatment, (b) 6 Spin-treatment and (c) 9 Spin-treatment of as Deposited Mesoporous Silica Coating.

An infrared spectrum for the as-deposited mesoporous silica layer on the bare Mg alloy is shown in Figure 4.3. There are three peaks of particular interest that can be attributed to the presence of the mesoporous silica coating on the surface. The first is the (Si-O) peak at 1050-

1250 cm^{-1} which indicates the presence of silicate. The second is the (CH_2/CH_3) stretch at 2850-3000 cm^{-1} which confirms the presence of the surfactant in the coating. The third is the sharp peak at 3700 cm^{-1} which may be attributed to either Si-OH or Mg-OH functional groups. From Figure 4.3 (a), (b), and (c), It is clear that the deposited mesoporous silica coating is present in all cases and the increase in intensity of the Si-O band and surfactant peaks in these spectra indicates that the coating thickness increased with an increasing number of spin-treatments. It was also observed that the silicate peak at 1050-1250 cm^{-1} is composed of two overlapping bands which demonstrates that as the number of spin-treatments increases, the silane molecules efficiently condense with each other to form Si-O-Si bond at 1050 $cm^{-1}$and also condense with magnesium hydroxyl groups on the substrate surface to form Si-O-Mg bond at 1200 cm^{-1}, however, this peak at 1200 cm^{-1} could also be due to an Si-O-C bond indicative of the presence of some unhydrolyzed silane molecules.

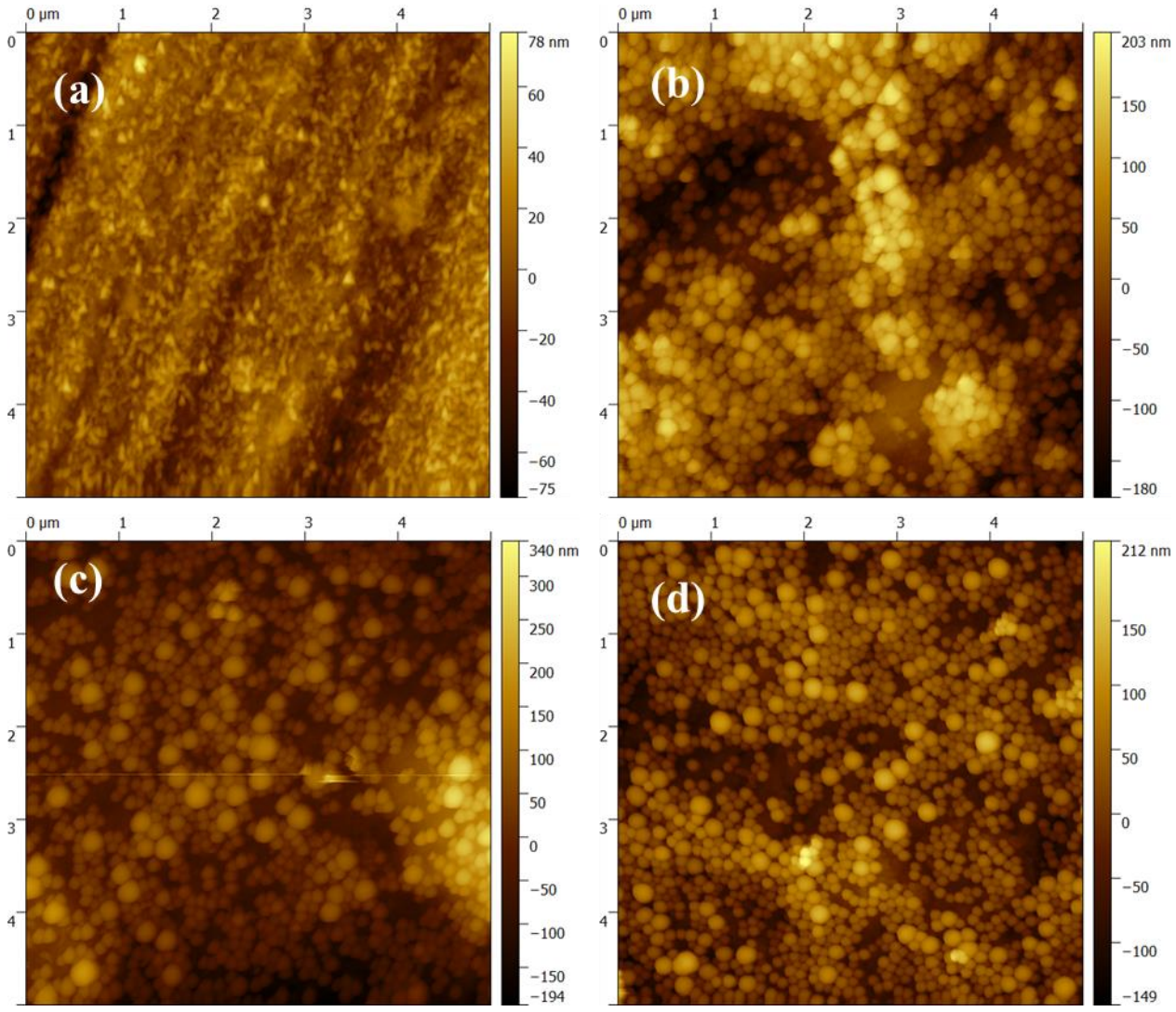

Figure 4.4: AFM Images of Mesoporous Silica Layer on Bare Magnesium Alloys as a Function of the Number of Treatments. (a) Uncoated Polished Mg AZ31 (b) 3 Spin-treatments, (c) 6 Spin-treatments and (d) 9 Spin-treatments of Mesoporous Silica Coating.

Atomic Force Microscopy (AFM) was used to determine the topography of the mesoporous silica layers that were deposited on the surface of the magnesium alloy substrate. Figure 4.4 (a) is representative the AFM image of the uncoated, polished magnesium alloy AZ31

and shows the polishing grooves on the surface of the substrate. Figure 4.4 b, c, and d show the AFM images of the magnesium alloy substrate after 3, 6 and 9 spin-treatments of the mesoporous silica coating. Upon comparison to the bare magnesium surface, it is clear that the polishing grooves of the magnesium substrate completely disappeared after spin coating due to the formation of a spherical particle layer on the surface of the samples. From Figure 4.4 (b, c, and d), it is clear the surface density of the mesoporous silica particles increases as a function of the number of spin-treatments which correlates with the observed increase in silica peak intensity from the infrared spectra in Figure 4.3. It is also clear from image (d) that the surface density of spherical particles increases to the point that a uniform layer of mesoporous silica is present on the surface. Therefore, 9 spin-treatments was chosen as the best condition to obtain a uniform film of mesoporous silica particles on the magnesium alloy substrate.

4.3.1.2.2 Deposition of the Mesoporous Silica Coating on the Sol-gel Silica Layer

After determining the best coating conditions for the mesoporous silica layer, the two part multilayer consisting of mesoporous silica layer on top of the sol-gel silica under layer was characterized before and after calcination. The coated samples were calcined at 350°C for 3h in order to remove the surfactant and therefore obtain the mesoporous structure.

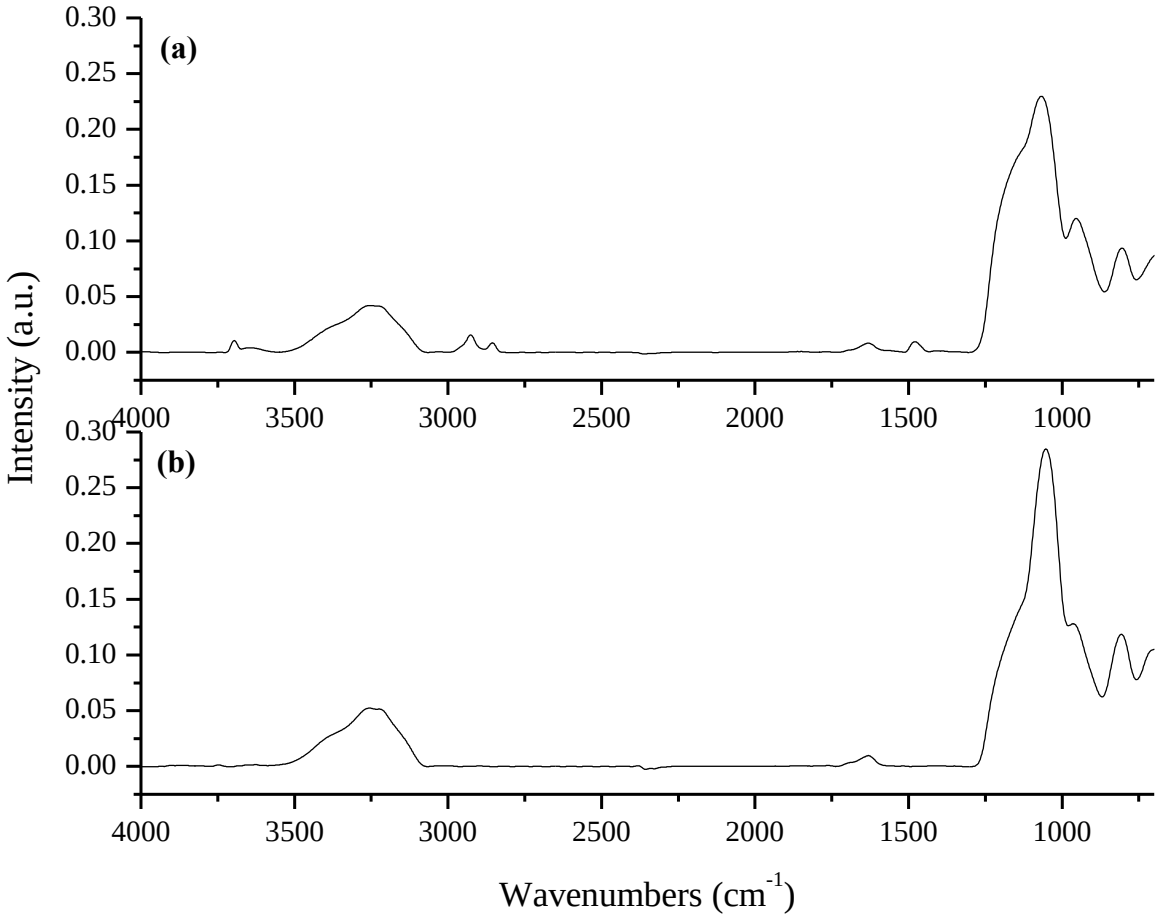

Figure 4.5: IR Spectra of Magnesium Alloy Coated with Sol-gel Silica Layer + Mesoporous Silica Layer Before (a) and After (b) Calcination.

Figure 4.5 shows the infrared spectra of the duplex coating consisting of a first layer of sol-gel silica and a second layer of mesoporous silica before and after calcination. The spectrum before calcination Figure 4.5 (a) indicates that the multi-layered film has all the peaks that are

indicative of the presence of a sol-gel silica layer and the as-deposited mesoporous silica film on the surface of the magnesium alloy.

In order to obtain the mesoporous structure of the top layer, the surfactant must be removed after the coating has been deposited on the surface. From the spectra after calcination Figure 4.5 (b), It was observed that the surfactant peaks disappeared completely after calcination of the coated magnesium substrate. Moreover, the peak at 3700 cm^{-1} which is due to the presence of either Mg-OH or silanol (Si-OH) peaks has completely disappeared after calcination. Thus, this peak can be attributed to the presence of Si-OH bonds due to incomplete condensation before calcination; thermal treatment leads to further condensation of the silanol groups converting them to silicate Si-O-Si or Si-O-Mg.

These results confirm the successful deposition of a uniform and thermally stable mesoporous silica film on top of the sol-gel silica layer.

4.3.1.3 Optimization of the Calcium Phosphate Coating Conditions (Layer 3)

4.3.1.3.1 Deposition of Calcium Phosphate (layer 3)

To determine the best coating conditions for the calcium phosphate (CaP) layer, the effect of varying the coating deposition time and the concentration was studied. The coated samples were analyzed by infrared microscopy to compare the thickness and uniformity of the calcium phosphate films deposited on the mesoporous silica + sol-gel silica coated magnesium alloys. Infrared spectroscopy was also used to identify the chemical composition of the calcium

phosphate layer while SEM-EDS was used for characterization of the surface morphology of the deposited calcium phosphate layer.

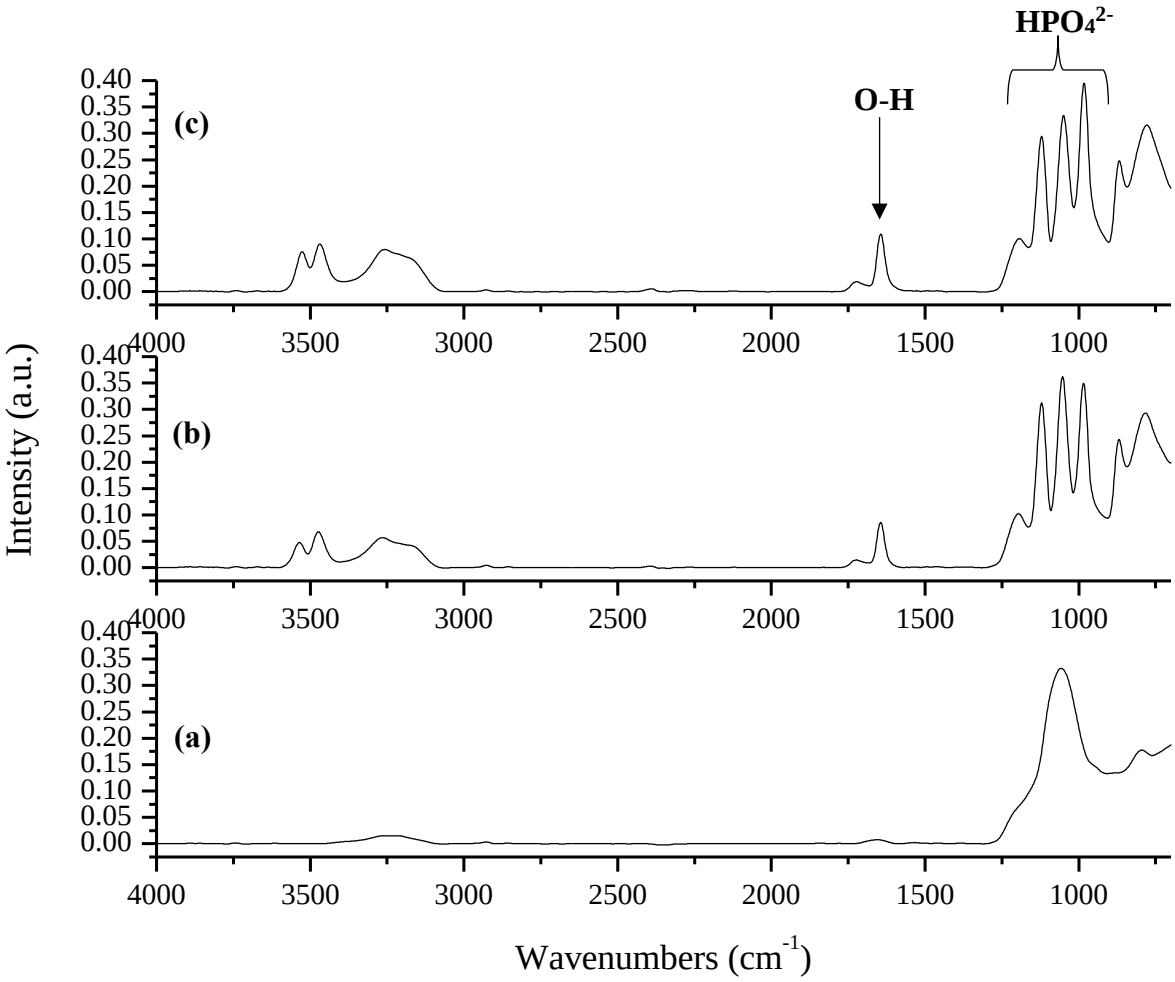

Figure 4.6: IR Spectra for Calcium Phosphate Deposited on Mesoporous Silica + Sol-gel Silica Coated Mg AZ31 after Immersion in a 3 mM Calcium Phosphate Solution for Various Deposition Times. (a) 1 Day, (b) 3 Days and (c) 7 Days Deposition Time in Calcium Phosphate Solution.

Figure 4.6 shows the IR spectra for calcium phosphate deposited on mesoporous silica coated Mg AZ31 from a 3 mM calcium phosphate solution as a function of immersion time. After a 1 day calcium phosphate deposition time (Figure 4.6 (a)), the spectrum shows a strong peak at 1050-1150 cm^{-1} which can be attributed to phosphate (PO_4^{3-}) or silicate peaks, both phosphorus and silicon were observed in the EDS spectra for this sample type (Table 4.1). The spectra after 3 and 7 days deposition (Figure 4.6 (b, c) show three strong peaks at 1122, 1052, and 984 cm^{-1} corresponding to phosphate present as brushite ($CaHPO_4.2H_2O$). A sharp peak (O-H bend) at 1640 cm^{-1} was also observed and is attributed to the presence of intercalated water within the brushite crystal lattice. The two peaks appearing as a doublet at 3527 and 3468 cm^{-1} are due to O-H stretch modes of the water in brushite [22,23].

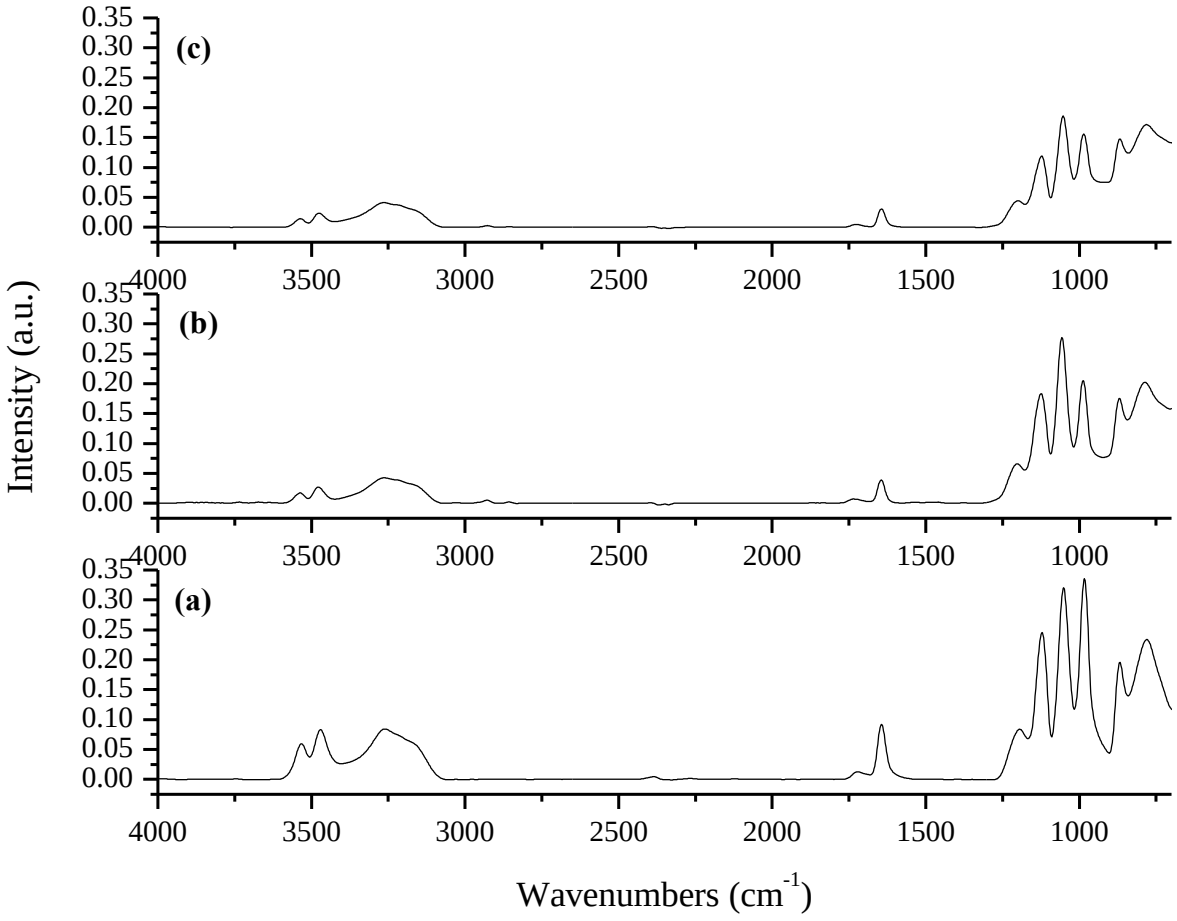

Figure 4.7: IR Spectra for Calcium Phosphate Deposited on Mesoporous Silica Coated Mg AZ31 after Immersion in a 6 mM Calcium Phosphate Solution for Various Deposition Times. (a) 1 Day, (b) 3 Days and (c) 7 Days Deposition Time in Calcium Phosphate Solution.

Figure 4.7 shows the IR spectra for calcium phosphate deposited on mesoporous silica coated Mg AZ31 from a 6 mM calcium phosphate solution as a function of immersion time. From Figure 4.7 (a, b, and c), all the spectra show three strong peaks at 1122, 1052, and 984

cm^{-1} corresponding to phosphate. The three peaks are attributed to the presence of the calcium phosphate coating on top of the mesoporous silica coating. This result suggests that the deposited calcium phosphate is brushite ($CaHPO_4.2H_2O$). However, Figure 4.7 (c) shows that increasing the deposition time to 7 days does not have a significant effect on the structure of the calcium phosphate layer. Therefore, only 1 day and 3 days deposition time were chosen for further optimization studies.

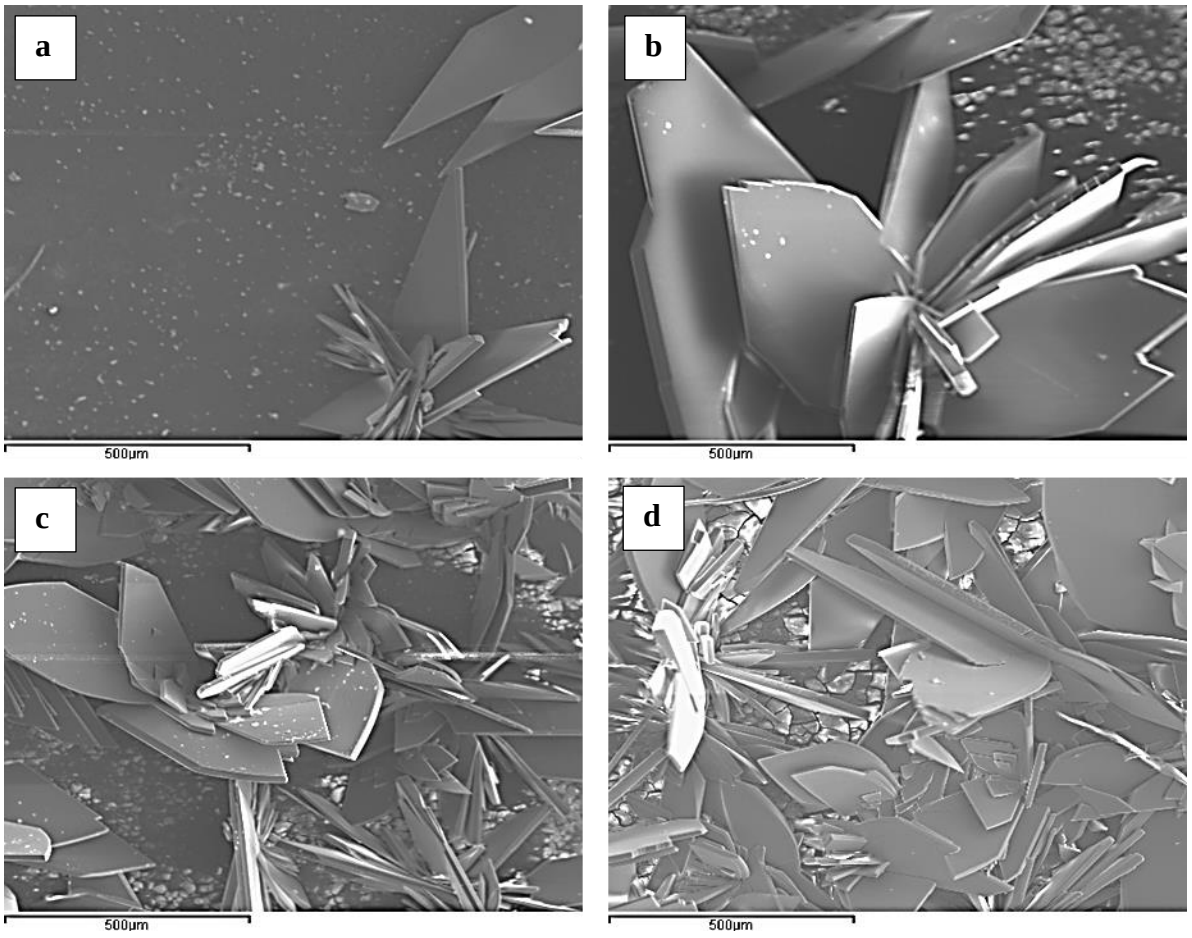

Figure 4.8: SEM Images for Calcium Phosphate Deposited on Mesoporous Silica Coated Mg AZ31 as a Function of Deposition Time and Concentration of Calcium Phosphate. (a) 1 Day and (b) 3 Days of Deposition Time in 3 mM Calcium Phosphate Solution. (c) 1 Day and (d) 3 Days of Deposition Time in 6 mM Calcium Phosphate Solution. Scale Bar = 500 µm.

The morphology and elemental composition of the calcium phosphate layer were characterized by SEM-EDS. Figure 4.8 shows the SEM images of the calcium phosphate deposited on mesoporous silica coated Mg AZ31 as a function of deposition time and concentration of calcium phosphate. The SEM images show that the deposited calcium

phosphate layer has a plate-like structure that is characteristic of brushite as shown in the literature and confirmed by our IR spectroscopy results [24].

The image of the calcium phosphate layer deposited with a 1 day deposition time and 3 mM of calcium phosphate (Figure 4.8 (a)) shows a high variability on the surface due to the formation of brushite (a plate-like structure) in some areas while other areas have small nodules on the flat surface. However, the atomic percentage of magnesium was very high in these samples as shown by the EDS analysis in Table 4.1. This indicates that the deposited calcium phosphate layer prepared with 3 mM of calcium phosphate and 1 day of deposition time was thin and non-uniform. However, after increasing the deposition time to 3 days (Figure 4.8 (b)), the surface was covered with more brushite which indicates that increasing the deposition time may increase the uniformity of the deposited calcium phosphate layer. Moreover, significant amounts of magnesium and silicon were detected on the flat areas of the 1 day and 3 days CaP coated samples prepared in a 3 mM calcium phosphate solution. The SEM images (a and b) coupled with the EDS results in (Table 4.1) suggest that the surface was not fully covered by calcium phosphate when the coating bath concentration was only 3 mM in calcium phosphate.

Figure 4.8 (c,d) show the SEM images of the calcium phosphate layer deposited from a 6 mM calcium phosphate solution. It is clear from these images that the surfaces were completely covered with crystalline brushite at the higher concentration as the plate-like brushite structures are present over the entire surface. Furthermore, the disappearance of magnesium and silicon from the EDS spectra coupled with the increasing calcium atomic percentage indicates that the thickness of the calcium phosphate layer increases when the concentration of calcium phosphate

in the solution is increased to 6 mM. However, the surface of the deposited calcium phosphate after increasing the deposition time from 1 day to 3 days (Figure 4.8 (d)) does not show a significant different on the structure and uniformity of the deposited calcium phosphate layer.

It is clear from the SEM images (Figure 4.8) and EDS analysis (Table 4.1) that the thickness and uniformity of the deposited calcium phosphate layer increases with an increase in the concentration of calcium phosphate. However, it seems that deposition time does not have a significant effect on the thickness of the brushite layer. Therefore, 1 day and 3 day samples prepared from a 6 mM of calcium phosphate solution were used for further study to determine the stability of the calcium phosphate coating on the mesoporous silica layer.

Table 4.2: The Atomic Percentage of Elements after Deposition of Calcium Phosphate on Mesoporous Silica Layer. Data are the Average of Three Spots of each Area.

Atomic %	[CaP]	3 mM		6 mM	
	Deposition Time	1 day	3 days	1 day	3 days
Mg	Flat Area	27.4±1.5	16.3±5.7	0	0
	Brushite Area	1.26±1.2	0	0	0
Si	Flat Area	9.70±1	3.51±0.35	0.21±0.36	0
	Brushite Area	0.70±0.57	0.07±0.06	0.06±0.05	0
P	Flat Area	9.78±0.96	13.82±0.68	12.49±12.63	7.09±2.73
	Brushite Area	10.57±5.07	14.73±1.77	13.41±1.58	7.20±3.3
Ca	Flat Area	0.3±0.24	3.60±1.46	40.64±7.57	34.26±10.27
	Brushite Area	16.45±6.76	16.90±6.00	11.65±3.28	13.14±7.51

4.3.1.3.2 Magnesium Release Rate in 3.5% NaCl Solution: Selection of the Optimum Coating Conditions for the Final Multi-layered Coating

Poor corrosion resistance is the major issue that has restricted the widespread use of magnesium alloys in biomedical application. The chemical and electrochemical reactivity of magnesium alloys are considered high when compared with other structural metals such as steel and aluminum alloys. The corrosion reaction of pure magnesium proceeds by an electrochemical reaction with water as shown in Reaction Scheme 4.2. This reaction produces hydrogen gas, magnesium ions and hydroxide ions. This corrosion reaction leads to precipitation of magnesium hydroxide at the surface. The film of $Mg(OH)_2$ can provide protection and reduce the corrosion rate of magnesium. However, in the presence of chloride anions, this film is readily converted into soluble $MgCl_2$ according to Reaction Scheme 4.3 [25]. As the hydroxide layer is converted to soluble $MgCl_2$, the underlying substrate is continually exposed to the corrosive media resulting in pitting corrosion of the substrate.

Reaction Scheme 4.2: Corrosion Reaction.

$$Mg_{(s)} + 2H_2O_{(l)} \rightarrow Mg(OH)_{2\,(s)} + H_{2\,(g)}$$

Reaction Scheme 4.3: Influence of Anions.

$$Mg(OH)_{2\,(s)} + 2Cl^-_{\,} \rightarrow MgCl_{2\,(aq)} + 2OH^-_{\,(aq)}$$

Therefore, an immersion test was performed to determine the best coating conditions for the calcium phosphate layer by comparing the amount of magnesium released into a 3.5% NaCl

solution as a function of time for the Mg alloys coated with the final multi-layered coating (sol-gel silica + mesoporous silica + calcium phosphate) and the uncoated material. The samples were also analyzed by ATR-FTIR and SEM-EDS after the corrosion test in order to identify the corrosion products on the surface.

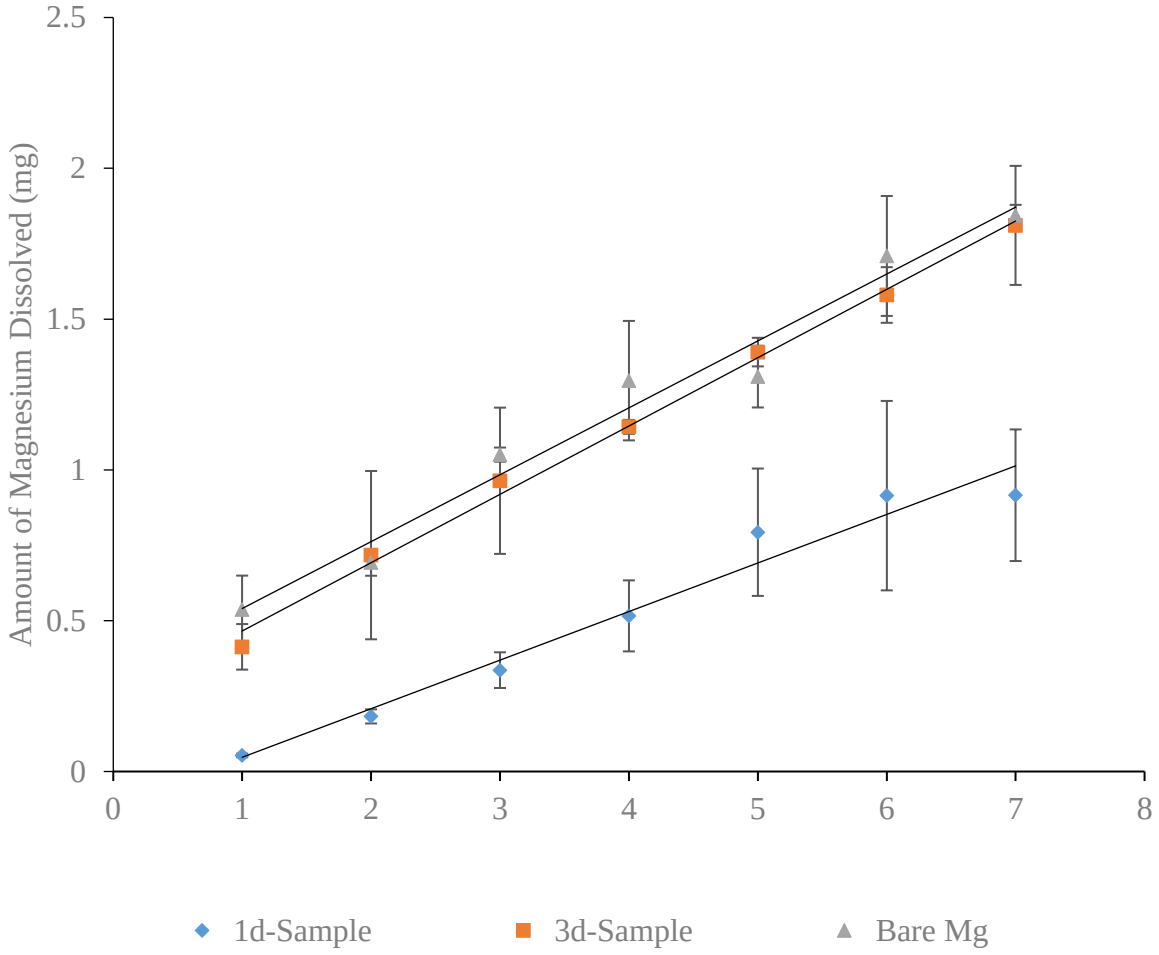

Figure 4.9: Amount of Magnesium Dissolved as a Function of Immersion Time in 3.5% NaCl. 1d-Sample (Multi-layered Sample Coated with 6 mM Calcium Phosphate and 1 day Deposition Time), 3d-Sample (Multi-layered Sample Coated with 6 mM Calcium Phosphate and 3 day Deposition Time) and Bare Magnesium (Uncoated Control).

Atomic absorption spectroscopy was used to determine the relative corrosion rate of unmodified Mg AZ31 in comparison to the multilayer coatings prepared by immersion in a 6 mM calcium phosphate solution for 1 and 3 days. The samples were immersed in 3.5% NaCl for a total of 7 days. The total amount of magnesium dissolved into the NaCl solution during the corrosion test was measured daily for the duration of the experiment. Figure 4.9 is a graph of the amount of magnesium dissolved into the NaCl solution as a function of immersion time for each sample. Each data point represents an average of 3 samples; the error bars are the sample to sample standard deviations. Both the 3 day calcium phosphate coated samples and uncoated magnesium alloys show a high rate of magnesium release into solution which continued until the end of this study. In comparison, the release of magnesium into the solution from the samples coated with calcium phosphate for 1 day continued up to 5 days but at a slower rate than the 3 day coated sample and uncoated sample. The degradation rate was calculated from the slope of the plots as shown in Table 4.2.

Table 4.3: The Degradation Rate of Uncoated and Coated Magnesium Alloys in 3.5% NaCl Solution.

Samples	Uncoated Mg alloy	3 days CaP coated samples	1 day CaP coated samples (0-5 day)	1 day CaP coated samples (6-7 day)
Degradation (mg/day)	0.221	0.226	0.181	0.001

Upon comparison of the 1 day and 3 day coated sample, there is a significant difference in the rate of degradation which indicates that the final multi-layered coating with 1day deposition time in 6 mM calcium phosphate had a good influence on the corrosion resistance of the magnesium alloy. Moreover, it is observed from this study that longer deposition times for the calcium phosphate layer does not improve the corrosion resistance of magnesium alloys since longer deposition time may lead to partial dissolution of some of the under-layer coatings (mesoporous silica and sol-gel layers) during the deposition of calcium phosphate.

Therefore, it can be concluded that the optimum conditions for deposition of calcium phosphate layer on mesoporous silica coated Mg alloys are high calcium phosphate concentration (6 mM) and low deposition time (1 day) since this produces a stable, thick and uniform layer. Thus, these samples were selected for further characterization.

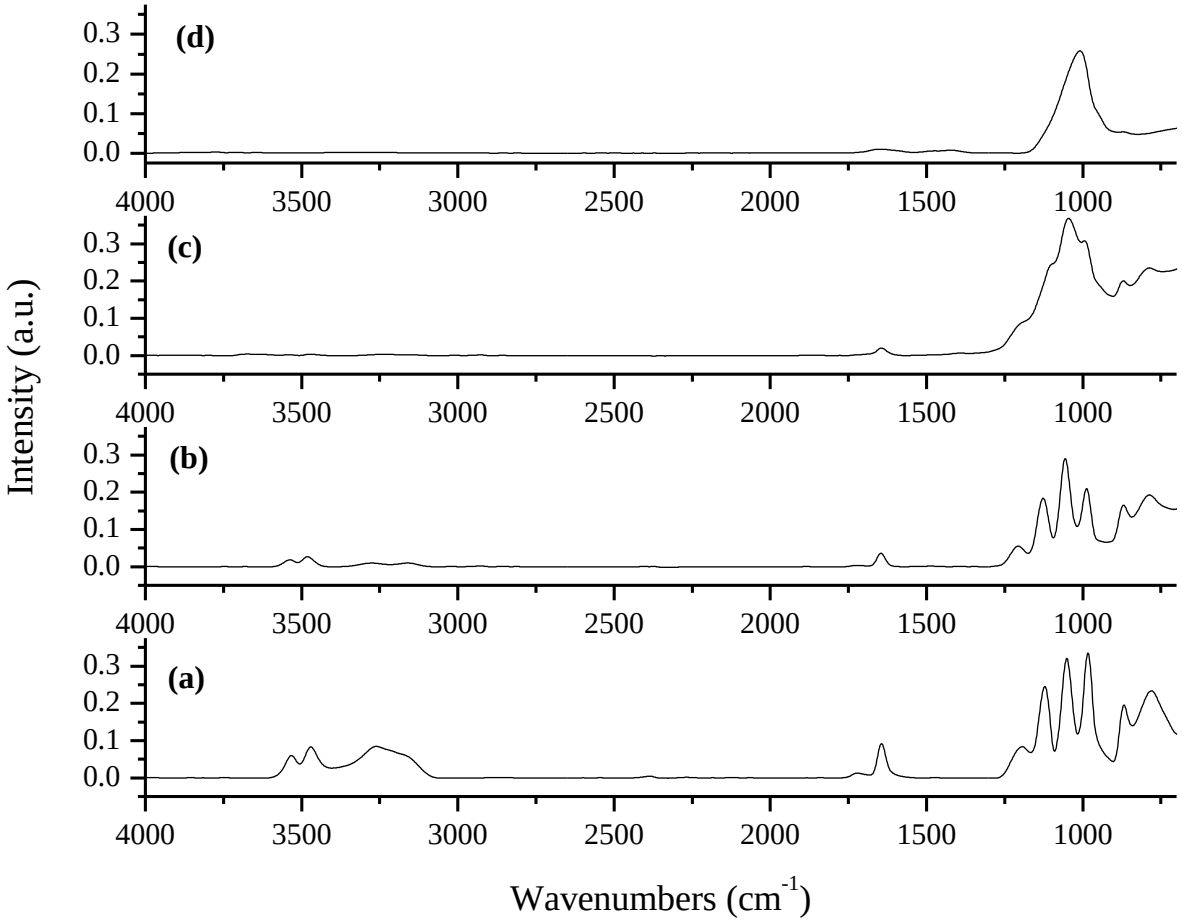

Figure 4.10: IR Spectra for the Final Multi-layered Coating Prepared with 6 mM Calcium Phosphate Solution and 1 Day of Deposition Time before and after Immersion in 3.5% NaCl Solution. (a) The Final Multi-layered Coating before Corrosion Test, (b) 1 Day, (c) 3 Days, (d) 7 Days after Corrosion Test

Figure 4.10 shows infrared spectra for magnesium alloys coated with the final multi-layered coating before and after immersed in 3.5% NaCl for 1, 3 and 7 days. As shown in this

figure, the multilayer coating is stable after 1day immersion in 3.5% NaCl. However, after 3 days in 3.5% NaCl, the three strong peaks that indicate the presence of brushite were gradually converted to one broad peak at 1050 cm^{-1} corresponding to PO_4^{3-}. This may indicate that the initial brushite layer is gradually converted to an amorphous calcium phosphate layer.

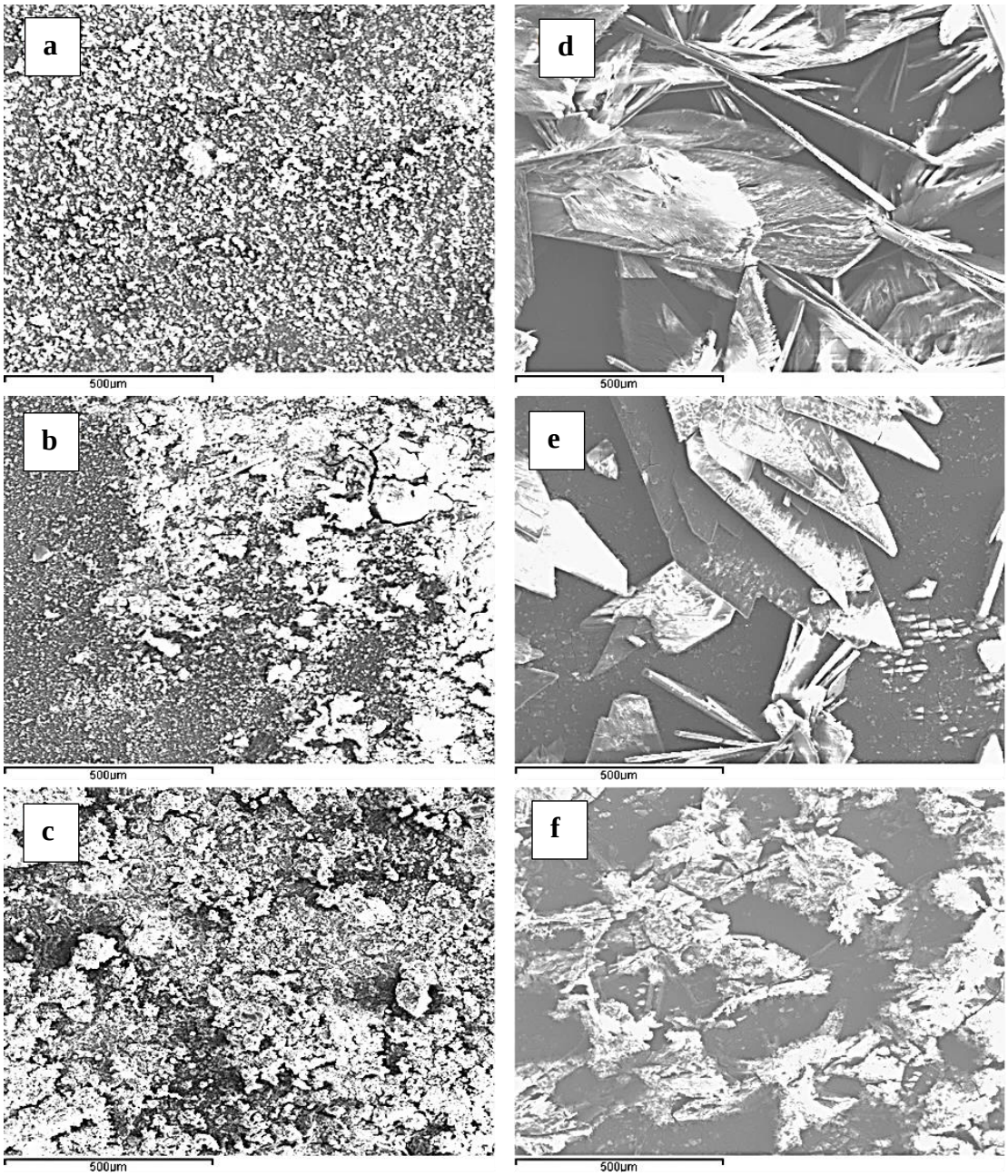

Figure 4.11: SEM Images for Uncoated Control of Magnesium (a, b, c) and the Final Multi-layered Coating of Calcium Phosphate Deposited on Mesoporous Silica Coated Mg AZ31 (d, e, f) after 1 Day, 3 Days, and 7 Days Immersion in NaCl Solution. Scale Bar = 500 µm.

Figure 4.11 shows SEM images of the coated and uncoated magnesium alloys after immersion in 3.5% NaCl for different times. It is observed from the SEM images (a,b,c) that the uncoated sample is completely covered with a layer that is likely magnesium hydroxide and soluble magnesium chloride after immersion in 3.5% NaCl as expected due to its high corrosion rate. After a 7 day immersion in the 3.5% NaCl solution, the surface of the uncoated magnesium alloy was completely covered with a thick layer of magnesium hydroxide or chloride. EDS confirmed the presence of magnesium, oxygen and chlorine on the surface of these samples as shown in Table 4.3.

In contrast, the SEM images Figure 4.11 (d,e) for the coated sample after one and three days of immersion in 3.5% NaCl, show that the calcium phosphate coating is still present and that there are no significant differences in its morphology compared to the coated samples before the corrosion test (Figure 4.8 (c)). These images still show the same morphology and the plate-like structure of brushite that was observed in the as-deposited CaP coating. After seven days of immersion in 3.5% NaCl, a layer of calcium phosphate is still observed on the surface of the coated samples but with a different morphology. This change in structure occurs as the brushite layer is converted to an amorphous calcium phosphate layer after 7 days of immersion in NaCl solution as shown in Figure 4.11 (f). However, the gradual decrease of the atomic percentage of calcium and phosphate coupled with the increase of the atomic percentage of magnesium on the coated surface with increasing immersion time in NaCl solution as shown in Table 4.4 indicates the gradual dissolution of the calcium phosphate layer. This mirrors the trend observed for the

corrosion rate of the final multi-layer coated samples; as the calcium phosphate layer degrades, the corrosion rate increases.

Table 4.4: The Atomic Percentage of Elements on the Surface of Magnesium Alloy AZ31 after Corrosion in NaCl Solution. Data are the Average of at least Eight Spots of each Sample.

Atomic %	1 day	3 days	7 days
Mg	42.32±4.07	42.95±10.19	42.06±9.55
O	57.50±4.44	50.95±11.94	56.17±6.38
Cl	0	2.56±4.12	1.77±3.74

Table 4.5: The Atomic Percentage of Elements on the Final Multi-layered Coating of Calcium Phosphate Deposited on Mesoporous Silica Coated Mg AZ31 after Corrosion in NaCl Solution. Data are the Average of at Least Eight Spots of each Sample. *Due to the Changing Morphology of the Coating after 7 Days of Immersion, it was Difficult to Define the Flat Areas from the Brushite on the Surface. Therefore the 7-days Results are Reported as One Area.

Atomic %	Time	1 day	3 day	7 days (both area)
Mg	Flat Area	1.15±0.0	0	3.83±0.61
	Brushite Area	0.34±0.22	1.21±0.39	
Si	Flat Area	1.78±0.0	0.25±0.35	0.84±1.04
	Brushite Area	0	0.19±0.12	
P	Flat Area	20.62±0.0	7.81±1.25	14.69±1.37
	Brushite Area	13.19±7.12	10.64±3.45	
Ca	Flat Area	41.26±0.0	56.95±7.80	17.55±4.52
	Brushite Area	41.30±13.98	20.34±14.00	

4.3.2 Characterization of the Final Multi-layered Coating on Magnesium Alloys

The previous section of this study confirmed the successful production of the multilayered coating on the magnesium alloy surface. In the next sections, the cross section of the final multi-layered coating, its degradation in simulated biological fluid and its cell cytotoxicity were characterized.

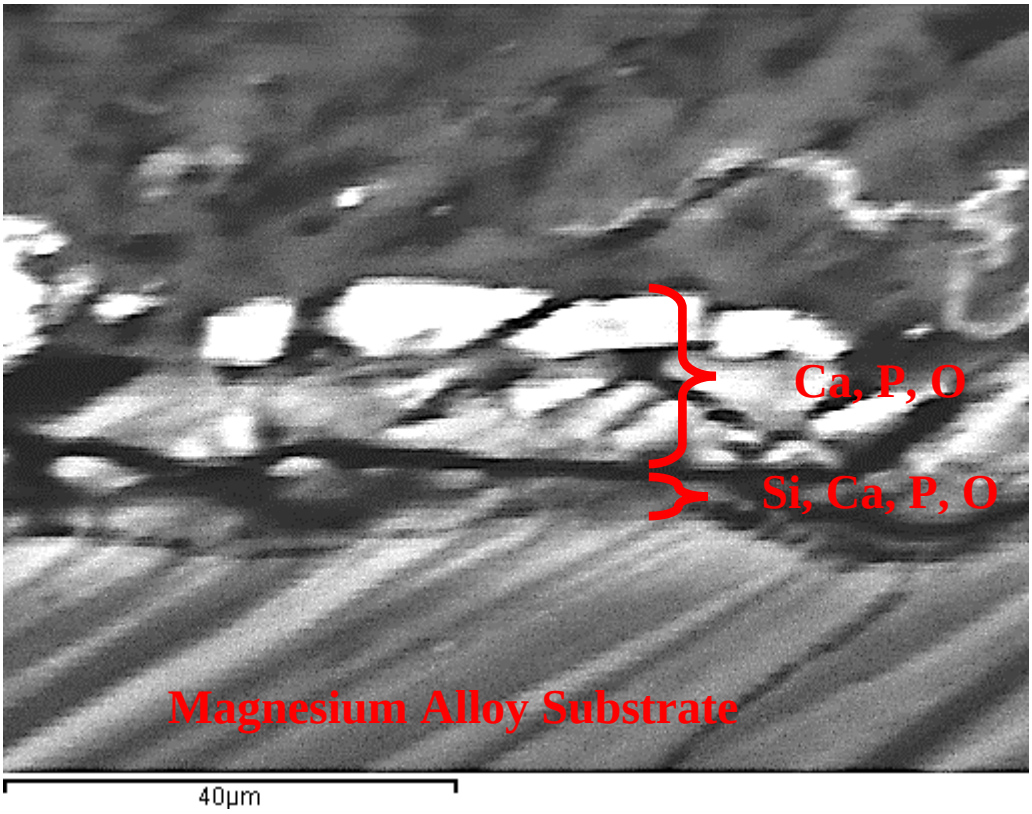

Figure 4.12: SEM image of the Cross Section of the Final Multi-layered Coating Deposited on Magnesium Alloy Substrate.

Figure 4.12 shows SEM image of the cross section of the final multi-layered coating on magnesium alloys substrate. A cross sectional image was used to observe the homogenous formation of the layers on the Mg alloy samples and to determine the thicknesses of the final multi-layered coatings. From the cross-sectional view, the thickness of the coating was measured to be around 20 μm and the coating was composed of two layers as marked in Figure 4.12. The sol-gel silica and mesoporous silica inner layer directly on top of the underlying magnesium alloy substrate and the dense outer layer is the calcium phosphate layer. However, The EDS analysis also detected the presence of calcium and phosphorus in the inner mesoporous silica layer which indicates the ingrowth of the calcium phosphate film into the pores of the mesoporous layer. Also, EDS mapping revealed that the calcium and phosphorus were homogeneously distributed throughout the inner layer. The ingrowth of the calcium phosphate layer into the pores of the mesoporous silica layer may have several advantages including increased corrosion resistance and improved adhesion.

Therefore, a thick, uniform, and stable multi-layered coating was successfully deposited on the magnesium alloy substrate. The final multi-layered coating consists of a sol-gel silica layer followed by a spin coated of mesoporous silica layer and finally a calcium phosphate coating.

4.3.3 *In Vitro* Characterization of the Properties of the Final Multi-layered Coating

Ideal coatings for biodegradable metallic implant materials should enable biodegradation at a desired rate and they should only protect the surface for a limited time until the healing process occurs [26]. In addition, they must be biocompatible and non-toxic. Depending on the intended application the ability to promote osseointegration, bioactivity, antibacterial properties or local drug delivery capability may also be very important characteristics.

Therefore, it is very important to study the *in vitro* degradation behaviour and cytotoxicity of the multi-layered coating to determine the stability and biocompatibility of the deposited coating on the biodegradable magnesium alloys in physiological solution.

4.3.3.1 *In Vitro* Biodegradation Behaviour of the Final Multi-layered Coating in Simulated Biological Fluid

The use of magnesium and its alloys as a biomaterial is promising due to their good biocompatibility and mechanical properties. However, their degradation rate is too high in body fluids in the first stages of the healing process. Orthopedic biomaterials need around three to four months to promote bone regeneration. The fast degradation of magnesium alloy in body fluid can lead to the occurrence of a second fracture [2]. Therefore, it is essential to understand the biodegradation behaviour of our coated Mg alloy in simulated body fluid (SBF). *In vitro* degradation tests were done by immersing the coated and uncoated samples in SBF at 37 °C for a 7 day period. The ion concentration and pH of the SBF solution are similar to that of human

blood plasma; this solution contains both calcium and phosphate ions which also make it a simple test for the ability of a biomaterial to induce calcium phosphate nucleation and growth at its surface. Therefore, this experiment was performed to determine the biodegradation rate of Mg alloys coated with the final multi-layered coating as well as to identify the biodegradation products on the surface.

One of the expected biodegradation products is the precipitation of calcium phosphate at the surface of the alloy. Calcium phosphates have very low K_{sp} values, especially at elevated pH. As the magnesium alloy degrades, the pH rises resulting in precipitation of calcium phosphate species. Since the SBF is supersaturated with calcium and phosphate, this reaction readily occurs during immersion in the SBF environment. Reaction Scheme 4.4 shows one such precipitation reaction that would result in the deposition of hydroxyapatite at the alloy surface [27]. The formation of a hydroxyapatite layer on the surface indicates good bioactivity of the implant in the physiological solution. This layer can form in direct contact with the surrounding tissue *in vivo* to enhance the osteointegration of the implant and can also improve both the corrosion rate and the biocompatibility of magnesium alloys in physiological solutions [27].

Reaction Scheme 4.4: Precipitation Reactions.

$$10Ca^{2+}{}_{(aq)} + 6PO_4^{3-}{}_{(aq)} + 2OH^-{}_{(aq)} \rightarrow Ca_{10}(PO_4)_6(OH)_{2\,(s)}$$

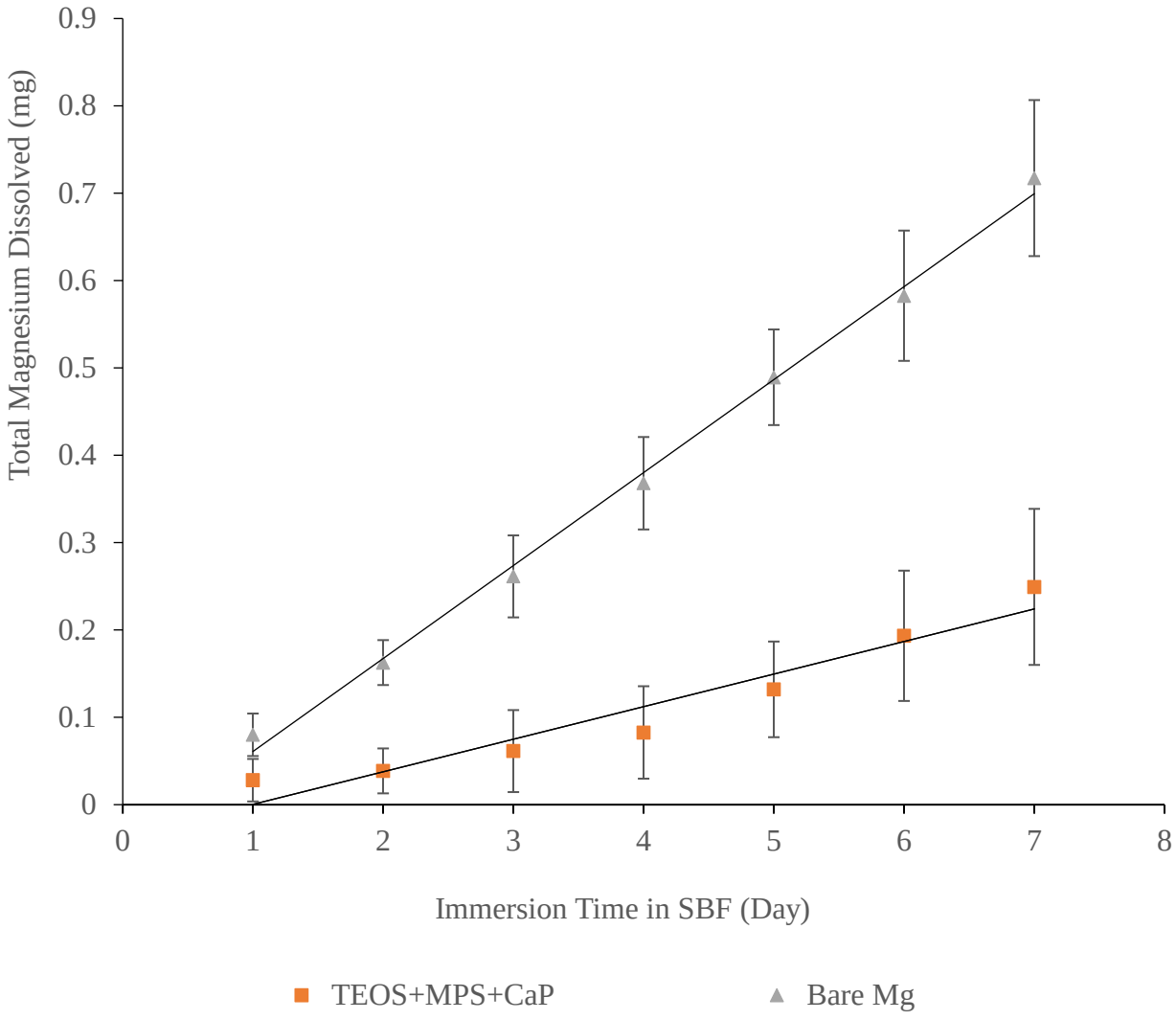

Figure 4.13: Amount of Magnesium Dissolved as a Function of Immersion Time in SBF for the Final Multi-layered Coating (TEOS+MPS+CaP) on Mg AZ31 and Uncoated Control of Magnesium (Bare Mg).

Atomic absorption spectroscopy was used to determine the biodegradation rate of the coated Mg alloys in SBF compared to the uncoated material. Figure 4.13 is a graph of the

cumulative amount of magnesium dissolved into the SBF solution as a function of time for a 7 day period. Each data point represents an average of 3 samples; the error bars are the sample to sample standard deviations. The uncoated magnesium alloy started to release magnesium ions into solution at a high linear rate which continued to the end of the study. By day 7, an average of about 0.71 ± 0.1 mg of magnesium has been released into the SBF solution. In comparison, the release of magnesium into the SBF solution from the final multilayered coated sample (TEOS+MPS+CaP) continued in a linear fashion as well but at a much slower rate than the uncoated sample. Specifically, the coated samples seem to have two linear parts: one starts from the beginning of the study up to 4 days which has a very slow degradation rate and the second part starts after day 4 up to the end of the study. This high magnesium ion release after 4 days is due to an increase in the degradation rate from pitting corrosion. Pitting corrosion was visually observed on the sample surfaces. In general, the degradation rate of the coated material increased with increasing immersion time which may indicate that the coating is beginning to break down as observed from the change in the slope of the plot as a function of immersion time. These results are reported in Table 4.5. However, the total amount of magnesium released into solution for the coated samples at 7 days is only about 0.249 ± 0.089 for the final multi-layered coating (TEOS+MPS+CaP). This suggests that the uncoated samples degrade at a rate that is at least 3 times greater than the coated samples. Therefore, the final multi-layered coating had a strong influence on the corrosion resistance of the magnesium alloy in simulated body fluids.

Table 4.6: The Degradation Rate of Uncoated and Coated Magnesium Alloys in SBF Solution.

Samples	Uncoated Mg Alloy	Coated Magnesium alloy (0-4 days)	Coated Magnesium alloys (5-7 days)
Degradation Rate (mg/day)	0.106	0.018	0.058

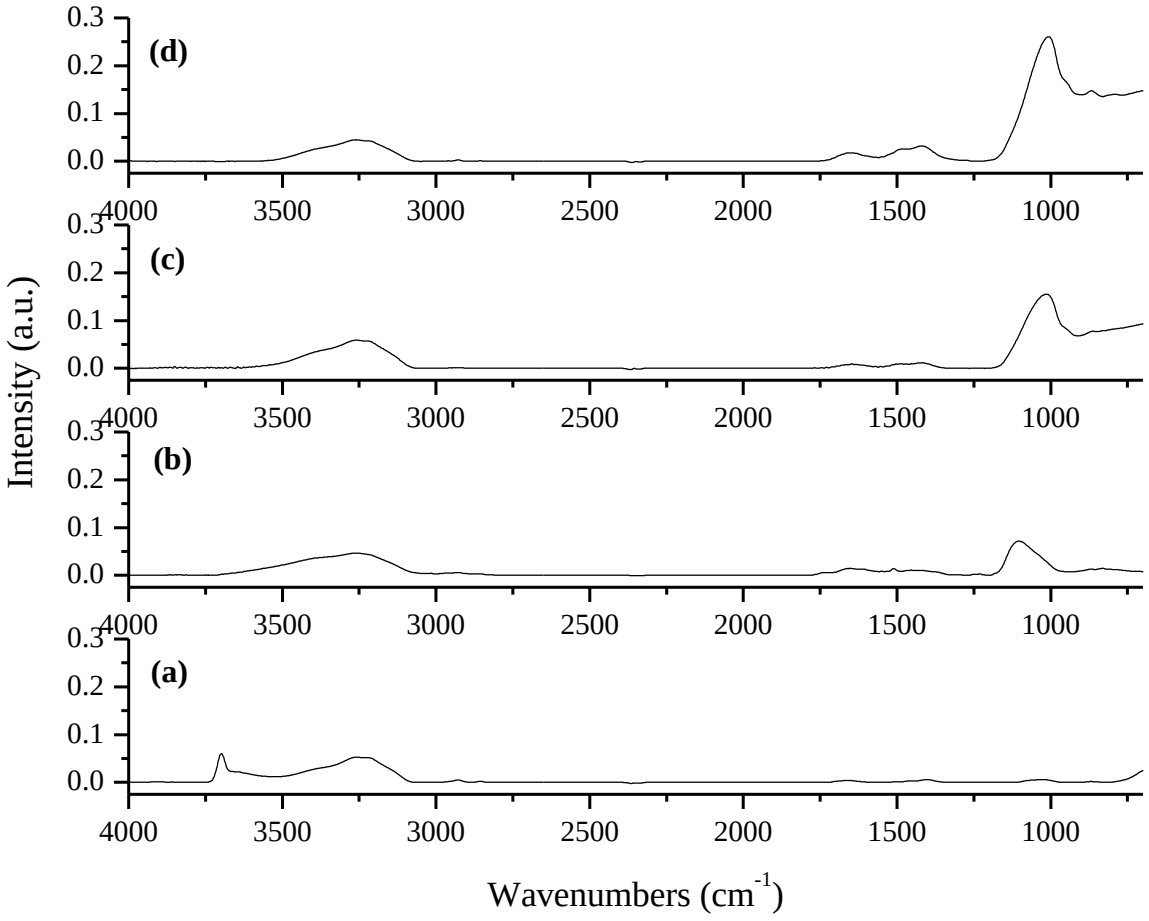

Figure 4.14: IR Spectra for the Bare Magnesium (Control) after Immersion in SBF for Various Periods of Time. (a) The Bare Magnesium before Biodegradation Test, (b) 1 Day, (c) 3 Days, (d) 7 Days after Biodegradation Test

Figure 4.14 shows infrared spectra for the bare magnesium (control) before and after immersion in SBF for various periods of time. After 1 day, 3 days and 7 days a new broad peak was observed at approximately 1050 cm^{-1} which confirms the presence of phosphate PO_4^{3-}.

Moreover, the phosphorus and calcium peaks observed in the EDS spectra confirm that the phosphate is due to the presence of a calcium phosphate layer at the surface. This indicates the formation of the biodegradation layer on the Mg alloy surface. Furthermore, the $Mg(OH)_2$ peak at 3700 cm^{-1} has disappeared due the formation of this layer on all the surface. No crystalline magnesium hydroxide is observed in the corrosion product. A carbonate peak at 1490 cm^{-1} is observed. This may be due to the presence of a mixed corrosion layer containing either calcium phosphate and magnesium or calcium carbonate.

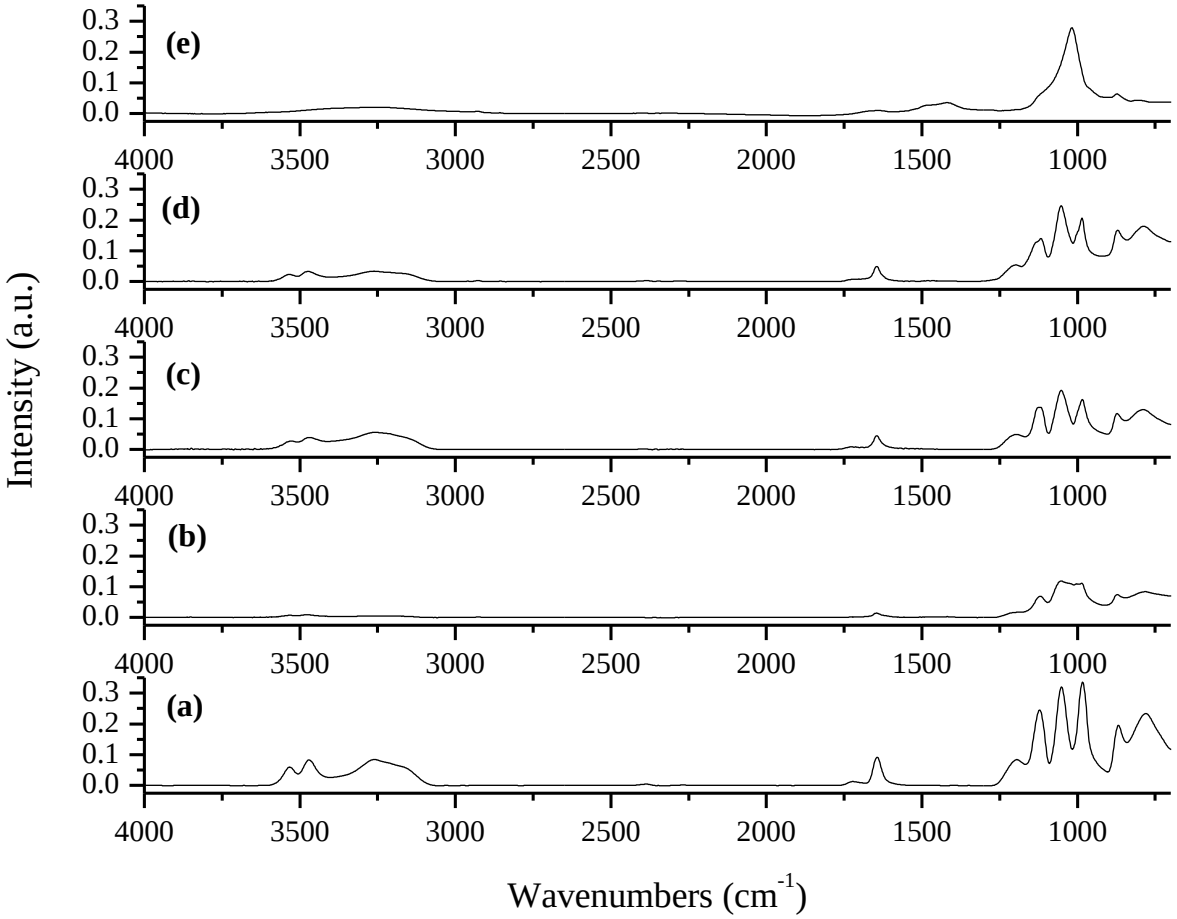

Figure 4.15: IR Spectra for the Final Multi-layered Coating after Immersion in SBF for Various Periods of Time. (a) The Final Multi-layered Coating before Biodegradation Test, (b) 1 Day, (c) 3 Days, (d and e) 7 Days after Biodegradation Test. Note That Two Type of Spectra were Observed after 7 Days of Immersion in SBF (d and e).

Figure 4.15 shows IR spectra of the final multi-layered coating after immersion in SBF for various periods of time. After immersion in SBF, all the samples still have three strong peaks

due to the presence of HPO_4^{2-} from brushite indicating that the final multilayer coating is stable. After 7 days of immersion in SBF, a broad peak representing PO_4^{3-} was observed in some spots of the sample surface such as the representative one in (Figure 4.15 (e)), indicating the formation of a new phase of calcium phosphate. This may be explained by the further deposition of calcium and phosphate from the SBF solution at the surface or it may indicate that the brushite layer gradually converts to the more stable hydroxyapatite mineral phase. A study by Li et al. showed that the brushite coating on a magnesium alloy was transformed into hydroxyapatite after immersion in SBF solution [28]. However, in another similar study by Huan et al. no hydroxyapatite was formed on the surface of the brushite coating on a Mg alloy after immersion in SBF for 7 days [29]. Therefore, different results were obtained from different studies depending on the stability of the brushite layer and the increase of the pH value during the immersion test. It was reported that brushite (dicalcium phosphate dihydrate) is always considered as a precursor for precipitation of hydroxyapatite and increasing the pH during immersion can promote the nucleation and growth of hydroxyapatite [28]. In our study, the SBF solution was changed every day to mimic physiological conditions; this would keep the pH from reaching higher and would therefore delay the transformation of the brushite to hydroxyapatite.

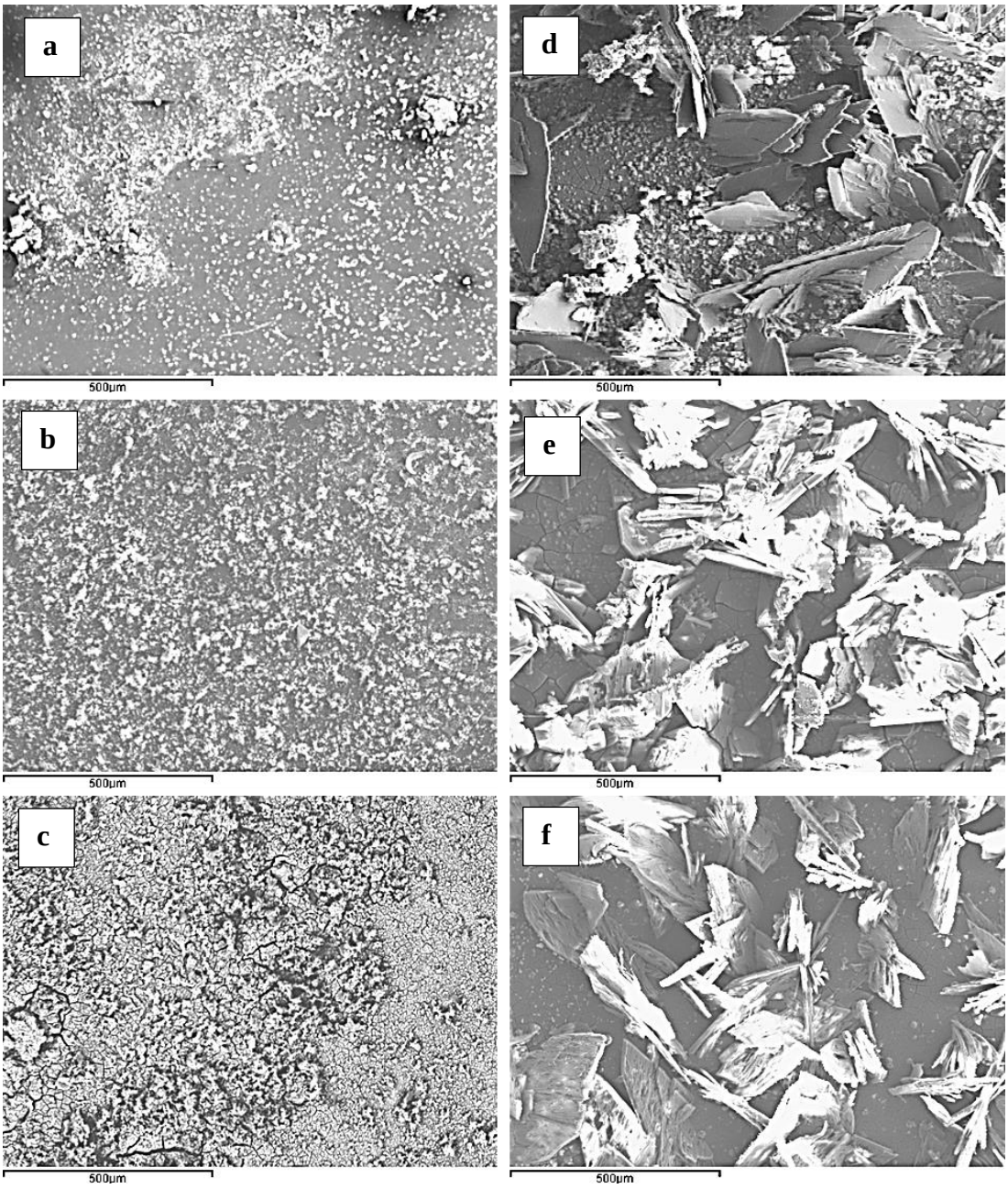

Figure 4.16: SEM Images for Uncoated Control of Bare Magnesium (a, b, c) and the Final Multi-layered Coating Deposited on Mg AZ31 Alloys (d, e, f) after 1 Day, 3 Days, and 7 Days Immersion in SBF Solution. Scale Bar = 500 µm.

Figure 4.16 shows SEM-EDS images of the coated and uncoated magnesium alloys after immersion in SBF for different times. It is observed from SEM images (a,b,c) that the uncoated sample is covered with a calcium phosphate layer after immersion in SBF. This was expected due to its high degradation rate that creates a high localized pH thus inducing precipitation of calcium phosphate at the interface. After 1 day and 3 days immersion in SBF, clusters of calcium phosphate and cracks were observed on the surface of the magnesium substrate. After a 7 day immersion period in the SBF solution, the surface of the uncoated magnesium alloy was completely covered with a thick layer of calcium phosphate. The presence of both calcium and phosphorus on these samples surfaces was confirmed by EDS as shown in Table 4.6. The gradual decrease in the atomic percentage of magnesium and concomitant increase in the atomic percentage of calcium and phosphorus confirms that the thickness of the corrosion product increased as a function of immersion time in the SBF.

Moreover, the SEM images Figure 4.16 (b, e, f) show the final multi-layered coating deposited on magnesium alloys after immersion in SBF. These images confirm the stability of the brushite layer that was deposited on the mesoporous silica coating since the images still show the platelet structure of brushite even after 7 days of immersion in SBF. The presence of calcium and phosphorus and also silicon in the EDS analysis after seven days also confirms the stability of the multi-layered coating on magnesium alloys (Table 4.7).

Furthermore, it was observed from the EDS results that the Ca/P ratio after 7 days on the brushite area and flat area increased to 1.22 and 1.44, respectively, which indicates the formation of amorphous calcium phosphate due to the further deposition of calcium and phosphate from the

SBF solution. This change was also confirmed by the presence of a phosphate peak (PO_4^{3-}) in the IR results (Figure 4.15 (e)).

Thus, the EDS results and the phosphate peaks in the IR spectra suggest that the calcium phosphate layer may tend to be transformed into hydroxyapatite layer with longer deposition time [28,29]. This conversion should result in a decreased degradation rate since hydroxyapatite is less soluble than brushite.

Table 4.7: The Atomic Percentage of Elements on the Surface of Magnesium Alloy AZ31 after Immersion in SBF Solution. Data are the Average of at least Eight Spots of each Sample.

Atomic %	1 day	3 days	7 days
Mg	69±21.29	22.69±17.37	15.70±9.44
O	22.06±15.89	52.47±21.47	53.25±16.60
P	3.57±3.27	12.31±2.92	14.63±4.04
Ca	2.22±2.07	10.73±2.67	13.58±4.43

Table 4.8: The Atomic Percentage of Elements on the Surface of the Final Multi-layered Coating Deposited on Magnesium Alloys AZ31 after Immersion in SBF Solution. Data are the Average of at least Eight Spots of each Sample.

Atomic %	Time	1 day	3 days	7 days
Mg	Flat Area	2.33±2.31	0.74±0.45	2.62±1.16
	Brushite Area	0.40±0.51	0.58±0.11	1.06±0.50
Si	Flat Area	0.45±0.16	1.67±1.08	1.33±0.18
	Brushite Area	0.41±0.34	0.20±0.10	0.02±0.05
P	Flat Area	20.10±4.87	20.58±5.33	18.16±3.71
	Brushite Area	15.85±5.63	14.97±5.58	16.42±4.23
Ca	Flat Area	19.54±12.66	40.16±8.73	26.06±14.36
	Brushite Area	19.80±15.78	20.15±10.97	20.16±7.76

4.3.3.2 Cytotoxicity Evaluation of the Final Multi-layered Coating:

It is well known that the biocompatibility of biomaterials is as important as mechanical properties if not more so especially when metallic materials are used. Although magnesium is an

essential element for human metabolism and is itself non-toxic, the biocompatibility of magnesium and its alloys before and after modification must be investigated to ensure the biosafety of the additional elements used in the alloying and the surface modification procedure. Cytotoxicity testing is the first step for evaluating the biocompatibility of a new material designed for use in biomedical application. In this study, the cytotoxicity was evaluated by an indirect method to estimate the impact of the surface modification used in this study on cell viability. A magnesium-conditioned cell culture medium were prepared by incubating the uncoated and coated magnesium alloys in cell culture media for 72 hrs at 37ºC in a 5% CO_2 atmosphere. The cell viability was determined by exposing healthy cells to the conditioned medium for 24 hrs. The number of cells was determined using the CyQUANT assay as described in section 4.2.6.

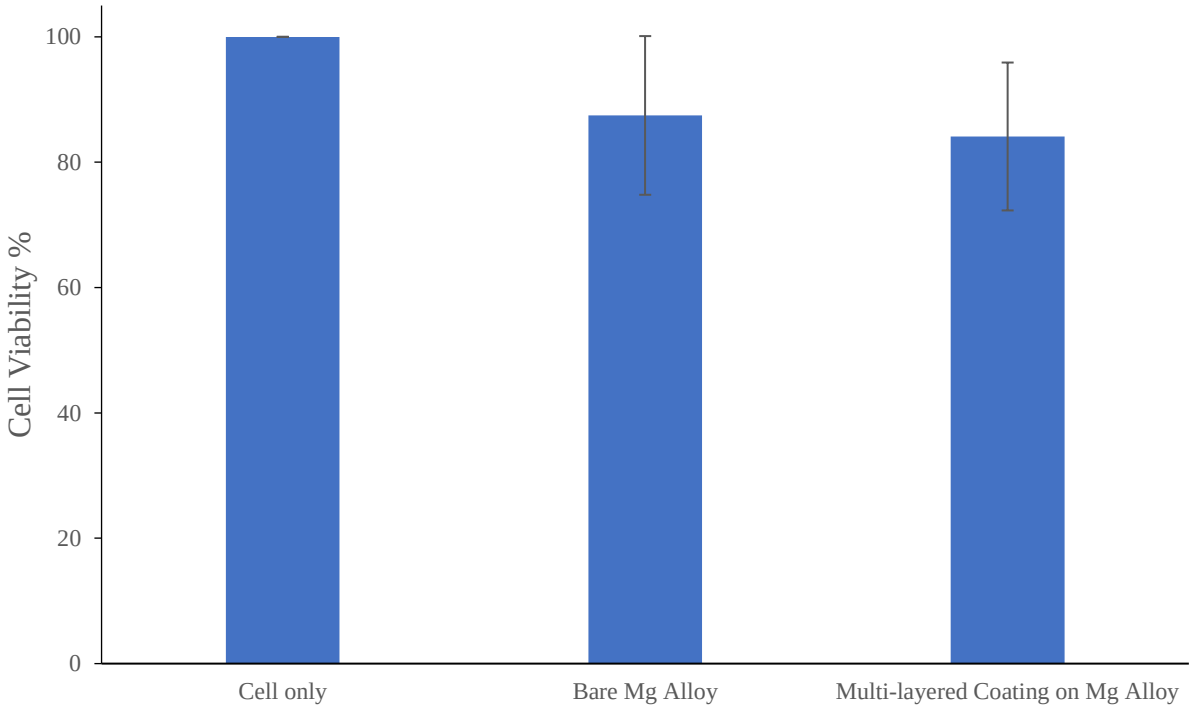

Figure 4.17: The Percentage of Saos-2 Cell Viability on the Final Multi-layered Coating and Bare Magnesium Alloy. Cells Only is the Positive Control. Data are the Average of 6 Samples (3 Replicates of 2 Independent Experiments).

Figure 4.17 shows the effect of coated and uncoated magnesium conditioned media on the Saos-2 cell viability. It was observed that the medium conditioned with the coated magnesium alloys yielded a cell viability similar to the medium conditioned with uncoated magnesium AZ31. No statistically significant difference in the cell viability between the uncoated and coated Mg alloys was observed ($p > 0.05$). The results show that the Mg alloy conditioned growth medium of coated and uncoated magnesium alloys have no cytotoxicity effect on the osteoblast cells (Saos-2 cell). The ISO definition of cytotoxicity states that a material is not cytotoxic unless the cell viability is reduced by more than 30% [30]. The cell

viability for both the uncoated Mg AZ31 and the coated Mg AZ31 in this study is reduced by less than 20%. This result suggests that all of the components of the multi-layered coating are biocompatible and non-toxic. Therefore, the *in vitro* cell studies demonstrate that the cytocompatibility of the multi-layered coating is acceptable for medical implant applications.

4.4 Conclusions

From the surface characterization results obtained, it can be concluded that a uniform and stable multi-layered coating consisting of silica sol-gel, mesoporous silica, and calcium phosphate layers was successfully deposited on magnesium alloy AZ31. Furthermore, the final multi-layered coating has good corrosion resistance in 3.5% NaCl solution. The *in vitro* biodegradation study showed that the degradation rate of the coated samples was significantly decreased indicating that the multi-layered coating was very effective in protecting the Mg alloy substrate from rapid degradation in SBF solution. Moreover, the cytotoxicity evaluation showed that the multi-layered coating was not cytotoxic to osteoblast cells. This type of coating may be promising for the surface modification of magnesium alloys that exhibit improved degradation resistance and biocompatibility and therefore provide a potential biodegradable material for application in bone repair.

References

1. Staiger, M. P., et al. "Magnesium and its alloys as orthopedic biomaterials: a review." *Biomaterials* 27.9 (2006): 1728-1734.
2. Gu, X. N., and Y.F. Zheng. "A review on magnesium alloys as biodegradable materials." *Frontiers of Materials Science in China* 4.2 (2010): 111-115.
3. Vasconcelos, D. C. L., et al. "Corrosion resistance of stainless steel coated with sol–gel silica." *Journal of Non-Crystalline Solids* 273.1 (2000): 135-139.
4. Thim, G. P., et al. "Sol-gel silica film preparation from aqueous solutions for corrosion protection." *Journal of Non-crystalline Solids* 273.1 (2000): 124-128.
5. Wang, D., and G. P. Bierwagen. "Sol-gel coatings on metals for corrosion protection." *Progress in Organic Coatings* 64.4 (2009): 327-338.
6. Asefa, T., and Z. Tao. "Mesoporous silica and organosilica materials-Review of their synthesis and organic functionalization." *Canadian Journal of Chemistry* 90.12 (2012): 1015-1031.
7. Gomez-Vega, J. M., et al. "Aligned bioactive mesoporous silica coatings for implants." *Journal of Materials Science: Materials in Medicine* 12.10-12 (2001): 923-927.
8. Wang, X., et al. "Mesoporous bioactive glass coatings on stainless steel for enhanced cell activity, cytoskeletal organization and AsMg immobilization." *Journal of Materials Chemistry* 20.31 (2010): 6437-6445.
9. Ehlert, N., et al. "Mesoporous silica coatings for controlled release of the antibiotic ciprofloxacin from implants." *Journal of Materials Chemistry* 21.3 (2011): 752-760.

10. Asefa, T., and Z. Tao. "Biocompatibility of mesoporous silica nanoparticles." *Chemical Research in Toxicology* 25.11 (2012): 2265-2284.
11. Nishiyama, N., et al. "Enhancement of structural stability of mesoporous silica thin films prepared by spin-coating." *Chemistry of Materials* 14.10 (2002): 4229-4234.
12. Miyata, H., and K. Kuroda. "Formation of a continuous mesoporous silica film with fully aligned mesochannels on a glass substrate." *Chemistry of Materials*12.1 (2000): 49-54.
13. Bruinsma, P.J., et al. "Mesoporous silica synthesized by solvent evaporation: spun fibers and spray-dried hollow spheres." *Chemistry of Materials* 9.11 (1997): 2507-2512.
14. Hatton, B. D., et al. "Spin-coated periodic mesoporous organosilica thin films-towards a new generation of low-dielectric-constant materials." *Advanced Functional Materials*15.5 (2005): 823-829.
15. Cui, F. Z., et al. "Calcium phosphate coating on magnesium alloy for modification of degradation behavior." *Frontiers of Materials Science in China* 2.2 (2008): 143-148.
16. Liu, Q., et al. "The role of surface functional groups in calcium phosphate nucleation on titanium foil: a self-assembled monolayer technique." *Biomaterials* 23.15 (2002): 3103-3111.
17. Zheng, C. Y., et al. "Calcium phosphate coating of Ti-Nb-Zr-Sn titanium alloy." *Materials Science and Engineering:* C 27.4 (2007): 824-831.
18. Ou, C., et al. "Effect of Ca and P ion concentrations on the structural and corrosion properties of biomimetic Ca-P coatings on ZK60 magnesium alloy." *International Journal of Electrochemical Science* 8 (2013): 9518-9530.
19. Xu, L., et al. "In vitro and in vivo evaluation of the surface bioactivity of a calcium phosphate coated magnesium alloy." *Biomaterials* 30.8 (2009): 1512-1523.

20. Al Hegy, A. "Deposition and characterization of mesoporous silica coatings on magnesium alloys". *M.SC. Thesis*. Laurentian University of Sudbury, 2014.
21. Serra, A., X. Ramis, and X., Fernández-Francos. "Epoxy sol-gel hybrid thermosets." *Coatings* 6.1 (2016): 8.
22. Hirsch, A., et al. "Infrared absorption spectrum of brushite from first principles." *Chemistry of Materials* 26.9 (2014): 2934-2942.
23. Idowu, B., et al. "In vitro osteoinductive potential of porous monetite for bone tissue engineering." *Journal of Tissue Engineering* 5 (2014): 2041731414536572.
24. Song, Y., et al. "Electrodeposition of Ca-P coatings on biodegradable Mg alloy: in vitro biomineralization behavior." *Acta Biomaterialia* 6.5 (2010): 1736-1742.
25. Makar, G. L., and J. Kruger. "Corrosion of magnesium." *International Materials Reviews* 38.3 (1993): 138-153.
26. Hornberger, H., S. Virtanen, and A. R. Boccaccini. "Biomedical coatings on magnesium alloys–a review." *Acta Biomaterialia* 8.7 (2012): 2442-2455.
27. Wang, Y., et al. "Corrosion process of pure magnesium in simulated body fluid." *Materials Letters* 62.14 (2008): 2181-2184.
28. Li, Kaikai, et al. "Microstructure, in vitro corrosion and cytotoxicity of Ca-P coatings on ZK60 magnesium alloy prepared by simple chemical conversion and heat treatment." *Journal of Biomaterials Applications* 28.3 (2013): 375-384.
29. Huan, Z. G., et al. "In vitro degradation behavior and cytocompatibility of Mg–Zn–Zr alloys." *Journal of Materials Science: Materials in Medicine* 21.9 (2010): 2623-2635.

30. International Organization for Standardization, ISO 10993-5. "Biological evaluation of medical devices-Part 5: tests for in vitro cytotoxicity." (2009). 10993:5.

Chapter 5

5 Preliminary Results on the Immobilization of a Fibronectin Mimetic to the Surface of Superhydrophobic Magnesium and its Influence on Cell Adhesion.

Afrah Al Hegy, Joy E. Gray-Munro, Eric R. Gauthier

Dept. of Chemistry and Biochemistry and Materials Science Program, Laurentian University, Sudbury, Ontario, Canada, P3E 2C6

(Manuscript)

Abstract

Magnesium and its alloys have been widely investigated as a biodegradable implant material for use in fracture fixation devices such as screws, pins and plates. One of the major problems associated with using magnesium alloys as orthopaedic biomaterials is their rapid degradation in physiological solutions leading to a loss in mechanical properties prior to healing. Superhydrophobic surfaces are of interest to control the degradation of these materials due to their extreme water repellency, however, they are unsuitable for cell adhesion. In this study, a superhydrophobic magnesium alloy surface was modified with a fibronectin mimetic cell adhesive molecule. Infrared spectroscopy and contact angle analysis demonstrated that the cell adhesive molecule was successfully attached to the surface of superhydrophobic magnesium. However, although, fibronectin is a known cell adhesive protein, quantitative analysis of cell numbers using the CyQUANT assay indicate that cell adhesion was not enhanced on the surface modified material in comparison to the unmodified superhydrophobic magnesium alloy.

Keywords: Magnesium alloys, biocompatibility, superhydrophobic surface, cell adhesion, mussel adhesive protein, fibronectin mimetic

5.1 Introduction

The development of biodegradable metallic biomaterials for orthopaedic applications has become of interest in recent years [1]. These materials would provide the necessary stability during the initial stages of healing and promote tissue regeneration as they gradually degrade. Additionally, biodegradable metals are advantageous because they would eliminate both the toxic corrosion products associated with traditional metallic implants and the requirement for a second surgery to remove the implants after healing. Magnesium and its alloys are candidates for a new generation of biodegradable metallic biomaterials. Magnesium (Mg) and its alloys can dissolve or degrade in the body fluid during the healing process. The biodegradation of magnesium results in the release of non-toxic magnesium ions that can easily be excreted in the urine [2]. As well as its biocompatibility, Mg and its alloys have very similar mechanical properties to those of human bone resulting in decreased stress shielding and enhanced growth of new bone tissue [3]. However, the rate of magnesium degradation in the human body is normally too fast restricting their use in clinical applications. This fast degradation results in the formation of hydrogen gas cavities, rapid loss of mechanical integrity, and harmful host tissue reactions within the first week after implantation [4]. As biodegradable orthopedic implants, it is necessary that the rate of degradation meets the rate of healing of the bone tissue. Thus, it is required for the magnesium implant to stay stable for at least 12 weeks [3,4]. Therefore, it is important to develop methods to control the surface degradation rate of magnesium biomaterials after implantation.

Surface modifications play a very important role in the degradation of magnesium alloys in the human body. Several strategies for surface modification have been employed to improve the degradation rate of magnesium alloys such as chemical conversion coatings, polymer coatings, and silane coatings [5,6,7].

Surface modifications that produce superhydrophobic surfaces are interesting for controlling the degradation of these materials due to their extreme water repellency [8]. Superhydrophobic surfaces are surfaces with high water contact angles that are greater than 150° and low sliding angles (smaller than 5°). The best-known natural example of a superhydrophobic surface comes from the lotus leaf. The lotus leaf gets its superhydrophobicity from the combination of a hierarchical topography consisting of microscale papillae and a nanostructured low surface energy waxy cuticle. The structure of the lotus leaf can be mimicked on man-made surfaces to make them superhydrophobic. Generally, superhydrophobic surfaces are produced by creating a surface with micro/nanostructured roughness and then modifying the rough surface with hydrophobic substances [9,10]. A variety of techniques have been established to fabricate superhydrophobic surfaces on magnesium and magnesium alloys such as hydrothermal reaction, anodic oxidation, electrochemical deposition, sol-gel polymerization, electrospinning, chemical etching, and self-assembly techniques [11,12,13,14,15,16,17]. Zhang et al. fabricated a superhydrophobic surface on magnesium alloy AZ31 by the combination of the hydrothermal treatment method to get the hierarchical rough structures and post modification with stearic acid. The superhydrophobic surface showed a water contact angle of 157.6°. The corrosion results in 3.5% NaCl showed that the superhydrophobic coatings significantly improved the corrosion

resistance of the AZ31 alloy [15]. Wang et al. fabricated a layer of flower-like structures on a pure Mg surface by chemical etching followed by immersion in a stearic acid solution. The superhydrophobic surface showed a water contact angle of 154° with a sliding angle of about 3°. The superhydrophobic surface showed four times higher corrosion resistance than pure Mg after immersion in a 0.1 mol/L NaCl solution [16]. Furthermore, a study by Xu et al. successfully developed a superhydrophobic magnesium (Mg) alloy surface via an electrochemical machining process followed by coating with a fluoroalkylsilane film. The results confirmed the production of a superhydrophobic surface on the magnesium alloy as evidenced by a water contact angle of 165.2° and a water sliding angle of approximately 2°. The resulting superhydrophobic surface showed excellent corrosion resistance in different acidic solutions, alkaline solutions, and salt solutions (3.5 wt % of NaCl, Na_2SO_4, $NaClO_3$, and $NaNO_3$). In addition, the results of immersion in 3.5 wt % NaCl aqueous solution for 24 hrs did not change the superhydrophobicity of the surface as the contact angle remained at 160.5° after the test indicating the stability of the surface modification [17].

In recent years, researchers have focused on the application of superhydrophobic surfaces in area of biomaterials for the prevention of protein adsorption and for the prevention of bacterial cell growth on biomaterials. Pernites et al. prepared a superhydrophobic polythiophene film on various substrates resulting in the inhibition of both protein adsorption and bacteria cell adhesion to the surface [18]. Furthermore, Moradi et al. investigated the effect of superhydrophobicity on platelet adhesion to stainless steel and titanium substrates. The results showed that superhydrophobic surfaces are highly resistant to platelet adhesion demonstrating that

superhydrophobic surfaces on metals offer a novel method to improve the hemocompatibility of metallic substrates [19].

In the present study, the hierarchical surface topography and extreme water repellency has been reproduced on a Mg AZ31 surface via a combination of acid etching of the substrate followed by coating with a hydrophobic polysiloxane layer as described by Gray-Munro and Campbell [20]. The acid etching produced microscale features that are further described in the results and discussion section. The polysiloxane coating was produced by polymerization of poly(dimethylsiloxane) (PDMS) with 3-mercaptopropyltrimethoxysilane (MPTS). This coating has a nanoscale rod-like topography as shown in Figure 5.1. Together the microstructures, nanostructures and the low surface energy produce a superhydrophobic surface on Mg AZ31 [20]. Their study further demonstrated that the superhydrophobic Mg AZ31 surface was resistant to corrosion in 3.5% NaCl solution [20].

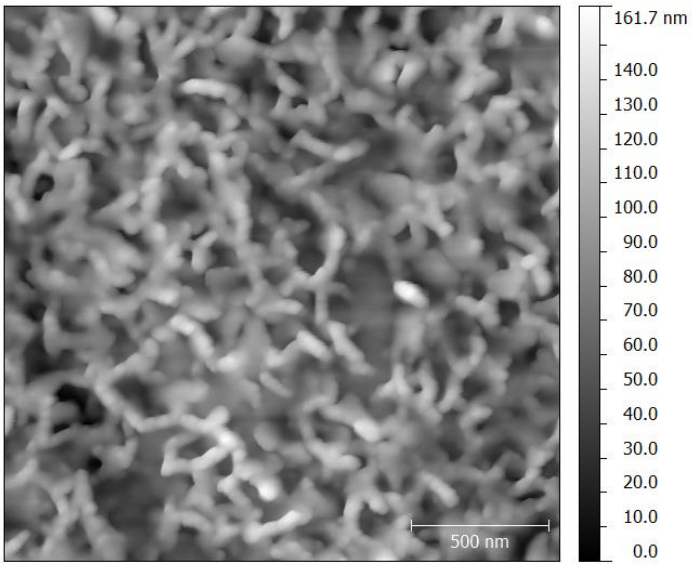

Figure 5.1: AFM Image of a Mixed MPTS/PDMS Coating on Magnesium Surface.

(Adapted from [20])

Although superhydrophobic surfaces decrease the rapid degradation of magnesium alloys, the interaction between the cells and the implant surfaces is also reduced leading to a decrease in the ability of the implant to induce bone regeneration and, therefore, limiting its biocompatibility.

Mimicking the structure and chemical composition of the extracellular matrix (ECM) through the attachment of ECM proteins has been shown to improve the biocompatibility of implant surfaces [21]. Cells bind to biomaterials surface through ligands found in proteins of the extracellular matrix. Integrins on the cell membrane interact with extracellular matrix (ECM) proteins such as fibronectin, laminin, and vitronectin through specific ligands. Fibronectin protein plays a very important role in cell attachment to substrate [22]. The arginylglycylaspartic

acid (RGD) amino acid sequence, which is commonly found in the cell adhesive protein fibronectin, is an essential recognition site for integrins on the cell membrane supporting cell adhesion and proliferation at biomaterials surfaces [21]. The attachment of the RGD peptide sequence to biomaterial surfaces has been shown to significantly improve osteoblast adhesion and proliferation on various implant surface such as titanium, polymers, and magnesium alloys [23,24,25].

A simple surface modification procedure was employed in this study to attach a fibronectin mimic to the surface of the superhydrophobic Mg AZ31 surface. This method involved immobilization of MAPTrix-F-RGD, a mussel adhesive protein containing the RGD sequence to the surface. Mussel adhesive proteins (MAPs) are a natural "glue" that has been shown to strongly adhere to virtually any material. They are generally rich in 3,4-dihydryoxyphenylalanine (DOPA) that has a catechol functional group that is believed to impart the strong adhesion characteristic of these proteins [26]. MAPs have been successfully coated onto a variety of material surface via one-step procedures such as deposition, precipitation or spin coating [26,27]. The mussel adhesive protein used in this study, MAPTrix-F-RGD, is a commercially available mussel adhesive protein that has been shown to enhance cell adhesion and proliferation on some substrates [28,29].

The objective of this study was to develop a method for the immobilization of the MAPTrix-F-RGD protein to the superhydrophobic Mg AZ31. In addition, the influence of this surface modification on Saos-2 osteoblast adhesion to the modified surfaces in comparison to unmodified superhydrophobic surfaces was determined using the CyQuant assay.

5.2 Material and Methods

5.2.1 Materials

Mg AZ31 foil (0.81 mm thickness) was purchased from Alfa Aesar Ltd (US). Sodium hydroxide was purchased from Sigma-Aldrich (Canada). Acetone (reagent grade) was purchased from Caledon Laboratory Chemicals (Canada). Ethyl alcohol (95%) and methanol were purchased from Commercial Alcohols (Canada). Concentrated sulphuric acid was purchased from Fisher Chemical LTD. 30% hydrogen peroxide, 3-mercaptopropyltrimethoxysilane (MPTS), poly(dimethylsiloxane) (PDMS) and MAPTrix-F-RGD were purchased from Sigma Aldrich Ltd. Bovine Calf Serum (BCS) and Trypan Blue were purchased from Fisher Scientific (Canada). McCoy's 5a and Trypsin/EDTA (1X) were purchased from Corning (Canada). Phosphate Buffered Saline (PBS) (1X) and Penicillin-Streptomycin Solution were purchased from HyClone (Canada). The CyQUANT cell proliferation assay was purchased from Life Technologies (Canada). All chemicals were used as received without further purification. The Saos-2 cell line was purchased from American Type Culture Collection (US) and cultured for further experiments.

5.2.2 Sample Preparation

Mg AZ31 alloy sheet (0.81 mm thickness) was cut into circular discs with a diameter of 1.27 cm and then polished to a 9 micron surface finish to remove the gross oxide layer. In order to clean and remove any excess polishing oil from the surface of the alloys, they were sonicated in acetone for 20 minutes and then rinsed in deionized water for 30 seconds.

5.2.3 Preparation of Superhydrophobic Magnesium Surfaces

5.2.3.1 Two-step Etching Procedure

A two-step etching procedure was employed to produce the microstructure of the superhydrophobic surface. In the first step the polished magnesium AZ31 sample was immersed into 20 mL of a 2% (v/v) H_2SO_4 solution for 4 minutes at 80ºC with sonication. In the second step the samples were immersed into 20 mL of a 20% (v/v) H_2O_2 solution with sonication for 2.5 minutes at 80ºC. The etched samples were rinsed with copious amounts of deionized water and air-dried.

5.2.3.2 Polysiloxane Coating

The coating solution was prepared by mixing MPTS: PDMS in a molar ratio of 100:1. First of all, a 1% MPTS solution was prepared by mixing 1 mL of MPTS (in methanol) with 0.484 mL of deionized water. The solution was adjusted to pH 4 using 0.05 M H_2SO_4. The pH adjusted solution was stirred for 90 minutes at room temperature to promote hydrolysis of the MPTS molecules. Then, 31 µL of PDMS was added to the 1% MPTS solution. The polysiloxane solution was allowed to stir for 24 hours to allow condensation between the hydrolyzed MPTS and the hydroxyl terminated PDMS molecules prior to coating. Then the etched samples were deposited in the coating solution for 24 hours at 50 ºC. After coating, the samples were dried before curing in an oven for 1h at 100 °C.

5.2.4 Deposition of MAPTrix-F-RGD Protein

The MAPTrix-F-RGD protein was deposited using two different methods:

Method 1. The as received MAPTrix-F-RGD solution was diluted in a 50 mM sodium bicarbonate buffer solution at pH 8.5. Then, 600 µL of the diluted protein solution (0.25 mg/mL) was deposited onto the superhydrophobic Mg AZ31 samples and they were incubated at 37 °C for 3 hours. At the end of the 3 hours, the alloys were rinsed with deionized water and air-dried.

Method 2. The MAPTrix-F-RGD solution was diluted using a methanol: deionized water mixture in a 2:3 volume ratio. Then, 300 µL of the diluted protein solution (0.25 mg/mL) was deposited onto a superhydrophobic Mg AZ31 sample and they were incubated at 37 °C overnight until the liquid evaporated completely. The samples were then rinsed with deionized water and air-dried.

5.2.5 Surface Characterization

5.2.5.1 ATR-FTIR Microscopy

Attenuated Total Reflection Fourier Transform Infrared microscopy (ATR-FTIR) was used to analyze the surface chemistry of the samples. A Bruker Optics Hyperion infrared microscope with an attenuated total reflectance objective and a germanium crystal was employed. The resolution of the spectrometer was $4\ cm^{-1}$ and 100 scans were taken per spectrum. The baseline and atmospheric compensation function of the OPUS software was used to correct all spectra. Spectra were collected in a minimum of three spots per sample.

5.2.5.2 Contact Angle Analysis

Contact angle goniometry was used to evaluate the wettability of the surfaces after each stage of the surface modification. A PG-2 Pocket Goniometer was used to determine the static contact angles with 6 µL of purified 18 MΩ water. Each data point represents an average of 6 samples; the error bars are the sample to sample standard deviations.

5.2.5.3 Scanning Electron Microscopy and Energy Dispersive X-ray Spectroscopy (SEM-EDS)

Scanning electron microscopy and energy dispersive X-ray spectroscopy (SEM-EDS) were used to evaluate the surface morphology of the superhydrophobic surface. SEM images were obtained using a JEOL 6400 field emission SEM operated at 20kV, 1 nA and 10^{-6} Torr. An Oxford EDS detector was used to determine the elemental composition of the sample surface. Samples to be analyzed were coated with a thin film of carbon to render the sample conductive.

5.2.6 Cell Culture

Saos-2 cells were cultured in McCoy's 5a cell culture medium containing 15% Bovine Calf Serum and 1% penicillin/streptomycin at 37ºC in a 5% CO_2 atmosphere. The cell culture medium was changed every two days. Once the cells grew to about 70-80% confluence, the cells were washed with PBS and detached from the flask with Trypsin/EDTA and then centrifuged at 2500 rpm for 5 minutes. The supernatant was discarded, and the cells were resuspended in fresh McCoy's medium. The number of cells in the suspension was determined by the trypan blue dye using a Neubauer hemocytometer.

5.2.7 Cell Adhesion Test

All samples were sterilized in 70% ethanol before the adhesion experiment, and then rinsed with warm, sterile PBS. The samples were then placed in the wells of a 24-well plate. In order to evaluate the adhesion of cells on the superhydrophobic Mg AZ31, 40,000 cells in 2 mL of McCoy's medium were allowed to adhere on the substrates for 3 hours at 37^{o}C in a 5% CO_2 atmosphere. After the incubation period, the Mg alloys were rinsed with warm PBS in order to remove nonadherent cells, then stored at -20^{o}C overnight for the cells to lyse. Later, the cell number was determined using the CyQUANT assay, following the manufacturer's instructions. Briefly, 200 µL of CyQUANT solution was added to each sample and incubated for 5 minutes. At the end of the incubation period, 100 µL of the CyQUANT solution was pipetted from each well to a black fluorescent 96-well plate (Costar) and the fluorescence intensity of each solution was measured with a Fluostar Optima spectrofluorometer. The cell number was then determined using a calibration curve of cell number vs. fluorescence intensity. In addition, cells grown on the bare well surface were applied as a positive control group. The experiment was repeated two times on different days to ensure the reliability of the results. Each individual experiment consisted of 3 superhydrophobic samples, 3 MAPTrix-F-RGD modified superhydrophobic samples and 3 positive controls.

5.3 Results and Discussion

5.3.1 Characterization of Superhydrophobic Surfaces

In order to ensure the successful production of the superhydrophobic Mg AZ31 surface, ATR-FTIR spectroscopy and contact angle analysis were performed to characterize the surface of the samples after each step of the surface modification procedure.

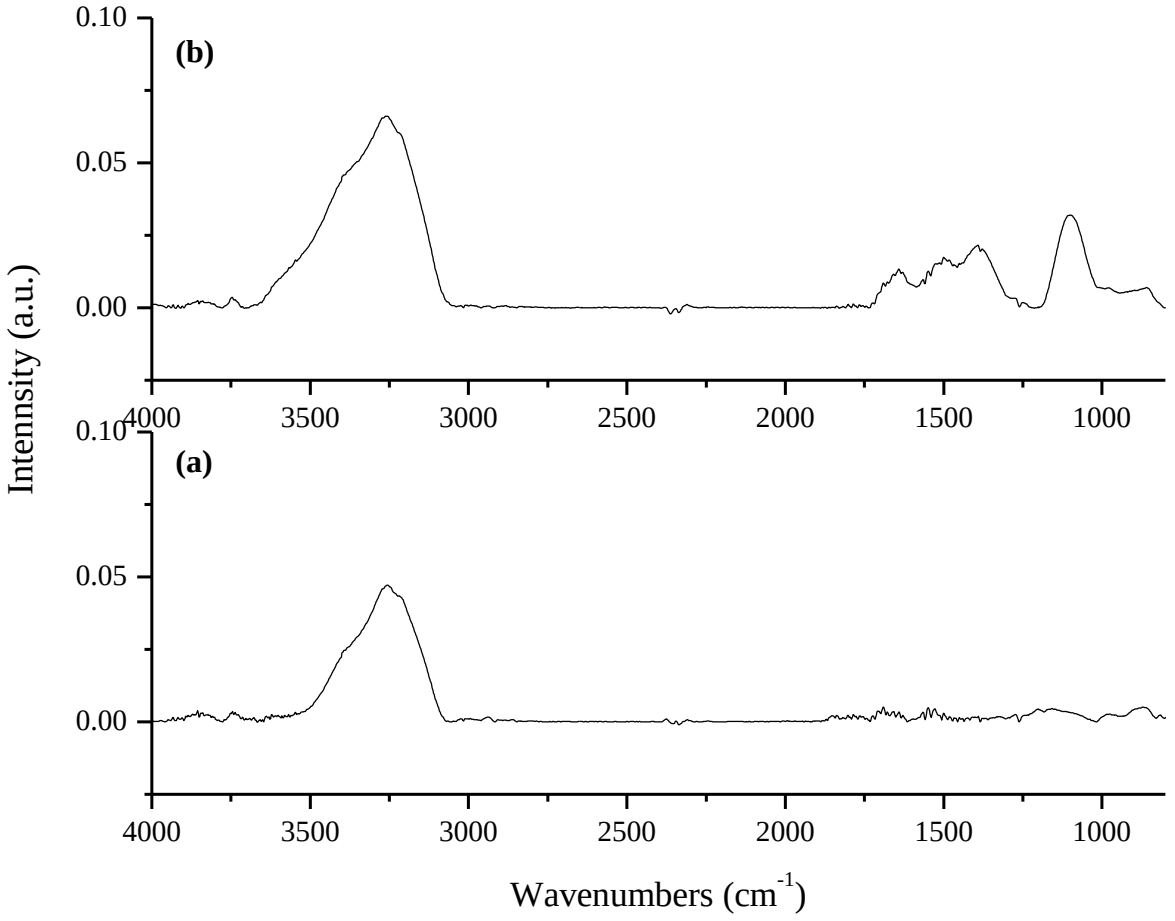

Figure 5.2: Infrared Spectra of Mg Alloy before and after Etching. (a) Polished and (b) Etched Samples.

ATR-FTIR spectroscopy was employed to confirm the surface chemistry of the magnesium alloys after each modification. Figure 5.2 shows the ATR-FTIR spectra of the Mg AZ31 samples after polished and etching. The spectrum of the polished magnesium alloy shows a small peak at 3750 cm^{-1} which indicates the presence of $Mg(OH)_2$ and a broad peak (3080-

3460 cm^{-1}) from the O-H stretch of adsorbed water at the surface. The spectrum of magnesium after the two-step etching process shows a broad carbonate stretch band centered at 1400 cm^{-1} due to the reaction of the magnesium surface with the carbon dioxide in the atmosphere. In addition, a peak at 1100 cm^{-1} was observed. The peak is due to the presence of sulphate (SO_4^{2-}) at the surface and indicates the formation of magnesium sulphate during etching in sulphuric acid.

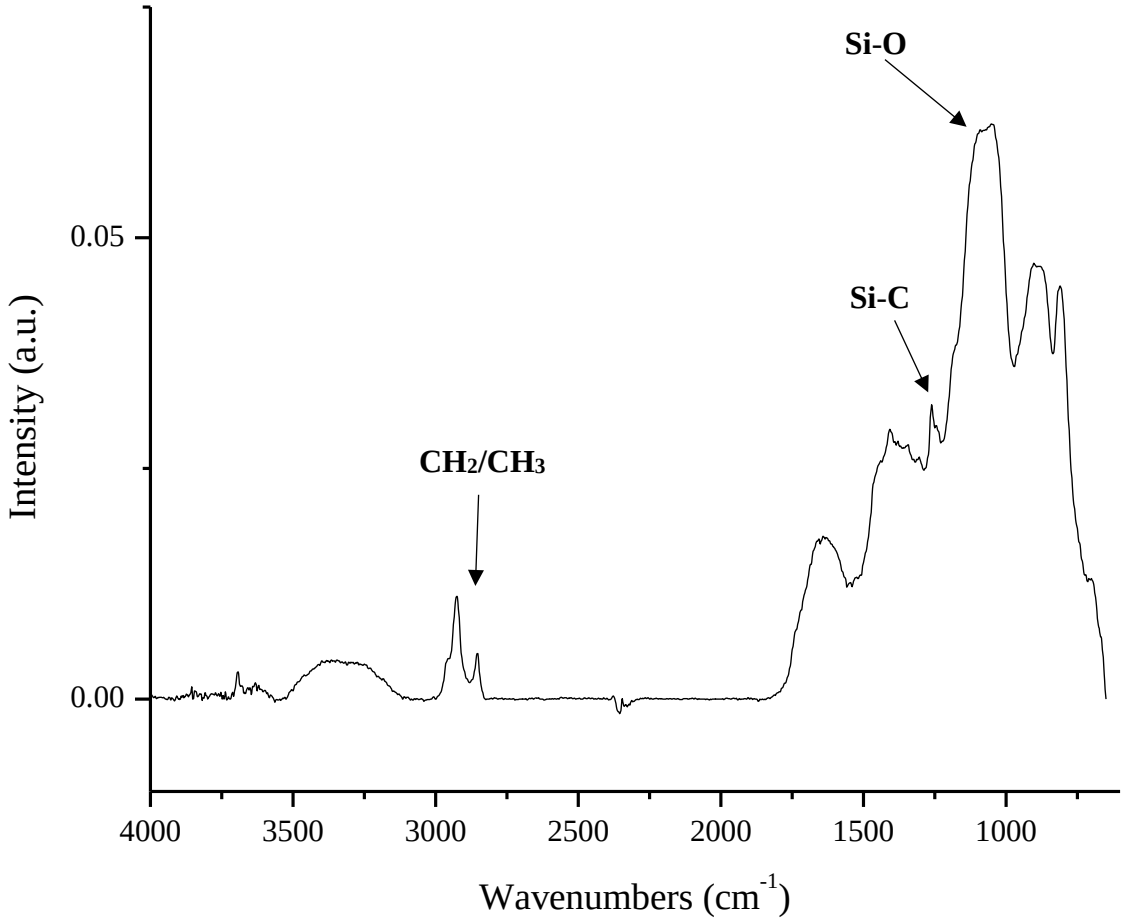

Figure 5.3: Infrared Spectrum of Hydrophobic Polysiloxane Coating on Polished Magnesium Alloys.

The deposition of a hydrophobic layer on the top of the rough surface is a very important step to produce a superhydrophobic surface. A hydrophobic polysiloxane layer was deposited by using MPTS and PDMS as both of these compounds are hydrophobic. MPTS was present as a linker molecule to bind the polysiloxane layer to the magnesium alloy surface. After hydrolysis

of the MPTS molecules, a condensation reaction between the terminal hydroxyl groups on the PDMS molecules and the silanol groups of MPTS will occur to link the two hydrophobic compounds together. Then, by further condensation of the silanol of MPTS with hydroxyl groups on the magnesium alloy surface, the polysiloxane layer will covalently bond to the surface of magnesium. Figure 5.3 shows the ATR-FTIR spectra of the hydrophobic polysiloxane coating deposited on the polished magnesium alloy. There are three peaks that confirm the presence of the polysiloxane coating on the surface of the polished magnesium alloy sample. The first is the (Si-O-Si) peak at 1050-1200 cm^{-1} which indicates the presence of silicate. The second is the (Si-CH_3) peak at 1260 cm^{-1} which confirms the polymerization of MPTS with PDMS. The third is the (C-H) stretch at 2850-3000 cm^{-1} which confirms the presence of the alkyl functional groups of the MPTS and PDMS molecules. These three peaks were preferred for confirming the presence of the hydrophobic siloxane coating on the sample surfaces as there is no interference from peaks due to the polished and etched substrates.

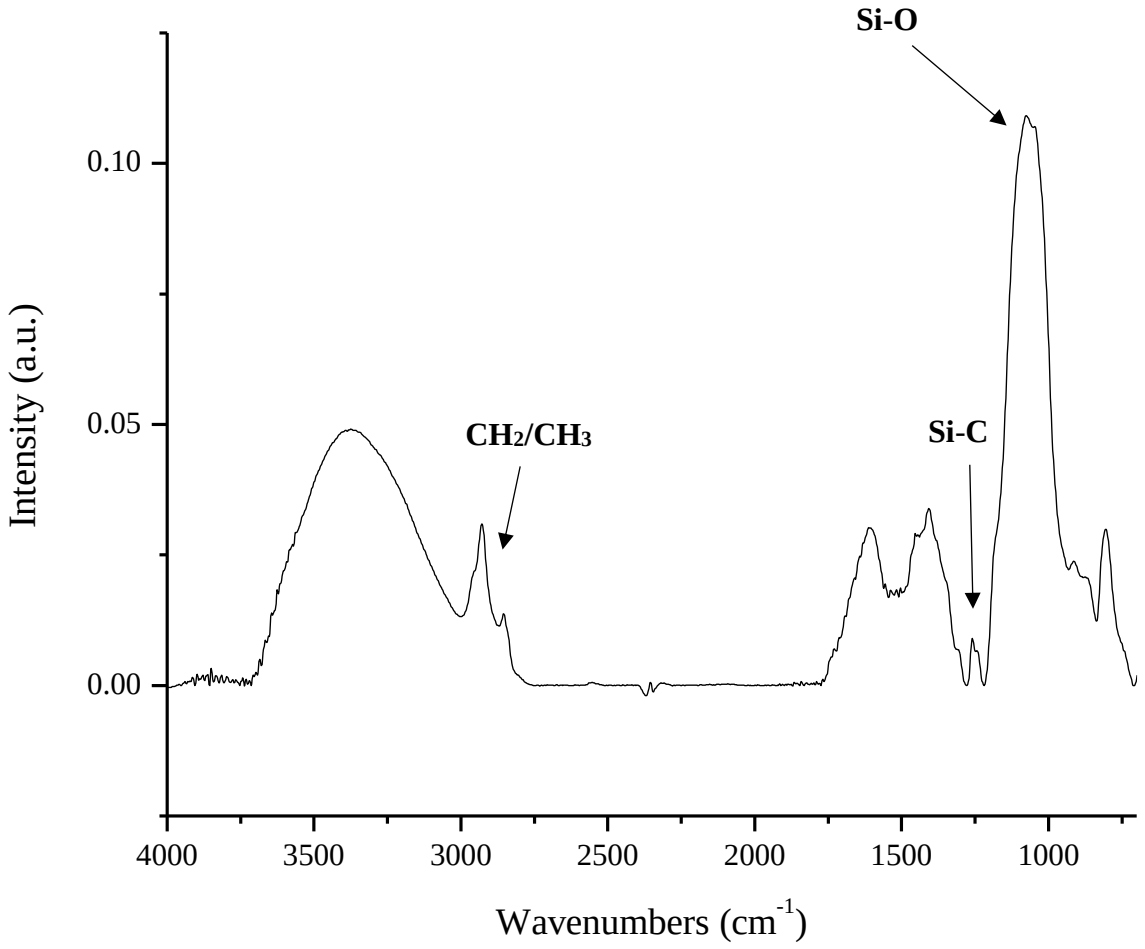

Figure 5.4: Infrared Spectrum of Superhydrophobic Surface of Magnesium Alloys

In order to produce a superhydrophobic surface, it is necessary to have a combination of surface roughness and hydrophobic surface chemistry. Figure 5.4 shows an ATR-FTIR spectrum of the superhydrophobic surface produced by depositing a hydrophobic polysiloxane layer on the etched magnesium alloy surface. The presence of Si-O-Si, Si-CH_3 and C-H stretch peaks in the spectrum indicate the successful deposition of the hydrophobic polysiloxane coating on the etched magnesium alloys.

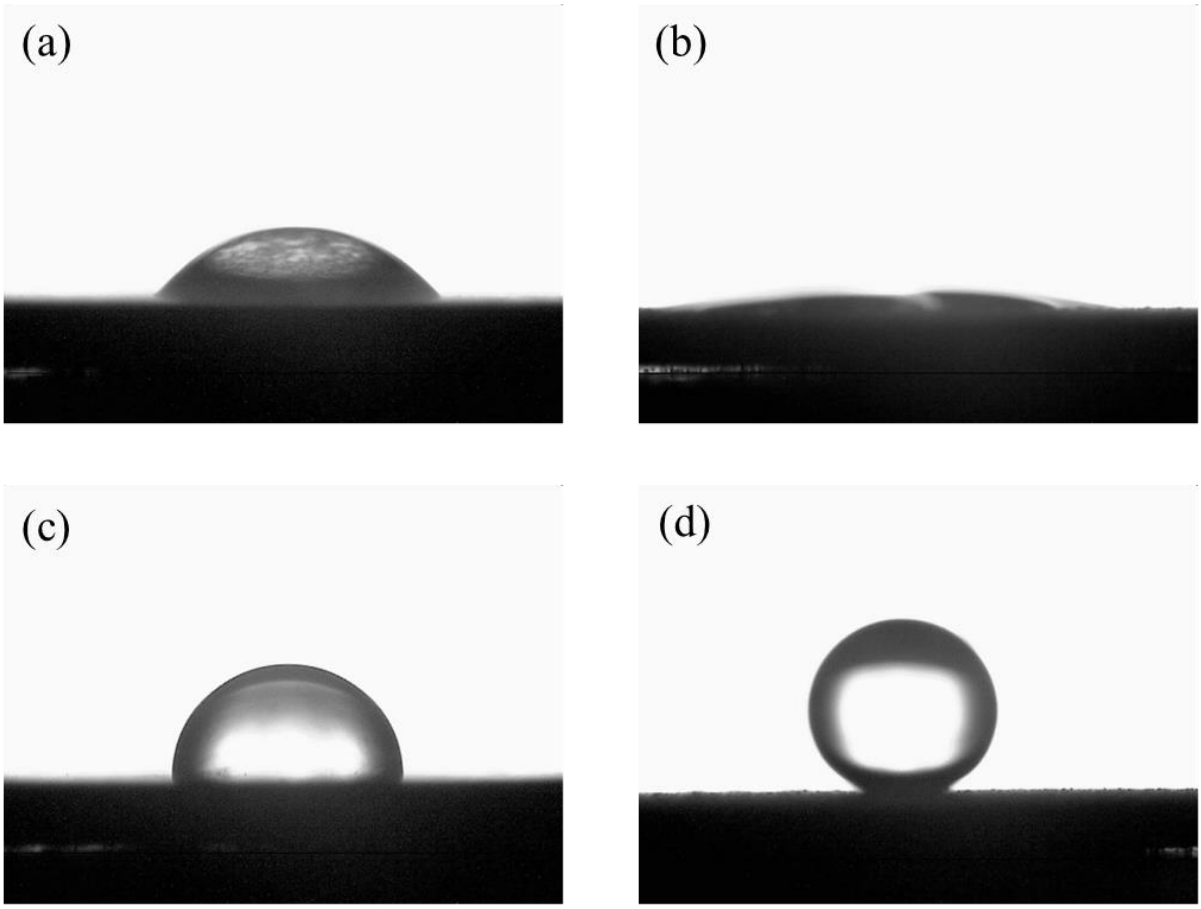

Figure 5.5: Images of Geometric Water Contact Angles of (a) Polished Surface, (b) Etched Surface, (c) Polysiloxane Coating on Polished Surface, and (d) Polysiloxane Coating on Etched Surface (Superhydrophobic Surface).

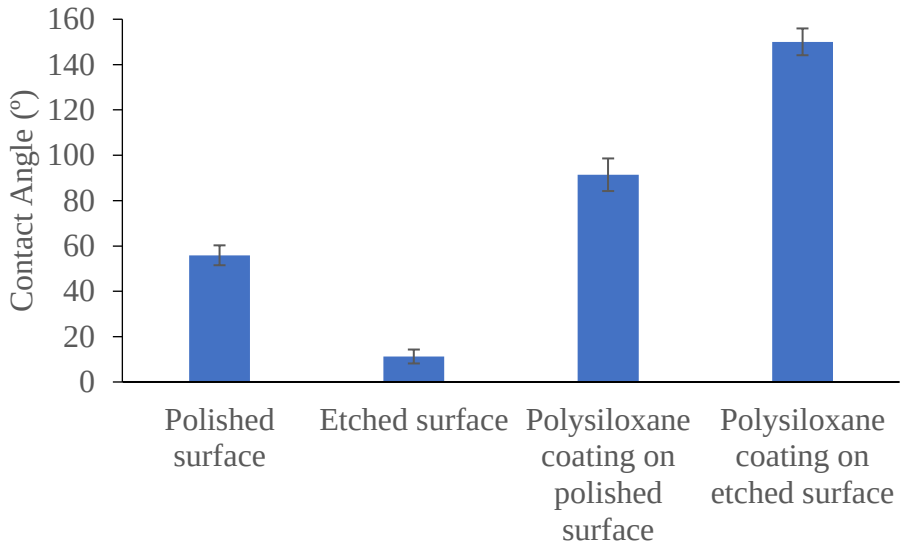

Figure 5.6: Water Contact Angle Measurements of (a) Polished Surface, (b) Etched Surface, (c) Polysiloxane Coating on Polished Surface, and (d) Polysiloxane Coating on Etched Surface. Each Data Point Represents an Average of 6 Samples; the Error Bars are the Sample to Sample Standard Deviations.

To evaluate the wettability of the surface, contact angle analysis was performed after each step of the surface modification procedure. Figure 5.5 and Figure 5.6 show the images of the water droplets and the measured contact angles alloys after each step of the superhydrophobic surface modification procedure. The contact angle of the polished magnesium substrates was (55.8°±4.3°), indicating that the polished and cleaned Mg AZ31 surfaces were slightly hydrophilic while the etched surfaces were very hydrophilic with low contact angles (11.2°± 3.0°) due to the surface roughness produced during acid etching. The contact angle of the polysiloxane coating on apolished magnesium alloys was (91.4°± 7.1°) indicating a slightly hydrophobic surface due to the hydrophobic nature of the MPTS and PDMS molecules.

To produce a superhydrophobic surface, a combination of a rough surface topography with a hydrophobic surface chemistry is needed. Combining both the etched surface and the hydrophobic polysiloxane coating produced a superhydrophobic surface on magnesium alloys that is confirmed by its high contact angle of 150.0°± 5.9°.

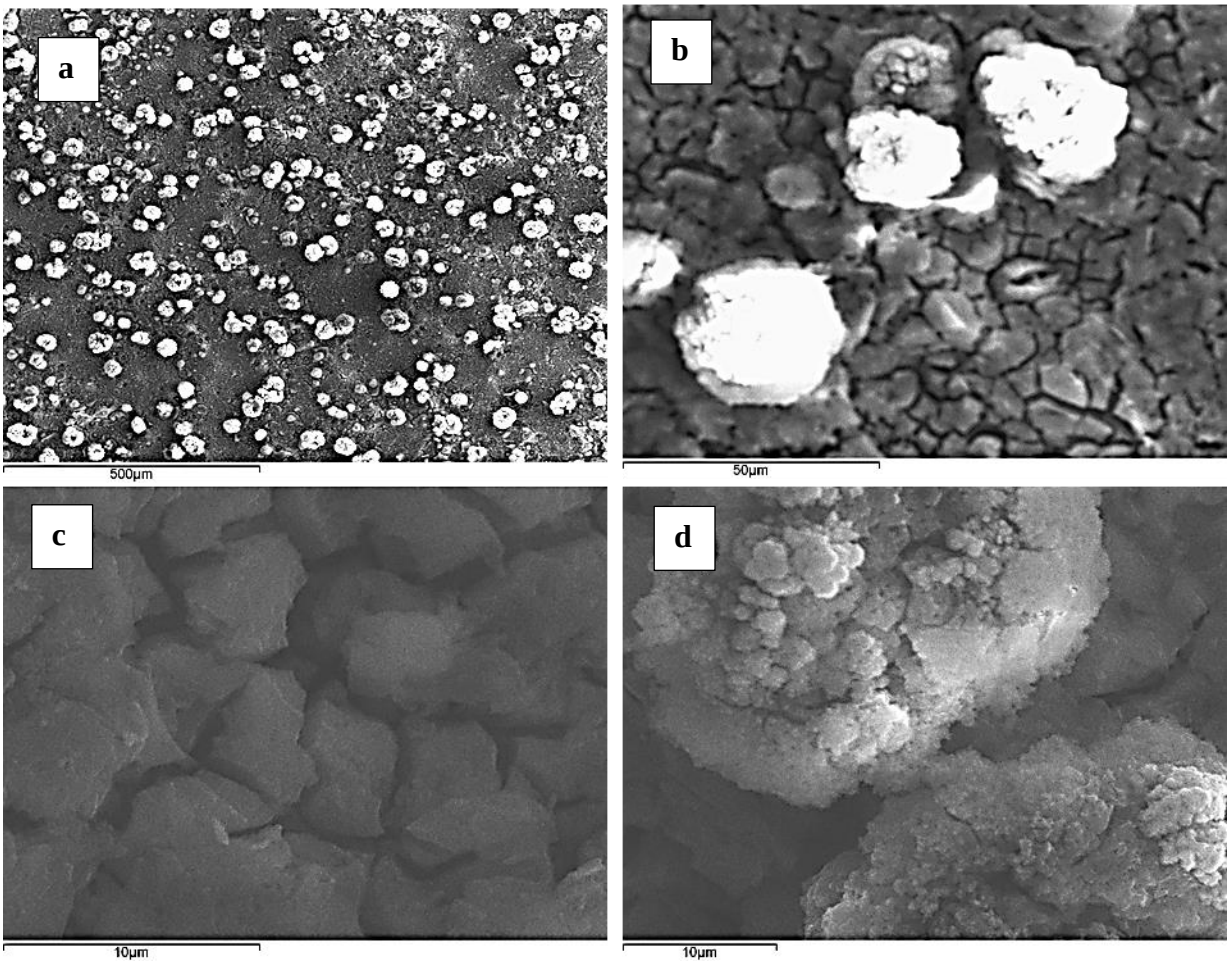

Figure 5.7: SEM Images of the Superhydrophobic Surface of Magnesium Alloy at Different Magnifications. (a) Full Superhydrophobic Surface at Low Magnification 500µm, (b) Full Surface at High Magnification with a Scale of 50µm (c) Flat Area at High Magnification with a Scale of 10µm (d) Spherical Particles at High Magnification with a scale of 10µm.

The topography of the etched surface was observed using SEM microscopy. Figure 3.7 shows the SEM images of the etched magnesium alloy surface at different magnifications. The surface image in Figure 5.7 (a) shows randomly distributed spherical particles over the whole surface. At higher magnification image (b), it is evident that the size of these spherical particles is approximately 25 μm diameter. These protrusions provided the microstructures that are necessary to mimic the superhydrophobic surface of the lotus leaf. Also, at high magnification image (c) of the flat area, it is clear that there are cracks on the flat area of the surface. Moreover, image (d) shows the spherical particles at higher magnification; this image shows that the micro-scale particles are composed of smaller particles of variable size. This set of images illustrates the complex topography produced by the etching process. In addition, Figure 5.1 showed that when the polysiloxane coating was added an additional nanoscale rod like topography was added to the surface.

5.3.2 Deposition of MAPTrix-F-RGD Protein on the Superhydrophobic Surface

The previous section of this study confirmed the successful reproducibility of the superhydrophobic surface. In order to improve the biocompatibility of the superhydrophobic surface, further surface modification by immobilization of the cell adhesive molecule MAPTrix-F-RGD protein was employed. The presence of the RGD peptide in this MAPTrix-F-RGD protein should help to mimic the extracellular matrix. The RGD sequence is a well-known unique amino acid sequence that can be specifically recognized by integrins on the cell

membrane thus supporting cell adhesion and proliferation at biomaterials surfaces [21]. In order to optimize the best deposition conditions for the immobilization of the MAPTrix-F-RGD protein on the superhydrophobic surfaces, two different methods were tested as described in section 5.2.4. The modified samples were analyzed by infrared microscopy and contact angle analysis to confirm the deposition of the MAPTrix-F-RGD protein on the superhydrophobic surface.

5.3.2.1 Deposition of MAPTrix-F-RGD Protein Using Sodium Bicarbonate Solution

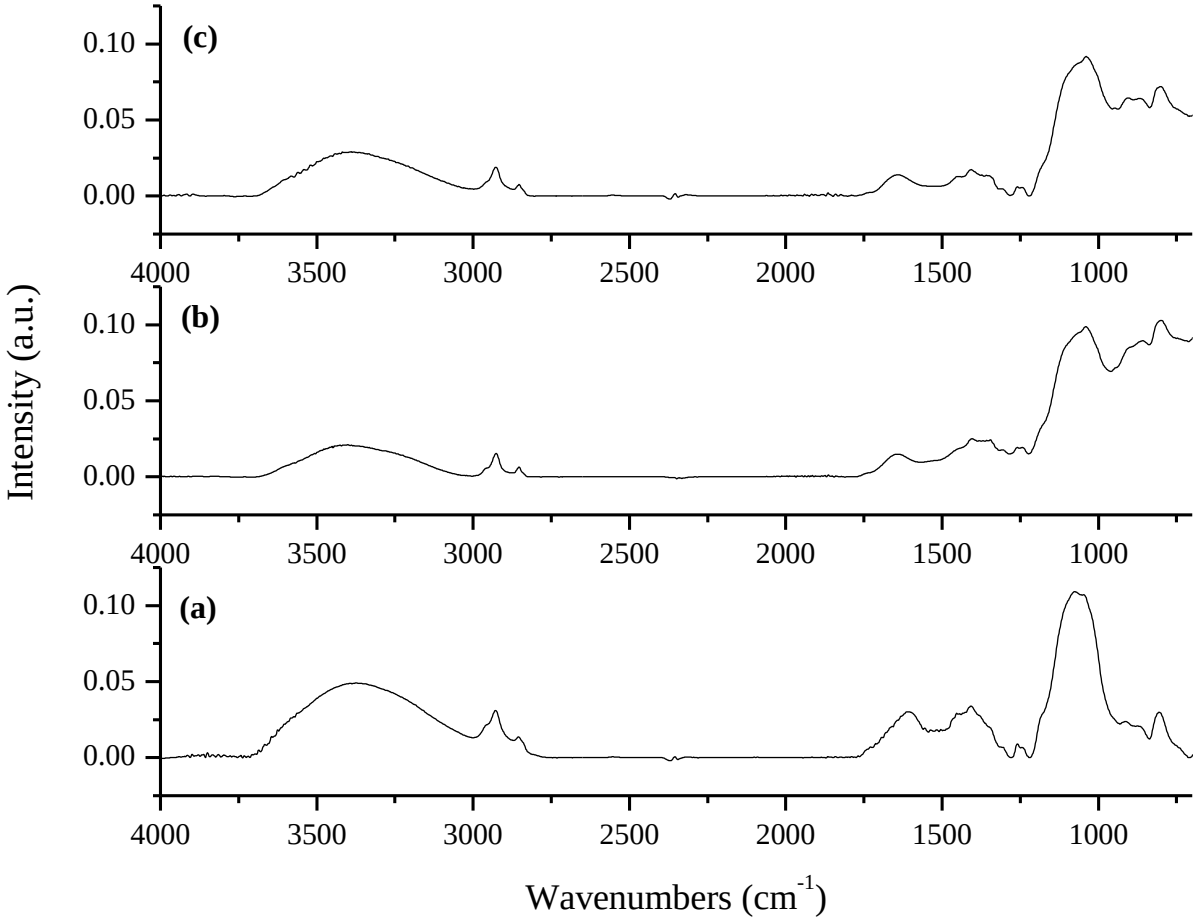

Figure 5.8: Infrared Spectra of MAPTrix-F-RGD Protein Deposited on Superhydrophobic Surface Using Sodium Bicarbonate Solution and Various Concentration of MAPTrix-F-RGD Protein. (a) Superhydrophobic Surface and after Deposition of (b) 0.1 mg mL^{-1} and (c) 0.25 mg mL^{-1} of MAPTrix-F-RGD Protein for 3 hours Deposition Time.

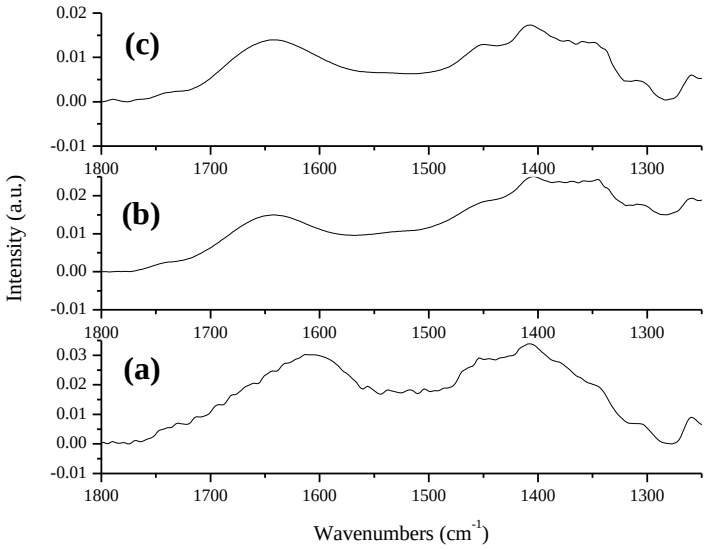

Figure 5.9: Partial Infrared Spectra of Superhydrophobic Surface before and after Deposition of MAPTrix-F-RGD Protein. (a) Superhydrophobic Surface and after Deposition of (b) 0.1 mg mL^{-1} and (c) 0.25 mg mL^{-1} of MAPTrix-F-RGD Protein for 3 hours Deposition Time.

Figure 5.8 and Figure 5.9 show the ATR-FTIR spectra of superhydrophobic surfaces of magnesium alloys before and after deposited MAPTrix-F-RGD protein with various concentrations using sodium bicarbonate solution as the solvent. MAPTrix-F-RGD is a protein and therefore it can be identified by the presence of the amide I (C=O stretch at 1650 cm^{-1}) and amide II (N-H bend at 1500 cm^{-1}). The spectra of the superhydrophobic surfaces after deposition of MAPTrix-F-RGD protein (0.1 mg mL^{-1} and 0.25 mg mL^{-1}) are similar to those of the unmodified superhydrophobic surface. A slight shift of the peak at 1610 cm^{-1} to 1650 cm^{-1} was observed which could be related to the presence of the amide I band of the protein. The

differences subtle in the spectra due to overlapping peaks from the superhydrophobic surface itself. However, the contact angle measurements after modification with MAPTrix-F-RGD dropped from 150.03° ± 5.90° to 26.36°± 7.31° and 27.24°± 4.3° for samples modified with 0.1 mg mL^{-1} and 0.25 mg mL^{-1} MAPTrix-F-RGD respectively.

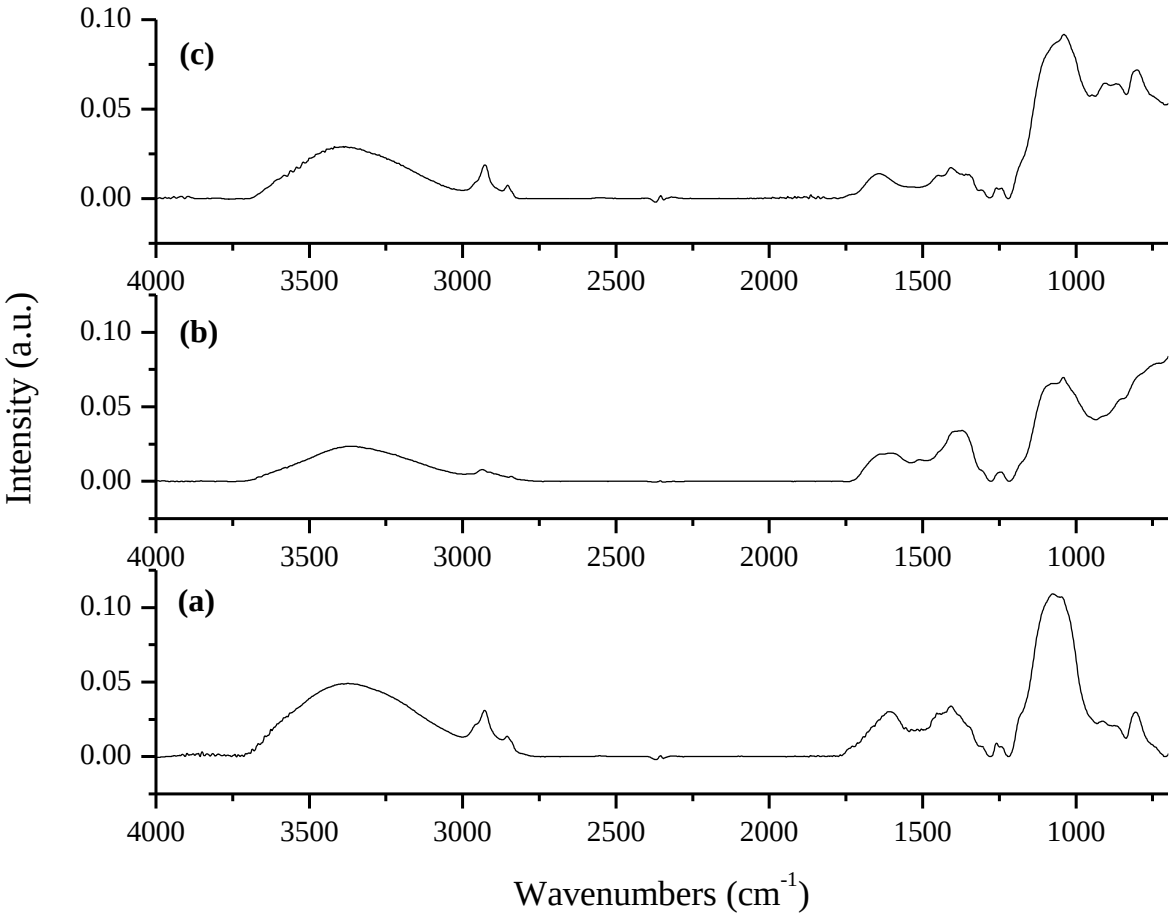

Figure 5.10: Infrared Spectra of MAPTrix-F-RGD Protein Deposited on Superhydrophobic Surface Using Sodium Bicarbonate Solution at Concentration of 0.25 mg mL^{-1} and Various Deposition Time. (a) Superhydrophobic Surface and (b, c) after 1 and 3 hours of Deposition MAPTrix-F-RGD Protein.

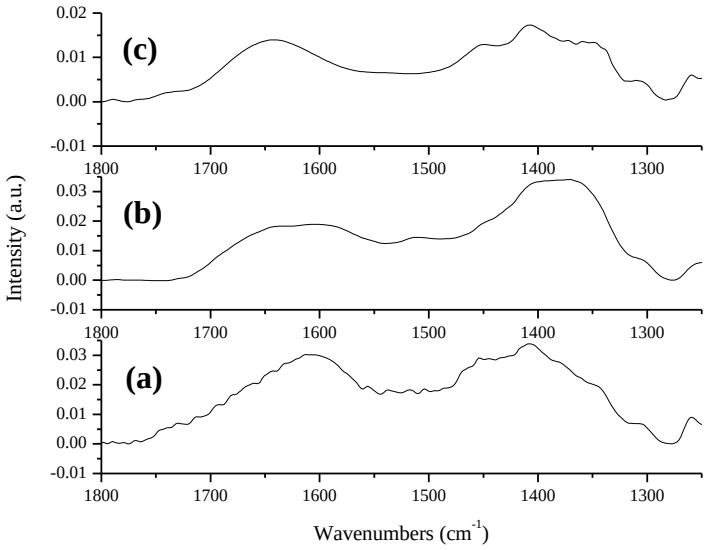

Figure 5.11: Partial Infrared Spectra of Superhydrophobic Surface before and after Deposition of MAPTrix-F-RGD Protein. (a) Superhydrophobic Surface and (b, c) after 1 and 3 hours of Deposition MAPTrix-F-RGD Protein.

Figure 5.10 and Figure 5.11 show the ATR-FTIR spectra of superhydrophobic surfaces of magnesium alloys before and after deposited MAPTrix-F-RGD protein using sodium bicarbonate solution at concentration of 0.25 mg mL^{-1} and various deposition time. The spectra of the superhydrophobic surfaces after 1 and 3 hours of MAPTrix-F-RGD protein deposition are similar to those of the unmodified superhydrophobic surface. There is only a slight shift of the peak from 1610 cm^{-1} peak to 1650 cm^{-1} was observed which could be related to the presence of the amide I band of the protein.

5.3.2.2 Deposition of MAPTrix-F-RGD Protein Using the Mixture of Methanol and Water Solution

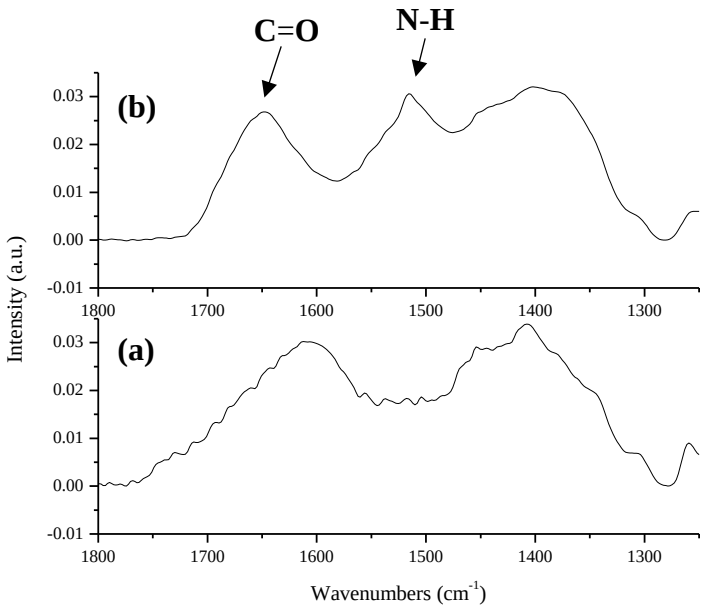

Figure 5.12: Partial Infrared Spectra of MAPTrix-F-RGD Protein Deposited on Superhydrophobic Surface of Magnesium Alloys Using a Methanol/Water Solution. (a) Superhydrophobic Surface and (b) after Deposition of MAPTrix-F-RGD Protein.

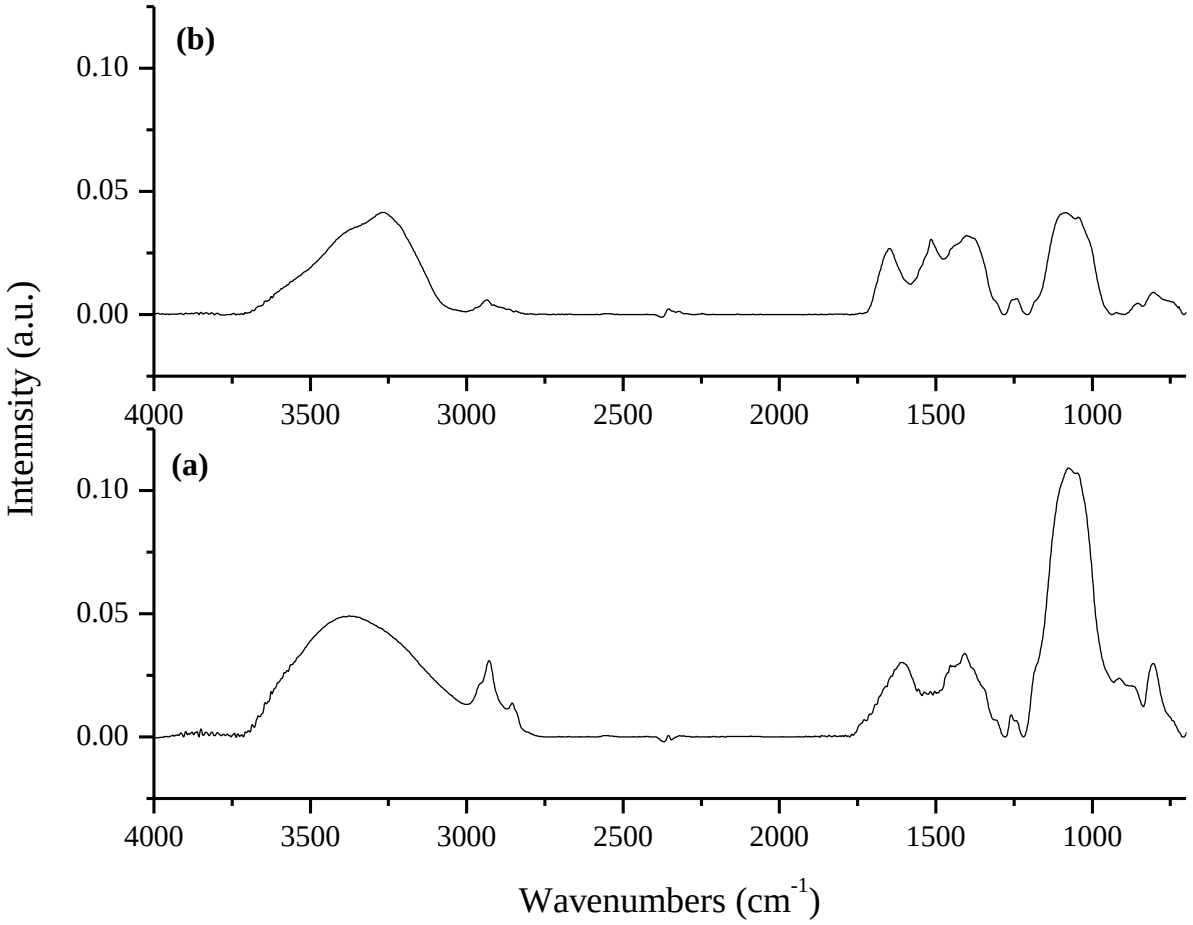

Figure 5.13: Infrared Spectra of MAPTrix-F-RGD Protein Deposited on Superhydrophobic Surface of Magnesium Alloys Using a Methanol/Water Solvent. (a) Superhydrophobic Surface and (b) after Deposition of MAPTrix-F-RGD Protein.

Figure 5.12 shows the partial ATR-FTIR spectra of MAPTrix-F-RGD protein deposited on superhydrophobic surface of magnesium alloys using the mixture of methanol and water as a solvent (0.25 mg mL^{-1} of MAPTrix-F-RGD). The spectrum of the superhydrophobic surface

after deposition of MAPTrix-F-RGD (b) shows a new peak at 1515 cm^{-1} which indicates the presence of amide II band (N-H stretch). Despite overlapping with adsorbed water peak (O-H), the amide I peak at 1650 cm^{-1} was clearly observed and the peak becomes sharper than before modification. Therefore, these observations confirm the successful deposition of MAPTrix-F-RGD protein on the superhydrophobic surface using the mixture of methanol and water as a solvent.

Figure 5.13 shows the whole ATR-FTIR spectra of MAPTrix-F-RGD protein deposited on superhydrophobic surface of magnesium alloys using the mixture of methanol and water as a solvent in comparison to superhydrophobic surface before modification. It is clear from the whole spectrum that all peaks indicating the presence of the polysiloxane coating are still present after the deposition of the Maptrix-F-RGD protein. Thus, the methanol/water solvent had no impact on the underlying polysiloxane coating.

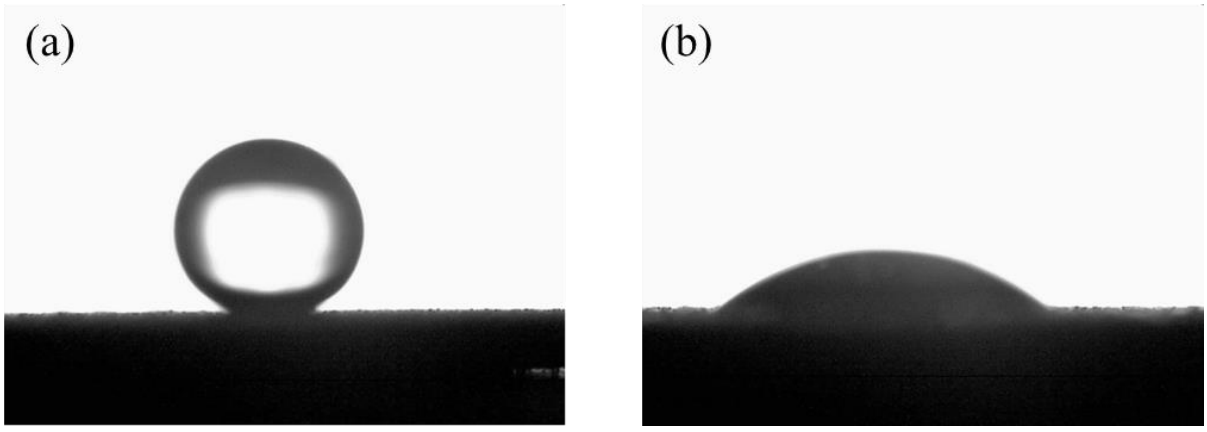

Figure 5.14: Images of Geometric Water Contact Angles of (a) Superhydrophobic Surface and (b) MAPTrix-F-RGD Modified Superhydrophobic Surface Using a Methanol/water Mixture as Solvent.

The influence of the MAPTrix-F-RGD protein on the wettability of the superhydrophobic surface was evaluated by contact angle analysis. Figure 5.14 shows water droplets on the superhydrophobic surface of magnesium alloys before and after deposition of MAPTrix-F-RGD protein. A significant change in the water contact angle from 150.0°± 5.9° to 39.3º ± 5 indicates that the surface was successfully modified through MAPTrix-F-RGD protein and that the presence of the protein increased the hydrophilicity of the surface.

5.3.3 Evaluation of the Biocompatibility of MAPTrix-F-RGD Protein Deposited on Superhydrophobic Surface of Magnesium Alloy AZ31

While superhydrophobic surfaces decrease the rapid degradation of magnesium alloys, the interaction between the cells and the superhydrophobic surface is also reduced leading to poor cell adhesion and limited biocompatibility. It is well known that hydrophilic surfaces

typically enhance cell adhesion on biomaterials [30]. A study by Lim et al. observed that the osteoblastic cells exhibited greater adhesion and proliferation on hydrophilic surfaces than on hydrophobic surfaces [30]. Therefore, it was expected that the presence of the RGD ligand coupled with the improved wettability of the surface would lead to improved cell adhesion for the MAPTrix-F-RGD modified superhydrophobic surfaces in comparison to the unmodified superhydrophobic surfaces. This is important because cell adhesion on biomaterials surfaces is an essential step for evaluating the biocompatibility of implants to ensure successful ossteoconduction and osseointegration of the implant with bone tissue [31]. In particular, a study performed in our lab by Yang et al. demonstrated successful adhesion and proliferation of SAOS-2 cells on a magnesium alloy surface through the covalent attachment of RGD peptides.

The biocompatibility of MAPTrix-F-RGD modified superhydrophobic surfaces was evaluated by comparing the number of cells adhered on the modified surface versus the superhydrophobic control sample.

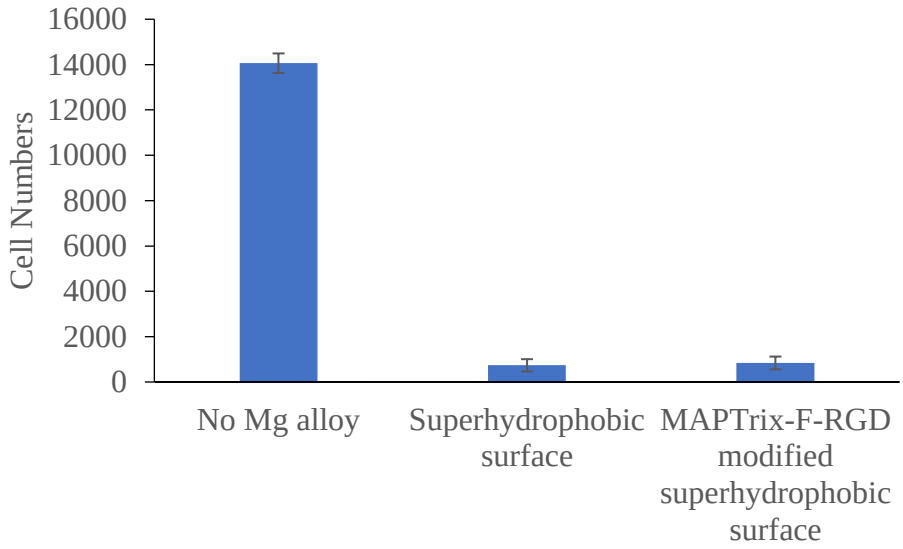

Figure 5.15: Cell Numbers of (Saos-2 Cell) Adhered on Superhydrophobic Surface before and after Deposition of MAPTrix-F-RGD Protein using Sodium Bicarbonate Solution. The Data are the Average of 3 Replicates and the Experiment was Repeated Two Times to Ensure Reproducibility.

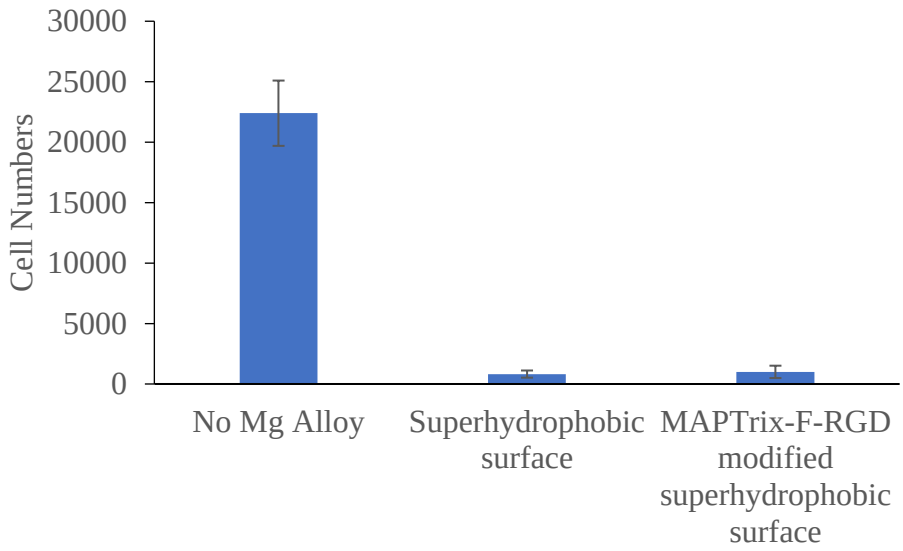

Figure 5.16: Cell Numbers of (Saos-2 Cell) Adhered on Superhydrophobic Surface before and after Deposition of MAPTrix-F-RGD Protein using the Mixture of Methanol and Water Solution. The Data are the Average of 3 Replicates and the Experiment was Repeated Two Times to Ensure Reproducibility.

Figure 5.15 shows the number of Saos-2 cells adhered on the superhydrophobic surface before and after deposition of MAPTrix-F-RGD from a sodium bicarbonate solution and Figure 5.16 shows the number of Saos-2 cell adhered on the superhydrophobic surface before and after deposition of MAPTrix-F-RGD protein from a methanol/water mixture. Cells grown on the bare well surface (No Mg alloy) was applied as a positive control group.

Also, a preliminary study was performed for MAPTrix-F-RGD protein deposited on the well surface to investigate the cell adhesion capability of this molecule in the absence of

superhydrophobic and modified superhydrophobic magnesium alloys. The results were positive and indicated that cells readily adhered to these surfaces.

As observed in Figure 5.15 and Figure 5.16, the average number of cells adhered to the modified superhydrophobic surface is similar to the average number of cells adhered to the superhydrophobic surface. Although, infrared spectroscopy confirmed that the cell adhesive molecule was successfully immobilized to the surface and that the surface wettability was greatly improved, cell adhesion was not improved on the MAPTrix-F-RGD modified superhydrophobic samples. Possible reasons for this behaviour are discussed below.

It is well known that morphology, wettability, topography, and chemical composition of a biomaterial surface all have a strong influence on cell behavior [32]. However, the influence of surface properties on cell behavior is still not fully understood. Many scientists have debated the roles of various surface properties on the cell adhesion efficiency due to the complex relationship between these properties. For example, hydrophilic surfaces are generally known to have a higher affinity for cells while superhydrophobic surfaces have been generally reported to prevent cell adhesion. Dowling et al. reported that the adhesion and proliferation of osteoblast cells were prevented on superhydrophobic surfaces [33]. However, in another study, Zangi et al. synthesized superhydrophobic surfaces with microscale and nanoscale features; they found that the sample with a micro-scale rough structure and superhydrophobic behavior accelerated cell attachment and proliferation while the sample with a nano-scale rough structure and superhydrophobic behavior strongly inhibited cell adhesion [34]. Therefore, it was concluded from this study that surface topography plays a more significant role in cell adhesion than

superhydrophobicity [34]. In contrast, other studies have suggested that micro-scale surface topography enhances the anti-adhesive properties of the implant material surface since it significantly reduced the adhesion of macrophages and fibroblast cells [35,36].

Therefore, our results and the inhibition of cell adhesion on both the superhydrophobic surface and the MAPTrix-F-RGD modified superhydrophobic surface may be attributed to the topography of the superhydrophobic surface. The superhydrophobic magnesium surface prepared in this study has a hierarchical surface topography consisting of micron scale papillae produced during etching (approximately 25 μm diameter spherical particles) and a nanoscale rod like structure from the polysiloxane overcoating. Many studies have demonstrated that nano-scale topography can inhibit or reduce cell adhesion [34,37]. This inhibition has been attributed to the amount and the conformation of the protein adsorbed on the surface [38].

In addition, the height of the micron scale particles present on the superhydrophobic surface, may be an obstacle to cell adhesion and spreading because they are on the order of the cell size. Many studies have also reported that micro-scale topographies with different shapes, sizes, heights and surface distribution can affect cell adhesion [35,36]. This effect can be either positive or negative, some studies have shown that micron scale topographies enhance cell adhesion [34,37,39]. However, the effect of topography is very complex with cell behavior being dependent on the type, size, height and regularity of the feature and also the cell size and type. Le Saux et al. synthesised surfaces that had topographical features with various pyramids height, RGD ligands were immobilized on these surfaces to study the effect of these topographical features on cell adhesion. The cell behaviour results after immobilization of RGD ligands on

these surfaces demonstrated that surfaces with micro-scaled pyramids, which had the highest height values, reduced the cell adhesion compared to flat surfaces. Furthermore, although it is known that the RGD ligands influence cell behavior, the presence of RGD ligands on their micro scale surfaces did not enhance the cell adhesion [40].

Accordingly, on the surfaces prepared in this study, the nano-scale particles coupled with the large height of the micro-scale particles and their overall surface distribution may be the reasons that cell adhesion is inhibited on the MAPTrix-F-RGD modified superhydrophobic surface despite its known cell adhesive properties and the improved wettability of our modified surfaces. Changes to the surface etching procedure may be an option to control this topography to give microscale particles with smaller height; this may lead to an improvement in cell adhesion on the modified superhydrophobic surface.

5.4 Conclusion

In this study, a superhydrophobic Mg AZ31 surface was successfully reproduced through a combination of rough hierarchical topography and a hydrophobic overlayer. It is well-known that superhydrophobic surfaces reduce the interaction between the cell and the surface. Therefore, a simple method for modifying the superhydrophobic surface was employed to mimic the extracellular matrix (ECM). The superhydrophobic surface was successfully modified with cell adhesive MAPTrix-F-RGD protein. However, the results from the cell adhesion test demonstrated that MAPTrix-F-RGD protein on the superhydrophobic surface did not improve the cell adhesion to the superhydrophobic surfaces. This is likely due the complex topography of the surface.

References

1. Prasad, K., et al. "Metallic biomaterials: Current challenges and opportunities." *Materials* 10.8 (2017): 884.

2. Walker, J., et al. "Magnesium biomaterials for orthopedic application: a review from a biological perspective." *Journal of Biomedical Materials Research Part B: Applied Biomaterials* 102.6 (2014): 1316-1331.

3. Zheng, Y. F., et al. "Biodegradable metals." *Materials Science and Engineering: R: Reports* 77 (2014): 1-34.

4. Liu, C., et al. "Biodegradable magnesium alloys developed as bone repair materials: a review." *Scanning* 2018 (2018): 9216314.

5. Zeng, R. C., et al. "Corrosion resistance of calcium-modified zinc phosphate conversion coatings on magnesium-aluminium alloys." *Corrosion Science* 88 (2014): 452-459.

6. Zomorodian, A., et al. "Corrosion resistance of a composite polymeric coating applied on biodegradable AZ31 magnesium alloy." *Acta Biomaterialia* 9.10 (2013): 8660-8670.

7. Dalmoro, V., et al. "Hybrid organophosphonic-silane coating for corrosion protection of magnesium alloy AZ91: The influence of acid and alkali pre-treatments." *Surface and Coatings Technology* 357 (2019): 728-739.

8. Wang, Z., et al. "Facile and fast fabrication of superhydrophobic surface on magnesium alloy." Applied Surface Science 271 (2013): 182-192.

9. Yan, Y. Y., N. Gao, and W. Barthlott. "Mimicking natural superhydrophobic surfaces and grasping the wetting process: A review on recent progress in preparing superhydrophobic surfaces." *Advances in Colloid and Interface Science* 169.2 (2011): 80-105.

10. Yeganeh, M., and N. Mohammadi. "Superhydrophobic surface of Mg alloys: A review." *Journal of Magnesium and Alloys* (2018): 59-70.

11. Ishizaki, T., et al. "Corrosion resistance and chemical stability of super-hydrophobic film deposited on magnesium alloy AZ31 by microwave plasma-enhanced chemical vapor deposition." *Electrochimica Acta* 55.23 (2010): 7094-7101.

12. Ishizaki, T., Y. Masuda, and M. Sakamoto. "Corrosion resistance and durability of superhydrophobic surface formed on magnesium alloy coated with nanostructured cerium oxide film and fluoroalkylsilane molecules in corrosive NaCl aqueous solution." *Langmuir* 27.8 (2011): 4780-4788.

13. Liang, J., et al. "Fabrication of superhydrophobic surface on magnesium alloy." *Chemistry Letters* 36.3 (2007): 416-417.

14. Song, J., et al. "Fabrication of superhydrophobic surfaces with hierarchical rough structures on Mg alloy substrates via chemical corrosion method." *Micro & Nano Letters* 7.3 (2012): 204-207.

15. Zhang, F., et al. "Fabrication of the superhydrophobic surface on magnesium alloy and its corrosion resistance." *Journal of Materials Science & Technology* 31.11 (2015): 1139-1143.

16. Wang, Y., et al. "Super-hydrophobic surface on pure magnesium substrate by wet chemical method." *Applied Surface Science* 256.12 (2010): 3837-3840.

17. Xu, W., et al. "Rapid fabrication of large-area, corrosion-resistant superhydrophobic Mg alloy surfaces." *ACS applied Materials & Interfaces* 3.11 (2011): 4404-4414.

18. Pernites, R. B., et al. "Tunable protein and bacterial cell adsorption on colloidally templated superhydrophobic polythiophene films." *Chemistry of Materials* 24.5 (2011): 870-880.

19. Moradi, S., et al. "Effect of extreme wettability on platelet adhesion on metallic implants: From superhydrophilicity to superhydrophobicity." *ACS Applied Materials & Interfaces* 8.27 (2016): 17631-17641.

20. Gray-Munro, J. E., and J. Campbell. "Mimicking the hierarchical surface topography and superhydrophobicity of the lotus leaf on magnesium alloy AZ31." *Materials Letters*189 (2017): 271-274.

21. Gray-Munro, J. E. "Biomimetic surface modifications of magnesium and magnesium alloys for biomedical applications." *Surface Modification of Magnesium and its Alloys for Biomedical Applications*. Woodhead Publishing, 2015. 271-299.

22. Hynes, R. O. "Integrins: bidirectional, allosteric signaling machines." *Cell* 110.6 (2002): 673-687.

23. Chollet, C., et al. "The effect of RGD density on osteoblast and endothelial cell behavior on RGD-grafted polyethylene terephthalate surfaces." *Biomaterials* 30.5 (2009): 711-720.

24. Dettin, M., et al. "Covalent surface modification of titanium oxide with different adhesive peptides: Surface characterization and osteoblast-like cell adhesion." *Journal of Biomedical Materials Research Part A: An Official Journal of The Society for Biomaterials* 90.1 (2009): 35-45.

25. Yang, X., et al. "Influence of mixed organosilane coatings with variable RGD surface densities on the adhesion and proliferation of human osteosarcoma Saos-2 cells to magnesium alloy AZ31." *Bioactive Materials* 2.1 (2017): 35-43.

26. Jo, Y. K., et al. "Biomimetic surface engineering of biomaterials by using recombinant mussel adhesive proteins." *Advanced Materials Interfaces* 5.9 (2018): 1800068.

27. Dalsin, J. L., et al. "Protein resistance of titanium oxide surfaces modified by biologically inspired mPEG-DOPA." *Langmuir* 21.2 (2005): 640-646.

28. Hwang, D. S., S. B. Sim, and H. J. Cha. "Cell adhesion biomaterial based on mussel adhesive protein fused with RGD peptide." *Biomaterials* 28.28 (2007): 4039-4046.

29. Hwang, D. S., J. H. Waite, and M. Tirrell. "Promotion of osteoblast proliferation on complex coacervation-based hyaluronic acid-recombinant mussel adhesive protein coatings on titanium." *Biomaterials* 31.6 (2010): 1080-1084.

30. Lim, J. Y., et al. "Systematic variation in osteoblast adhesion and phenotype with substratum surface characteristics." *Journal of Biomedical Materials Research Part A: An Official Journal of The Society for Biomaterials* 68.3 (2004): 504-512.

31. Albrektsson, T., and C. Johansson. "Osteoinduction, osteoconduction and osseointegration." *European Spine Journal* 10.2 (2001): S96-S101.

32. Yousefi, S. Z., P.S. Tabatabaei-Panah, and J. Seyfi. "Emphasizing the role of surface chemistry on hydrophobicity and cell adhesion behavior of polydimethylsiloxane/TiO_2 nanocomposite films." *Colloids and Surfaces B: Biointerfaces* 167 (2018): 492-498.

33. Dowling, D. P., et al. "Effect of surface wettability and topography on the adhesion of osteosarcoma cells on plasma-modified polystyrene." *Journal of Biomaterials Applications* 26.3 (2011): 327-347.

34. Zangi, S., et al. "Tuning cell adhesion on polymeric and nanocomposite surfaces: Role of topography versus superhydrophobicity." *Materials Science and Engineering:* C63 (2016): 609-615.

35. Robotti, F., et al. "A micron-scale surface topography design reducing cell adhesion to implanted materials." *Scientific Reports* 8.1 (2018): 10887.

36. Lamichhane, S., et al. "Polytetrafluoroethylene topographies determine the adhesion, activation, and foreign body giant cell formation of macrophages." *Journal of Biomedical Materials Research Part A* 105.9 (2017): 2441-2450.

37. Hejazi, I., et al. "Investigating the role of surface micro/nano structure in cell adhesion behavior of superhydrophobic polypropylene/nanosilica surfaces." *Colloids and Surfaces B: Biointerfaces* 127 (2015): 233-240.

38. Di Mundo, R., et al. "Cell adhesion on nanotextured slippery superhydrophobic substrates." *Langmuir* 27.8 (2011): 4914-4921.

39. Santander-Borrego, M., et al. "Hydrogels with lotus leaf topography: investigating surface properties and cell adhesion." *Langmuir* 33.2 (2017): 485-493.

40. Le Saux, G., et al. "The relative importance of topography and RGD ligand density for endothelial cell adhesion." *PloS one* 6.7 (2011): e21869.

Chapter 6

6 Conclusions and Future Directions

The objective of the first project was to demonstrate the applicability of the cyanine dye for the *in vitro* evaluation of the biocompatibility of biodegradable magnesium materials by both direct and indirect methods. This study demonstrates a quick and reliable assay to evaluate the biocompatibility of biodegradable magnesium alloys by both direct and indirect methods. The CyQUANT assay provides a more accurate assessment of the overall in vitro biocompatibility of biodegradable metals than the more commonly used assays that are depending on chemical reduction. Upon comparison of the direct and indirect methods, it is evident these two techniques provide complementary information. In the case of the direct method, it was observed that the cells were able to adhere to the surface of Mg AZ31, which would not have been possible using an indirect assay. On the other hand, the magnesium-conditioned medium was shown to be only slightly toxic to the cells using the indirect method. Therefore, the indirect method can be used to quantify the cytotoxicity of the magnesium alloys while the direct method can be used to measure the cell adhesion and proliferation. The results of the direct and indirect methods indicate that in order to accurately determine the cytotoxicity as well as the biocompatibility of biodegradable magnesium alloys, different factors such as the rapid pH change, hydrogen gas produced and deposition of biodegradation products during biocorrosion process must be taken into consideration.

The objective of the second project was to develop a surface modification strategy for magnesium alloys that controls both the degradation rate and the biocompatibility of these

materials. A multi-layered coating consisting of a sol-gel silica layer, a mesoporous silica layer and a layer of calcium phosphate was successfully deposited on magnesium alloy AZ31. The *in vitro* biodegradation test in physiological solutions (SBF) established that the multi-layer coating provides an excellent protection for the magnesium alloy substrate from rapid degradation. Moreover, the *in vitro* cell studies indicated the cytocompatibility of the multi-layered coating. These *in vitro* studies confirm that these multi-layered coatings are an effective surface modification strategy for controlling both the degradation rate and biocompatibility of magnesium alloys for medical applications in bone repair. Furthermore, longer investigation time of *in vitro* degradation studies are needed in this study to determine the bioactivity and degradation behaviour of brushite layer in simulated body fluid. Moreover, *in vitro* cell adhesion and proliferation studies are needed to have a more accurate assessment of the biocompatibility of the coating.

The objective of the third project was to prdevelop a method for the immobilization of the MAPTrix-F-RGD protein to the superhydrophobic Mg AZ31 and to study the influence of this surface modification on Saos-2 osteoblast adhesion to the modified surfaces in comparison to unmodified superhydrophobic surfaces. A superhydrophobic Mg AZ31 surface was successfully reproduced through a combination of rough hierarchical topography and a hydrophobic overlayer. A superhydrophobic magnesium alloy surface was successfully modified with a fibronectin mimetic cell adhesive MAPTrix-F-RGD protein using the mixture of methanol and water solution. However, the in vitro cell adhesion results demonstrated that MAPTrix-F-RGD protein on the superhydrophobic surface did not enhance the cell adhesion of

superhydrophobic surfaces probability due to the complex topography of the superhydrophobic surface. The nano-scale particles coupled with the large height of the microscale particles and their distribution on the surface may be the reasons that cell adhesion is inhibited on the MAPTrix-F-RGD modified superhydrophobic surface. Therefore, further experiments are required to explain the effect of the complex micro and nano scale topography of the superhydrophobic magnesium alloy surface on cell adhesion. The cell adhesion should be evaluated on smooth surfaces with the same surface chemistry as the superhydrophobic surfaces with and without MATRrix-F-RGD. In addition, etched surfaces without the nanoscale coating before and after addition of MAPTrix-F-RGD should be evaluated to determine if the anti-adhesive effect is due to the microscale features alone. Finally, surfaces with microscale particles of variable height and surface distribution should also be analyzed for their cell adhesive properties with and without the cell adhesive ligand.

In general, it is recommended that for studies involving magnesium alloys as a biomaterial, the structure, composition and morphology of the coated surface must always be considered to achieve stable, anti-corrosion and biocompatible magnesium implants. Combining nano-and micro-textures to mimic the hierarchical structure of bone tissue should be taken into account to improve the integrity at the bone/implant interface. Surface roughness is an important factor in cell attachment and corrosion behaviours of magnesium and its alloys but more research is needed in this area. Therefore, the effect of the surface roughness of magnesium and its alloys on the degradation rate and cell behavior should be widely studied under *in vitro* and *in vivo*

conditions. Besides the surface roughness, the effect of surface morphology and porosity on the corrosion behaviors of magnesium *in vivo* has not been fully investigated.

Curriculum Vitae

Name:	Afrah Alhegy
Post-secondary Education and Degrees:	King Faisal University Alhassa, Saudi Arabia 2003-2007 B.Sc. Chemical Education Laurentian University Sudbury, Ontario, Canada 2012-2014 M.A. Laurentian University Sudbury, Ontario, Canada 2014-2019 Ph.D.
Honours and Awards:	Ministry of Education in the Kingdom of Saudi Arabia. 2009-2019

Conference Presentations:

1. **Al Hegy, A.**, Gray-Munro, J. E., & Gauthier, E. R. "Evaluation of the Biocompatibility of Magnesium Alloys by Direct and Indirect Methods" presented at the 34th Annual Meeting of the Canadian Biomaterials Society (CBS 2018), Victoria, B.C., May 2018 (Poster)

2. **Al Hegy**, **A.** & Gray-Munro, J. E. "Development of Self-Healing Calcium Phosphate Coatings on Biodegradable Metallic Implant Materials" presented at the International Conference on 10th World Biomaterials Congress (WBC 2016), Montreal, QC, May 2016 (Poster)

3. **Al Hegy, A.** & Gray-Munro, J. E. "Development of Self-Healing Calcium Phosphate Coating on Biodegradable Metallic Implant Materials" presented at the 32th Annual Meeting of the Canadian Biomaterials Society (CBS 2015), Toronto, ON, May 2015 (Poster)

4. **Al Hegy, A.**, & Gray-Munro, J. E. "Deposition of a Mesoporous Silica Coating on Magnesium Alloy AZ31" presented at the Materials Science and Technology Conference, Montreal, QC, October 2013 (Oral Presentation)

5. **Al Hegy, A.** & Gray-Munro "Deposition of a Mesoporous Silica Coating on Magnesium Alloy AZ31" presented at the International Conference on Nanotechnology and Advanced Materials, Quebec, QC, August 2013 (Poster)

6. **Al Hegy, A.** & Gray-Munro"Deposition of a Mesoporous Silica Coating on Magnesium Alloy AZ31" presented at the Canadian Biomaterials Society Conference, Ottawa, ON, June 2013. (Poster)

Publications:

1. **Al Hegy, A**., Gray-Munro, J.E. & Gauthier, E.R. (Evaluation of the Biocompatibility of Magnesium Alloys by Direct and Indirect Methods) (in preparation)

2. **Al Hegy, A**., Gray-Munro, J.E. & Gauthier, E.R. (Development of a Biocompatible Calcium Phosphate Coating with Improved Degradation Resistance for Biodegradable Magnesium Implant Materials) (in preparation)

3. **Al Hegy, A**., Gray-Munro, J.E. & Gauthier, E.R. (Preliminary Results on the Immobilization of a Fibronectin Mimetic to the Surface of Superhydrophobic Magnesium and its Influence on Cell Adhesion) (in preparation)

4. Yang, X., **Al Hegy, A.**, Gauthier, E. R., & Gray-Munro, J. (2017). Influence of mixed organosilane coatings with variable RGD surface densities on the adhesion and proliferation of human osteosarcoma Saos-2 cells to magnesium alloy AZ31. Bioactive materials, 2(1), 35-43.

Published Abstract:

1. **Al Hegy**, **A.** & Gray-Munro, J. E. "Development of Self-Healing Calcium Phosphate Coatings on Biodegradable Metallic Implant Materials" *Front. Biotechnol. Conference Abstract: 10th World Biomaterials Congress.* Doi:10.3389/conf. FBIOE. 2016.01.02735

Appendices

Appendix 1: List of the References Used to Prepare Figure 3.2.

❖ Indirect MTT Assay

1. Jin, W., et al. "Improvement of corrosion resistance and biocompatibility of rare-earth WE43 magnesium alloy by neodymium self-ion implantation." *Corrosion Science* 94 (2015): 142-155.
2. Bian, D., et al. "In vitro and in vivo studies on biomedical magnesium low-alloying with elements gadolinium and zinc for orthopedic implant applications." *ACS Applied Materials & Interfaces* 10.5 (2018): 4394-4408.
3. Zhao, Y., et al. "Enhanced antimicrobial properties, cytocompatibility, and corrosion resistance of plasma-modified biodegradable magnesium alloys." *Acta Biomaterialia* 10.1 (2014): 544-556.
4. Jin, W., et al. "Hafnium-implanted WE43 magnesium alloy for enhanced corrosion protection and biocompatibility." *Surface and Coatings Technology* 306 (2016): 11-15.
5. Lin, X., et al. "In vitro degradation and biocompatibility of a strontium-containing micro-arc oxidation coating on the biodegradable ZK60 magnesium alloy." *Applied Surface Science* 288 (2014): 718-726.
6. Naujokat, H., et al. "Effects of degradable osteosynthesis plates of MgYREZr alloy on cell function of human osteoblasts, fibroblasts and osteosarcoma cells." *Journal of Materials Science: Materials in Medicine* 28.8 (2017): 126.

7. Cheng, M., et al. "Dual ions implantation of zirconium and nitrogen into magnesium alloys for enhanced corrosion resistance, antimicrobial activity and biocompatibility." *Colloids and Surfaces B: Biointerfaces* 148 (2016): 200-210.
8. Liao, Y., et al. "Cellular response of chondrocytes to magnesium alloys for orthopedic applications." *International Journal of Molecular Medicine* 36.1 (2015): 73-82.
9. Yang, H., et al. "Growth, in vitro biodegradation and cytocompatibility properties of nano-hydroxyapatite coatings on biodegradable magnesium alloys." *Journal of Alloys and Compounds* 672 (2016): 366-373.
10. Tian, J., et al. "Investigation of the antimicrobial activity and biocompatibility of magnesium alloy coated with HA and antimicrobial peptide." *Journal of Materials Science: Materials in Medicine* 26.2 (2015): 66.
11. Wang, Q., L. Tan, and K. Yang. "Cytocompatibility and hemolysis of AZ31B Magnesium alloy with si-containing coating." *Journal of Materials Science & Technology* 31.8 (2015): 845-851.
12. Makkar, P., et al. "Development and properties of duplex MgF2/PCL coatings on biodegradable magnesium alloy for biomedical applications." *PloS One* 13.4 (2018): e0193927.
13. Yu, K., et al. "In vitro and in vivo evaluation of novel biodegradable Mg-Ag-Y alloys for use as resorbable bone fixation implant." *Journal of Biomedical Materials Research Part A* (2018).

14. Mousa, H. M., et al. "In vitro degradation behavior and cytocompatibility of a bioceramic anodization films on the biodegradable magnesium alloy." *Colloids and Surfaces A: Physicochemical and Engineering Aspects* 488 (2016): 82-92.
15. Mousa, H. M., et al. "One-step anodization deposition of anticorrosive bioceramic compounds on AZ31B magnesium alloy for biomedical application." *Ceramics International* 41.9 (2015): 10861-10870.
16. Wang, C., et al. "In vitro degradation and cytocompatibility of a silane/Mg (OH) 2 composite coating on AZ31 alloy by spin coating." *Journal of Alloys and Compounds*714 (2017): 186-193.
17. Liu, C., et al. "Surface modification of magnesium alloy via cathodic plasma electrolysis and its influence on corrosion resistance and cytocompatibility." *Materials Letters* 132 (2014): 15-18.
18. Yang, H., et al. "In Vitro Corrosion and Cytocompatibility Properties of Nano-Whisker Hydroxyapatite Coating on Magnesium Alloy for Bone Tissue Engineering Applications." *International Journal of Molecular Sciences* 16.3 (2015): 6113-6123.
19. Gopi, D., et al. "Electrodeposition of a porous strontium-substituted hydroxyapatite/zinc oxide duplex layer on AZ91 magnesium alloy for orthopedic applications." *Journal of Materials Chemistry B* 2.34 (2014): 5531-5540.
20. Ma, W. H., et al. "Improved biological performance of magnesium by micro-arc oxidation." *Brazilian Journal of Medical and Biological Research* 48.3 (2015): 214-225.
21. Yan, T., et al. "Fluoride conversion coating on biodegradable AZ31B magnesium alloy." *Journal of Materials Science & Technology* 30.7 (2014): 666-674.

22. Homayun, B., and A. Afshar. "Microstructure, mechanical properties, corrosion behavior and cytotoxicity of Mg-Zn-Al-Ca alloys as biodegradable materials." *Journal of Alloys and Compounds* 607 (2014): 1-10.
23. Li, T., et al. "Effects of scandium addition on biocompatibility of biodegradable Mg–1.5 Zn–0.6 Zr alloy." *Materials Letters*215 (2018): 200-202.
24. Li, Z., et al. "In vitro and in vivo corrosion, mechanical properties and biocompatibility evaluation of MgF2-coated Mg-Zn-Zr alloy as cancellous screws." *Materials Science and Engineering: C* 75 (2017): 1268-1280.
25. Zhao, N., et al. "In vitro biocompatibility and endothelialization of novel magnesium-rare earth alloys for improved stent applications." *PloS One* 9.6 (2014): e98674.
26. Dehghanian, C., N. Aboudzadeh, and M. A. Shokrgozar. "Characterization of silicon-substituted nano hydroxyapatite coating on magnesium alloy for biomaterial application." *Materials Chemistry and Physics* 203 (2018): 27-33.
27. Wang, M. J., S. C. Chao, and S. K. Yen. "Electrolytic calcium phosphate/zirconia composite coating on AZ91D magnesium alloy for enhancing corrosion resistance and bioactivity." *Corrosion Science* 104 (2016): 47-60.
28. Zhu, B., et al. "Preparation and characterization of aminated hydroxyethyl cellulose-induced biomimetic hydroxyapatite coatings on the AZ31 magnesium alloy." *Metals* 7.6 (2017): 214.
29. Abdal-hay, A., et al. "Enhanced biocorrosion resistance of surface modified magnesium alloys using inorganic/organic composite layer for biomedical applications." *Ceramics International* 40.1 (2014): 2237-2247.

30. Lin, B., et al. "Preparation and characterization of dopamine-induced biomimetic hydroxyapatite coatings on the AZ31 magnesium alloy." *Surface and Coatings Technology*281 (2015): 82-88.
31. Pichler, K., et al. "Cellular reactions to biodegradable magnesium alloys on human growth plate chondrocytes and osteoblasts." *International Orthopaedics* 38.4 (2014): 881-889.
32. Chang, W. H., et al. "In vitro biocompatibility and antibacterial behavior of anodic coatings fabricated in an organic phosphate containing solution on Mg–1.0 Ca alloys." *Surface and Coatings Technology* 289 (2016): 75-84.
33. Mao, L., et al. "A promising biodegradable magnesium alloy suitable for clinical vascular stent application." *Scientific Reports* 7 (2017): 46343.
34. Mao, L., et al. "Enhanced biocompatibility and long-term durability in vivo of Mg-Nd-Zn-Zr alloy for vascular stent application." *Journal of Alloys and Compounds* 720 (2017): 245-253.
35. Liu, C., et al. "The in vitro biocompatibility and macrophage phagocytosis of Mg17Al12 phase in Mg–Al–Zn alloys." *Journal of Biomedical Materials Research Part A* 103.7 (2015): 2405-2415.
36. Cao, L., et al. "RGDC Peptide-Induced Biomimetic Calcium Phosphate Coating Formed on AZ31 Magnesium Alloy." *Materials* 10.4 (2017): 358.
37. Wang, J., et al. "Magnesium alloy based interference screw developed for ACL reconstruction attenuates peri-tunnel bone loss in rabbits." *Biomaterials* 157 (2018): 86-97.

38. Abdal-hay, A., et al. "Biocorrosion behavior of biodegradable nanocomposite fibers coated layer-by-layer on AM50 magnesium implant." *Materials Science and Engineering: C* 58 (2016): 1232-1241.
39. Jin, W., et al. "Enhanced corrosion resistance and biocompatibilty of PMMA-coated ZK60 magnesium alloy." *Materials Letters* 173 (2016): 178-181.
40. Zhu, B., et al. "Preparation of hydroxyapatite/tannic acid coating to enhance the corrosion resistance and cytocompatibility of AZ31 magnesium alloys." *Coatings* 7.7 (2017): 105.
41. Jin, W., et al. "Corrosion resistance and cytocompatibility of tantalum-surface-functionalized biomedical ZK60 Mg alloy." *Corrosion Science* 114 (2017): 45-56.
42. Meifeng, H., et al. "Effects of Li addition on the corrosion behaviour and biocompatibility of Mg (Li)–Zn–Ca metallic glasses." *Journal of Materials Science* (2018): 1-15.
43. Bakhsheshi-Rad, H. R., et al. "Drug delivery and cytocompatibility of ciprofloxacin loaded gelatin nanofibers-coated Mg alloy." *Materials Letters* 207 (2017): 179-182.
44. Bakhsheshi-Rad, H. R., et al. "Novel bi-layered nanostructured SiO2/Ag-FHAp coating on biodegradable magnesium alloy for biomedical applications." *Ceramics International* 42.10 (2016): 11941-11950.
45. Bakhsheshi-Rad, H. R., et al. "Drug release, cytocompatibility, bioactivity, and antibacterial activity of doxycycline loaded Mg-Ca-TiO2 composite scaffold." *Materials & Design* 139 (2018): 212-221.

46. Cui, T., et al. "Studies on biocompatibility of Mg-4.0 Zn-1.5 Sr alloy with coated of the laser surface processing combining alkaline treatment." *IOP Conference Series: Materials Science and Engineering*. Vol. 301. No. 1. IOP Publishing, 2018.
47. Bakhsheshi-Rad, H. R., et al. "In vitro degradation behavior, antibacterial activity and cytotoxicity of TiO2-MAO/ZnHA composite coating on Mg alloy for orthopedic implants." *Surface and Coatings Technology* 334 (2018): 450-460.
48. Willbold, E., et al. "Effect of the addition of low rare earth elements (lanthanum, neodymium, cerium) on the biodegradation and biocompatibility of magnesium." *Acta Biomaterialia* 11 (2015): 554-562.
49. Khalajabadi, S. Z., et al. "The effect of MgO on the biodegradation, physical properties and biocompatibility of a Mg/HA/MgO nanocomposite manufactured by powder metallurgy method." *Journal of Alloys and Compounds* 655 (2016): 266-280.
50. Agarwal, S., et al. "Enhanced corrosion protection and biocompatibility of a PLGA–silane coating on AZ31 Mg alloy for orthopaedic applications." *RSC Advances* 6.115 (2016): 113871-113883.
51. He, G., et al. "Addition of Zn to the ternary Mg–Ca–Sr alloys significantly improves their antibacterial properties." *Journal of Materials Chemistry B* 3.32 (2015): 6676-6689.
52. Huang, T., et al. "Microelectrode array-evaluation of neurotoxic effects of magnesium as an implantable biomaterial." *Journal of Materials Science & Technology* 32.1 (2016): 89-96.

53. Tian, P., D. Xu, and X. Liu. "Mussel-inspired functionalization of PEO/PCL composite coating on a biodegradable AZ31 magnesium alloy." *Colloids and Surfaces B: Biointerfaces* 141 (2016): 327-337.
54. Chen, Y., et al. "In vitro and in vivo assessment of the biocompatibility of an Mg–6Zn alloy in the bile." *Journal of Materials Science: Materials in Medicine* 25.2 (2014): 471-480.
55. Jia, Z. J., et al. "Micro-arc oxidization of a novel Mg–1Ca alloy in three alkaline KF electrolytes: Corrosion resistance and cytotoxicity." *Applied Surface Science* 292 (2014): 1030-1039.
56. Liu, L., et al. "The in vitro biological properties of Mg-Zn-Sr alloy and superiority for preparation of biodegradable intestinal anastomosis rings." *Medical Science Monitor: International Medical Journal of Experimental and Clinical Research* 20 (2014): 1056.
57. Huang, L., et al. "Carboxymethyl chitosan functionalization of CPED-treated magnesium alloy via polydopamine as intermediate layer." *Surface and Coatings Technology* 258 (2014): 664-671.
58. Wei, Z., et al. "Hemocompatibility and selective cell fate of polydopamine-assisted heparinized PEO/PLLA composite coating on biodegradable AZ31 alloy." *Colloids and Surfaces B: Biointerfaces* 121 (2014): 451-460.
59. Bahl, S., S. Suwas, and K. Chatterjee. "The control of crystallographic texture in the use of magnesium as a resorbable biomaterial." *RSC Advances* 4.99 (2014): 55677-55684.

60. Qiu, Xun, et al. "Preliminary research on a novel bioactive silicon doped calcium phosphate coating on AZ31 magnesium alloy via electrodeposition." *Materials Science and Engineering: C* 36 (2014): 65-76.
61. Anvari-Yazdi, A. F., et al. "Cytotoxicity assessment of adipose-derived mesenchymal stem cells on synthesized biodegradable Mg-Zn-Ca alloys." *Materials Science and Engineering: C* 69 (2016): 584-597.
62. Wu, Y., et al. "Unique antitumor property of the Mg-Ca-Sr alloys with addition of Zn." *Scientific Reports* 6 (2016): 21736.
63. Zeng, R.C., et al. "In vitro corrosion and cytocompatibility of a microarc oxidation coating and poly (l-lactic acid) composite coating on Mg–1Li–1Ca alloy for orthopedic implants." *ACS Applied Materials & Interfaces* 8.15 (2016): 10014-10028.
64. Neacsu, P., et al. "Characterization and in vitro and in vivo assessment of a novel cellulose acetate-coated mg-based alloy for orthopedic applications." *Materials* 10.7 (2017): 686.
65. Zhao, Q., W. Mahmood, and Y. Zhu. "Synthesis of dittmarite/Mg (OH) 2 composite coating on AZ31 using hydrothermal treatment." *Applied Surface Science* 367 (2016): 249-258.
66. Hong, D., et al. "Binder-jetting 3D printing and alloy development of new biodegradable Fe-Mn-Ca/Mg alloys." *Acta Biomaterialia* 45 (2016): 375-386.
67. Song, X., et al. "Investigation on the in vitro cytocompatibility of Mg-Zn-Y-Nd-Zr alloys as degradable orthopaedic implant materials." *Journal of Materials Science: Materials in Medicine* 29.4 (2018): 44.

68. Shen, C., et al. "Mechanical properties, in vitro degradation behavior, hemocompatibility and cytotoxicity evaluation of Zn–1.2 Mg alloy for biodegradable implants." *RSC Advances* 6.89 (2016): 86410-86419.
69. Mostofi, S., et al. "Effects of corroded and non-corroded biodegradable Mg and Mg alloys on viability, morphology and differentiation of MC3T3-E1 cells elicited by direct cell/material interaction." *PloS One* 11.7 (2016): e0159879.
70. Galvin, E., et al. "In vitro corrosion and biological assessment of bioabsorbable WE43 Mg alloy specimens." *Journal of Manufacturing and Materials Processing* 1.1 (2017): 8.
71. Bagha, P. S., et al. "Characterization of nanostructured biodegradable Zn-Mn alloy synthesized by mechanical alloying." *Journal of Alloys and Compounds* 735 (2018): 1319-1327.
72. Liu, J., et al. "Improved cytocompatibility of Mg-1Ca alloy modified by Zn ion implantation and deposition." *Materials Letters* 205 (2017): 87-89.
73. Bakhsheshi-Rad, H. R., et al. "Thermal characteristics, mechanical properties, in vitro degradation and cytotoxicity of novel biodegradable Zn-Al-Mg and Zn-Al-Mg-xBi alloys." *Acta Metallurgica Sinica (English Letters)* 30.3 (2017): 201-211.

❖ Indirect Other Assays

1. Fei, J., et al. "Biocompatibility and neurotoxicity of magnesium alloys potentially used for neural repairs." *Materials Science and Engineering: C* 78 (2017): 1155-1163.

2. Wang, W., et al. "Novel biocompatible magnesium alloys design with nutrient alloying elements Si, Ca and Sr: Structure and properties characterization." *Materials Science and Engineering: B* 214 (2016): 26-36.
3. Peng, F., et al. "Enhanced corrosion resistance and biocompatibility of magnesium alloy by Mg–Al-layered double hydroxide." *ACS Applied Materials & Interfaces* 8.51 (2016): 35033-35044.
4. Zhen, Z., et al. "Hemolysis and cytotoxicity mechanisms of biodegradable magnesium and its alloys." *Materials Science and Engineering: C* 46 (2015): 202-206.
5. Zhang, J., et al. "Effect of the addition CNTs on performance of CaP/chitosan/coating deposited on magnesium alloy by electrophoretic deposition." *Materials Science and Engineering: C* 58 (2016): 992-1000.
6. Zhang, L., et al. "Facile preparation of poly (lactic acid)/brushite bilayer coating on biodegradable magnesium alloys with multiple functionalities for orthopedic application." *ACS Applied Materials & Interfaces* 9.11 (2017): 9437-9448.
7. Pompa, L., et al. "Surface characterization and cytotoxicity response of biodegradable magnesium alloys." *Materials Science and Engineering: C* 49 (2015): 761-768.
8. Saha, P., et al. "Effects of grain refinement on the biocorrosion and in vitro bioactivity of magnesium." *Materials Science and Engineering: C* 57 (2015): 294-303.
9. Ding, Y., et al. "Mechanical properties, in vitro corrosion and biocompatibility of newly developed biodegradable Mg-Zr-Sr-Ho alloys for biomedical applications." *Scientific Reports* 6 (2016): 31990.

10. Zhou, Y. L., et al. "Microstructures, mechanical and corrosion properties and biocompatibility of as extruded Mg–Mn–Zn–Nd alloys for biomedical applications." *Materials Science and Engineering: C* 49 (2015): 93-100.
11. Wang, Y., et al. "Improved corrosion resistance and biocompatibility of a calcium phosphate coating on a magnesium alloy for orthopedic applications." *European Journal of Inflammation* 14.3 (2016): 169-183.
12. Kang, Y. G., et al. "Enhanced biocompatibility and osteogenic potential of mesoporous magnesium silicate/polycaprolactone/wheat protein composite scaffolds." *International Journal of Nanomedicine* 13 (2018): 1107.
13. Ding, Y., et al. "Mechanical properties, corrosion, and biocompatibility of Mg-Zr-Sr-Dy alloys for biodegradable implant applications." *Journal of Biomedical Materials Research Part B: Applied Biomaterials* (2017).
14. Gu, X. N., et al. "Degradation, hemolysis, and cytotoxicity of silane coatings on biodegradable magnesium alloy." *Materials Letters* 193 (2017): 266-269.
15. Peng, F., et al. "“Petal effect”-inspired superhydrophobic and highly adhesive coating on magnesium with enhanced corrosion resistance and biocompatibility." *Science China Materials* (2017): 1-14.
16. Bornapour, M., et al. "Surface characterization, in vitro and in vivo biocompatibility of Mg-0.3 Sr-0.3 Ca for temporary cardiovascular implant." *Materials Science and Engineering: C*67 (2016): 72-84.

17. Lee, H. P., D. J. Lin, and M. L. Yeh. "Phenolic modified ceramic coating on biodegradable Mg alloy: The improved corrosion resistance and osteoblast-like cell activity." *Materials* 10.7 (2017): 696.
18. Han, J., et al. "Tailoring the degradation and biological response of a magnesium–strontium alloy for potential bone substitute application." *Materials Science and Engineering: C*58 (2016): 799-811.
19. Kaabi Falahieh Asl, S., S. Nemeth, and M. J. Tan. "Novel biodegradable calcium phosphate/polymer composite coating with adjustable mechanical properties formed by hydrothermal process for corrosion protection of magnesium substrate." *Journal of Biomedical Materials Research Part B: Applied Biomaterials* 104.8 (2016): 1643-1657.
20. Liu, Y., et al. "Influence of biocompatible metal ions (Ag, Fe, Y) on the surface chemistry, corrosion behavior and cytocompatibility of Mg–1Ca alloy treated with MEVVA." *Colloids and Surfaces B: Biointerfaces* 133 (2015): 99-107.
21. Kubásek, J., et al. "Structure, mechanical characteristics and in vitro degradation, cytotoxicity, genotoxicity and mutagenicity of novel biodegradable Zn–Mg alloys." *Materials Science and Engineering: C* 58 (2016): 24-35.
22. Kim, Y. K., et al. "Effect of Ca-P compound formed by hydrothermal treatment on biodegradation and biocompatibility of Mg-3Al-1Zn-1.5 Ca alloy; in vitro and in vivo evaluation." *Scientific Reports* 7.1 (2017): 712.
23. Lin, D. J., et al. "Tailored coating chemistry and interfacial properties for construction of bioactive ceramic coatings on magnesium biomaterial." *Materials & Design* 89 (2016): 235-244.

24. Mousa, H. M., et al. "A multifunctional zinc oxide/poly (lactic acid) nanocomposite layer Coated on magnesium alloys for controlled degradation and antibacterial function." *ACS Biomaterials Science & Engineering* (2018).
25. Henderson, H. B., et al. "Mechanical and degradation property improvement in a biocompatible Mg-Ca-Sr alloy by thermomechanical processing." *Journal of the Mechanical Behavior of Biomedical Materials* 80 (2018): 285-292.
26. Zhang, Y., et al. "Effect of homogenization on microstructure characteristics, corrosion and biocompatibility of Mg-Zn-Mn-xCa alloys." *Materials* 11.2 (2018): 227.
27. Kraemer, M., et al. "Corrosion behavior, biocompatibility and biomechanical stability of a prototype magnesium-based biodegradable intramedullary nailing system." *Materials Science and Engineering: C* 59 (2016): 129-135.
28. Peng, F., et al. "Enhanced corrosion resistance and biocompatibility of magnesium alloy by Mg–Al-layered double hydroxide." *ACS Applied Materials & Interfaces* 8.51 (2016): 35033-35044.
29. Guo, Y., et al. "Biocompatibility and osteogenic activity of guided bone regeneration membrane based on chitosan-coated magnesium alloy." *Materials Science and Engineering: C* (2019).
30. Ren, Y., et al. "Rapid coating of AZ31 magnesium alloy with calcium deficient hydroxyapatite using microwave energy." *Materials Science and Engineering: C* 49 (2015): 364-372.
31. Zhang, J., et al. "Influence of proteins and cells on in vitro corrosion of Mg–Nd–Zn–Zr alloy." *Corrosion Science* 85 (2014): 477-481.

32. Jung, O., et al. "Optimized in vitro procedure for assessing the cytocompatibility of magnesium-based biomaterials." *Acta Biomaterialia* 23 (2015): 354-363.
33. Bagherifard, S., et al. "Effects of nanofeatures induced by severe shot peening (SSP) on mechanical, corrosion and cytocompatibility properties of magnesium alloy AZ31." *Acta Biomaterialia* 66 (2018): 93-108.

❖ Direct MTT Assay

1. Razavi, M., et al. "In vivo assessments of bioabsorbable AZ91 magnesium implants coated with nanostructured fluoridated hydroxyapatite by MAO/EPD technique for biomedical applications." *Materials Science and Engineering: C* 48 (2015): 21-27.
2. Kumar, R. M., et al. "Electrophoretic deposition of hydroxyapatite coating on Mg–3Zn alloy for orthopaedic application." *Surface and Coatings Technology* 287 (2016): 82-92.
3. Yang, Q., et al. "Atomic layer deposited ZrO2 nanofilm on Mg-Sr alloy for enhanced corrosion resistance and biocompatibility." *Acta Biomaterialia* 58 (2017): 515-526.
4. Wang, S. H., C. W. Yang, and T. M. Lee. "Evaluation of microstructural features and in vitro biocompatibility of hydrothermally coated fluorohydroxyapatite on AZ80 Mg alloy." *Industrial & Engineering Chemistry Research* 55.18 (2016): 5207-5215.
5. Razavi, M., et al. "In vivo study of nanostructured akermanite/PEO coating on biodegradable magnesium alloy for biomedical applications." *Journal of Biomedical Materials Research Part A* 103.5 (2015): 1798-1808.

6. Jaiswal, S., et al. "Mechanical, corrosion and biocompatibility behaviour of Mg-3Zn-HA biodegradable composites for orthopaedic fixture accessories." *Journal of the Mechanical Behavior of Biomedical Materials* 78 (2018): 442-454.
7. Xu, Q., et al. "Performance of hydroxyapatite coatings electrodeposited on micro-arc oxidized magnesium alloys using a static magnetic field." *RSC Advances* 5.19 (2015): 14458-14464.
8. Singh, S., et al. "Sol-gel derived hydroxyapatite coating on Mg-3Zn alloy for orthopedic application." *Jom* 67.4 (2015): 702-712.
9. Shen, S., et al. "Microwave aqueous synthesis of hydroxyapatite bilayer coating on magnesium alloy for orthopedic application." *Chemical Engineering Journal* 309 (2017): 278-287.
10. Razavi, M., et al. "In vivo study of nanostructured diopside (CaMgSi2O6) coating on magnesium alloy as biodegradable orthopedic implants." *Applied Surface Science* 313 (2014): 60-66.
11. Razavi, M., et al. "Surface microstructure and in vitro analysis of nanostructured akermanite (Ca2MgSi2O7) coating on biodegradable magnesium alloy for biomedical applications." *Colloids and Surfaces B: Biointerfaces* 117 (2014): 432-440.
12. Sunil, B. R., et al. "In vitro and in vivo studies of biodegradable fine grained AZ31 magnesium alloy produced by equal channel angular pressing." *Materials Science and Engineering: C* 59 (2016): 356-367.

13. Sunil, B. R., et al. "Nano-hydroxyapatite reinforced AZ31 magnesium alloy by friction stir processing: a solid state processing for biodegradable metal matrix composites." *Journal of Materials Science: Materials in Medicine* 25.4 (2014): 975-988.
14. Sunil, B. R., et al. "Friction stir processing of magnesium–nanohydroxyapatite composites with controlled in vitro degradation behavior." *Materials Science and Engineering: C*39 (2014): 315-324.
15. Kim, Y. K., et al. "Characterization and biocompatibility of a calcium-containing AZ31B alloy as a biodegradable material." *Journal of Materials Science* 50.13 (2015): 4672-4682.
16. Jiang, S., et al. "Synthesis and characterization of magnesium phytic acid/apatite composite coating on AZ31 Mg alloy by microwave assisted treatment." *Materials Science and Engineering: C* 91 (2018): 218-227.
17. Prakash, C., et al. "Synthesis, characterization, corrosion and bioactivity investigation of nano-HA coating deposited on biodegradable Mg-Zn-Mn alloy." *Surface and Coatings Technology* 346 (2018): 9-18.
18. Ramya, M., et al. "Hydroxyapatite particle (HAp) reinforced biodegradable Mg-Zn-Ca metallic glass composite for bio-implant applications." *Biomedical Physics & Engineering Express* 4.2 (2018): 025039.
19. Charyeva, O., et al. "Biocompatibility of magnesium implants in primary human reaming debris-derived cells stem cells in vitro." *Journal of Orthopaedics and Traumatology* 17.1 (2016): 63.

20. Liu, J., et al. "A novel biodegradable and biologically functional arginine-based poly (ester urea urethane) coating for Mg-Zn-Y-Nd alloy: enhancement in corrosion resistance and biocompatibility." *Journal of Materials Chemistry B* 5.9 (2017): 1787-1802.
21. Wang, B., et al. "Mussel-inspired nano-multilayered coating on magnesium alloys for enhanced corrosion resistance and antibacterial property." *Colloids and Surfaces B: Biointerfaces*157 (2017): 432-439.
22. Nayak, S., et al. "Strengthening of Mg based alloy through grain refinement for orthopaedic application." *Journal of the Mechanical Behavior of Biomedical Materials* 59 (2016): 57-70.
23. Kayhan, S. M., et al. "Experimental and numerical investigations for mechanical and microstructural characterization of micro-manufactured AZ91D magnesium alloy disks for biomedical applications." *Materials & Design* 93 (2016): 397-408.
24. Jiang, T., et al. "Upregulation of cell proliferation via Shc and ERK1/2 MAPK signaling in SaOS-2 osteoblasts grown on magnesium alloy surface coating with tricalcium phosphate." *Journal of Materials Science: Materials in Medicine* 26.4 (2015): 158.
25. Hanas, T., et al. "Tailoring degradation of AZ31 alloy by surface pre-treatment and electrospun PCL fibrous coating." *Materials Science and Engineering: C* 65 (2016): 43-50.
26. Tian, P., X. Liu, and C. Ding. "In vitro degradation behavior and cytocompatibility of biodegradable AZ31 alloy with PEO/HT composite coating." *Colloids and Surfaces B: Biointerfaces* 128 (2015): 44-54.

❖ Direct Other Assays

1. Witecka, A., A. Yamamoto, and W. Swieszkowski. "Improvement of cytocompatibility of magnesium alloy ZM21 by surface modification." *Magnesium Technology 2014*. Springer, Cham, 2014. 375-380.
2. Pan, C. J., et al. "Effects of self-assembly of 3-phosphonopropionic acid, 3-aminopropyltrimethoxysilane and dopamine on the corrosion behaviors and biocompatibility of a magnesium alloy." *Materials Science and Engineering: C* 67 (2016): 132-143.
3. Pan, C. J., et al. "Improving corrosion resistance and biocompatibility of magnesium alloy by sodium hydroxide and hydrofluoric acid treatments." *Applied Sciences* 7.1 (2016): 33.
4. Jiang, Y., et al. "Polydopamine Mediated Assembly of Hydroxyapatite Nanoparticles and Bone Morphogenetic Protein-2 on Magnesium Alloys for Enhanced Corrosion Resistance and Bone Regeneration." *Journal of Biomedical Materials Research Part A* (2017).
5. Zhang, D., et al. "In vitro degradation and cytocompatibility of magnesium alloy coated with Hf/PLLA duplex coating." *Materials Letters* 213 (2018): 249-252.
6. Kannan, M. B., R. Walter, and A. Yamamoto. "Biocompatibility and in vitro degradation behavior of magnesium-calcium alloy coated with calcium phosphate using an unconventional electrolyte." *ACS Biomaterials Science & Engineering* 2.1 (2015): 56-64.

7. Witecka, A., et al. "Influence of biodegradable polymer coatings on corrosion, cytocompatibility and cell functionality of Mg-2.0 Zn-0.98 Mn magnesium alloy." *Colloids and Surfaces B: Biointerfaces* 144 (2016): 284-292.
8. Zhang, L. C., et al. "Biofunctionization of biodegradable magnesium alloy to improve the in vitro corrosion resistance and biocompatibility." *Applied Surface Science* 451 (2018): 20-31.
9. Ma, C., et al. "Laser surface modification of Mg-Gd-Ca alloy for corrosion resistance and biocompatibility enhancement." *Applied Surface Science* 445 (2018): 211-216.
10. Pan, C., et al. "Corrosion resistance and biocompatibility of magnesium alloy modified by alkali heating treatment followed by the immobilization of poly (ethylene glycol), fibronectin and heparin." *Materials Science and Engineering: C* 70 (2017): 438-449.
11. Liu, J., and T. Xi. "Enhanced anti-corrosion ability and biocompatibility of PLGA coatings on MgZnYNd alloy by BTSE-APTES pre-treatment for cardiovascular stent." *Journal of Materials Science & Technology* 32.9 (2016): 845-857.
12. Wei, Z., et al. "In vitro degradation, hemolysis, and cytocompatibility of PEO/PLLA composite coating on biodegradable AZ31 alloy." *Journal of Biomedical Materials Research Part B: Applied Biomaterials* 103.2 (2015): 342-354.

❖ Direct CyQUANT Assy

1. Kim, S. M., et al. "Hydroxyapatite-coated magnesium implants with improved in vitro and in vivo biocorrosion, biocompatibility, and bone response." *Journal of Biomedical Materials Research Part A* 102.2 (2014): 429-441.

2. Kang, M. H., et al. "Poly (ether imide)-silica hybrid coatings for tunable corrosion behavior and improved biocompatibility of magnesium implants." *Biomedical Materials* 11.3 (2016): 035003.
3. Kim, S. M., et al. "Innovative micro-textured hydroxyapatite and poly (l-lactic)-acid polymer composite film as a flexible, corrosion resistant, biocompatible, and bioactive coating for Mg implants." *Materials Science and Engineering: C* 81 (2017): 97-103.
4. Gaur, S., et al. "Silane-Coated Magnesium Implants with Improved In-Vitro Corrosion Resistance and Biocompatibility." *Journal of Materials Science & Surface Engg* 4 (2016): 415-424.
5. Zhu, D., et al. "Biological responses and mechanisms of human bone marrow mesenchymal stem cells to Zn and Mg biomaterials." *ACS Applied Materials & Interfaces* 9.33 (2017): 27453-27461.
6. Yang, X., et al. "Influence of mixed organosilane coatings with variable RGD surface densities on the adhesion and proliferation of human osteosarcoma Saos-2 cells to magnesium alloy AZ31." *Bioactive Materials* 2.1 (2017): 35-43.